EVOLUTIONARY TOPOLOGY OPTIMIZATION OF A FOLDING MISSILE WING FOR STIFFNESS AND FREQUENCY

A THESIS SUBMITTED TO
THE GRADUATE SCHOOL OF NATURAL AND APPLIED SCIENCES
OF
MIDDLE EAST TECHNICAL UNIVERSITY

BY

ATA ÜRÜN

IN PARTIAL FULFILLMENT OF THE REQUIREMENTS
FOR
THE DEGREE OF MASTER OF SCIENCE
IN
AEROSPACE ENGINEERING

JANUARY 2023

Approval of the thesis:

EVOLUTIONARY TOPOLOGY OPTIMIZATION OF A FOLDING MISSILE WING FOR STIFFNESS AND FREQUENCY

submitted by **ATA ÜRÜN** in partial fulfillment of the requirements for the degree of **Master of Science** i**n Aerospace Engineering, Middle East Technical University** by,

Prof. Dr. Halil Kalıpçılar
Dean, Graduate School of **Natural and Applied Sciences** _____

Prof. Dr. Serkan Özgen
Head of the Department, **Aerospace Engineering** _____

Assoc. Prof. Dr. Melin Şahin
Supervisor, **Aerospace Engineering, METU** _____

Assoc. Prof. Dr. Ercan Gürses
Co-Supervisor, **Aerospace Engineering, METU** _____

Examining Committee Members:

Prof. Dr. Altan Kayran
Aerospace Engineering, METU _____

Assoc. Prof. Dr. Melin Şahin
Aerospace Engineering, METU _____

Assoc. Prof. Dr. Ercan Gürses
Aerospace Engineering, METU _____

Asst. Prof. Dr. Görkem Eğemen Güloğlu
Aerospace Engineering, METU _____

Assoc. Prof. Dr. Recep M. Görgülüarslan
Mechanical Engineering, TOBB ETU _____

Date: 25.01.2023

I hereby declare that all information in this document has been obtained and presented in accordance with academic rules and ethical conduct. I also declare that, as required by these rules and conduct, I have fully cited and referenced all material and results that are not original to this work.

Name Last name : Ata Ürün

Signature :

ABSTRACT

EVOLUTIONARY TOPOLOGY OPTIMIZATION OF A FOLDING MISSILE WING FOR STIFFNESS AND FREQUENCY

Ürün, Ata
Master of Science, Aerospace Engineering
Supervisor: Assoc. Prof. Dr. Melin Şahin
Co-Supervisor: Assoc. Prof. Dr. Ercan Gürses

January 2023, 123 pages

This thesis presents a study on the topology optimization of a folding wing structure for a cruise missile with the aim of minimizing the weight of the wing while maximizing its stiffness and/or maximizing the selected natural frequency values. The weight of the folding wing has a significant impact on the performance of the opening mechanism and the overall dynamic behavior of the missile. The Bi-directional Evolutionary Structural Optimization (BESO) method, a widely-used topology optimization technique, is employed in conjunction with the MSC NASTRAN finite element solver and MATLAB to optimize the wing topology. The proposed algorithm is first validated on benchmark cases and then applied to the folding wing structure to obtain the optimized designs.

The wing structure studied in this work is composed of two parts and two design volumes. In order to minimize its weight, several optimization studies are performed with different objectives. The first objective is to maximize stiffness and the design space is optimized for this purpose under the aerodynamic load. The second

objective is to maximize the first natural frequency which may be necessary if there are excitation sources (such as the missile's engine or the aircraft that carries it) at that frequency. Shifting the natural frequency of the structure away from the frequency of the excitation can be useful for many aerospace-related problems. At the same time, increasing the natural frequencies results in modes of lower amplitudes and this precaution can prevent structural damage and decrease the flutter risk. Lastly, a multi-objective study on wing structure by considering its stiffness and natural frequencies is shown. By using topology optimization, it is possible to tailor the structure to shift the natural frequencies in the desired direction and reduce its weight simultaneously.

The algorithm used in this thesis obtains several novel wing structures which are suitable for manufacturing using conventional chip removal methods and have efficient material distribution around the design volume. These structures are compared with each other, and conclusions are drawn about their effectiveness. Results show that the topology optimization algorithm used in this thesis is able to generate highly efficient topologies with improved stiffness and natural frequency values. Furthermore, the impact of different parameters of the Bi-directional Evolutionary Structural Optimization (BESO) method on the resulting structures is demonstrated in this thesis. Overall, this thesis illustrates the capabilities of the used topology optimization method in aerospace engineering by providing examples of folding wing structures and contributes a novelty to the literature by operating in multi-design domains simultaneously due to multiple components of the folding wing, while most of the studies on topology optimization only focus on single design space.

Keywords: Finite Element Method, Structural Optimization, Topology Optimization, Frequency Optimization, Bi-directional Evolutionary Structural Optimization (BESO), Folding-Wing

ÖZ

KATLANIR BİR FÜZE KANADININ DİRENGENLİK VE FREKANS İÇİN EVRİMSEL TOPOLOJİ OPTİMİZASYONU

Ürün, Ata
Yüksek Lisans, Havacılık ve Uzay Mühendisliği
Tez Yöneticisi: Doçent. Dr. Melin Şahin
Ortak Tez Yöneticisi: Doçent. Dr. Ercan Gürses

Ocak 2023, 123 sayfa

Bu tez, bir seyir füzesinin katlanabilir kanat yapısının topoloji optimizasyonu üzerine bir çalışma sunmaktadır. Amaç, kanadın ağırlığını en aza indirirken, direngenliğini ya da seçilen doğal frekans değerini mümkün olan en yüksek seviyede tutmaktır. Katlanabilir kanadın ağırlığı, açılma mekanizmasının performansında ve füzenin genel dinamik davranışında önemli bir etkiye sahiptir. Yaygın olarak kullanılan bir topoloji optimizasyon tekniği olan Çift-yönlü Evrimsel Yapısal Optimizasyon (BESO) yöntemi, MSC NASTRAN sonlu eleman çözücüsü ve MATLAB ile oluşturulan ortamda kanat topolojisini optimize etmektedir. Önerilen algoritma önce referans çalışmalarla doğrulanmakta ve daha sonra katlanabilir kanat yapısını optimize etmek için uygulanmaktadır.

Bu çalışmada incelenen kanat yapısı, iki parçadan ve iki tasarım hacminden oluşmaktadır. Ağırlığını en aza indirmek için, farklı amaçlarla çeşitli optimizasyon çalışmaları yapılmıştır. İlk amaç, direngenliği maksimize etmektir ve tasarım alanı, aerodinamik yük altında bu amaçla optimize edilmektedir. İkinci hedef, ilk doğal frekansı maksimize etmektir ve bu durum, roket motoru veya taşıyan platform gibi titreşim kaynaklarının ilgili frekansa yakın yayın yapması halinde gerekli

olabilmektedir. Yapının doğal frekans değerlerinin, tahrik kaynağının frekansından uzağa kaydırılması birçok havacılık probleminde faydalı olabilmektedir. Aynı zamanda, doğal frekans değerlerinin artırılması, daha düşük deplasmanlara sahip modlara sahip olunması ile sonuçlanmaktadır ve bu önlem yapıyı hasardan korumakta ve çırpınma riskini de azaltmaktadır. Son olarak, bu tezde kanadın direngenliğinin ve doğal frekans değerlerinin gözetildiği çok amaçlı bir çalışma da paylaşılmıştır. Topoloji optimizasyonu kullanılarak, yapının doğal frekansının daha yüksek değerlere kaydırılarak aynı anda ağırlığının da azaltılması mümkün olmaktadır.

Oluşturulan algoritma, konvansiyonel talaşlı imalat yöntemleriyle üretilebilen ve verimli materyal dağılımına sahip olan çeşitli yeni kanat yapılarını ortaya koymuştur. Bu yapılar birbirleriyle karşılaştırılmakta ve etkinlikleri hakkında sonuçlar çıkarılmaktadır. Sonuçlar, kullanılan algoritmanın iyileştirilmiş direngenlik ve doğal frekans değerlerine sahip oldukça verimli topolojiler elde etme kapasitesine sahip olduğunu göstermiştir. Ayrıca, Çift-yönlü Evrimsel Yapısal Optimizasyon (BESO) metodunun farklı parametrelerinin sonuçlanan yapılara etkisi bu tezde gösterilmektedir. Bu tez, kullanılan optimizasyon metodunun havacılık mühendisliğindeki kabiliyetlerini katlanan kanat yapısından örnekler vererek sunmaktadır. Ayrıca, tek tasarım hacmine odaklanan diğer topoloji optimizasyon çalışmalarının çoğunun aksine çoklu tasarım hacminde çalışarak literatüre yenilikçi bir katkıda da bulunmaktadır.

Anahtar Kelimeler: Sonlu Elemanlar Methodu, Yapısal Optimizasyon, Topoloji Optimizasyonu, Frekans Optimizasyonu, Çift-Yönlü Evrimsel Yapısal Optimizasyon (BESO), Katlanabilir-Kanat



To my wife, Pınar

ACKNOWLEDGMENTS

I would like to express my deepest gratitude and special thanks to my supervisor Assoc. Prof. Dr. Melin Şahin and Co-Supervisor Assoc. Prof. Dr. Ercan Gürses for their valuable guidance, patience and criticism throughout this challenging study.

I would like to thank my former company, Roketsan, and my former senior colleagues of Dr. Burcu Dönmez, Cuma Polat, Zafer Külünk and Gökhan Tüşün for their support and contributions to my engineering perspective.

Also, I would like to express heartfelt thanks to my mom, Şirin Sever and my father, Yener Ürün for their blessings and endless support in my whole life.

Finally, I would like to present my greatest gratitude to my wife, Pınar Şenocak Ürün, for her precious care, patience and understanding which she has selflessly provided during the past years.

TABLE OF CONTENTS

ABSTRACT v

ÖZ vii

ACKNOWLEDGMENTS x

TABLE OF CONTENTS xi

LIST OF TABLES xiv

LIST OF FIGURES xv

LIST OF ABBREVIATIONS xx

LIST OF SYMBOLS xxi

1 INTRODUCTION 1

1.1 Background and Motivation of the Study 2

1.2 Objectives of the Study 4

1.3 Limitations of the Study 4

1.4 Outline of the Thesis 5

2 LITERATURE REVIEW 7

2.1 Introduction 7

2.2 Structural Optimization Methods 7

2.2.1 Solid Isotropic Material with Penalization (SIMP) 11

2.2.2 Evolutionary Structural Optimization (ESO) 15

2.2.3 Bi-directional Evolutionary Structural Optimization (BESO) 17

2.2.4 Level Set Topology Optimization 23
2.2.5 Metaheuristic Methods 23
2.3 Comparison of the Topology Optimization Methods 24
2.4 Conclusion 26
3 OPTIMIZATION METHODOLOGY 27
3.1 Introduction 27
3.2 Calculations of Evolutionary Structural Optimization (ESO) Method 28
3.3 Calculations of Bi-directional Evolutionary Structural Optimization (BESO) Method 30
3.4 Filter Scheme 35
3.5 Constructed Algorithm in MATLAB 41
3.6 Conclusion 44
4 STRUCTURAL FINITE ELEMENT MODELLING AND PRELIMINARY ANALYSES OF THE FOLDING WING 45
4.1 Introduction 45
4.2 Mechanical Specifications of the Folding Wing Structure 45
4.3 Boundary Conditions and Loads on the Folding Wing Structure 49
4.4 Preliminary Static Analysis of the Folding Wing Structure 51
4.5 Preliminary Modal Analysis of the Folding Wing Structure 53
4.6 Conclusion 56
5 TOPOLOGY OPTIMIZATION OF THE FOLDING WING STRUCTURE 57
5.1 Introduction 57
5.2 Design Variables 57
5.3 Optimization for Stiffness Criteria 59

5.4 Optimization for Natural Frequency Criteria 63
5.4.1 Maximizing The First Natural Frequency 64
5.4.2 Maximizing the Third Natural Frequency 68
5.4.3 Separation of the Second and the Third Natural Frequencies 72
5.5 Multi-objective Study with Stiffness and Separation of Natural Frequencies 79
5.6 Comparison of All Final Topologies 85
5.7 Conclusion 87
6 CONCLUSION 89
6.1 General Conclusions 89
6.2 Recommendations for Future Work 90
7 REFERENCES 93
8 APPENDICES 99
A. Reference Studies 99
A.1 Michell Type Structure 99
A.2 2D Cantilever Beam 101
A.3 3D Cantilever Beam 103
B. 3D Cantilever Beam Mesh-independency Study 105
C. Minimum Filter Radius Selection 107
D. Stiffness Optimization for Load 2 and Load 3 111
E. Effect of Initial Guess on Optimization of 2D Cantilever Beam 113
F. Initial Guess Design for the Folding Wing 120

LIST OF TABLES

TABLES

Table 2-1 Flight Conditions of the Wing-Box 18
Table 2-2 Weighted Coefficients and Objective Results [26] 21
Table 4-1 Mechanical Properties of AL 7075-T6 46
Table 4-2 Element Properties 49
Table 4-3 Loads on the Folding Wing 50
Table 4-4 Mean Compliance and Maximum y Displacement Values of Three Different Load Cases 52
Table 4-5 First Three Natural Frequency Values of the Folding Wing Structure 53
Table 5-1 Summary of All Final Results with Natural Frequency and Mean Compliance Values 86
Table 8-1 Comparison between reference study [15] and constructed algorithm for ESO 100
Table 8-2 Comparison between reference study [38] and constructed algorithm for BESO 102
Table 8-3 Comparison between reference study [38] and constructed algorithm for 3D BESO 104
Table 8-4 Mesh-independency Results 106

LIST OF FIGURES

FIGURES

Figure 1-1 Roketsan Atmaca Cruise Missile [1] 2
Figure 2-1 Famous Michell Type Structure [4] 8
Figure 2-2 Three-bar Truss [5] 8
Figure 2-3 Recap of Optimization Categories [7] 10
Figure 2-4 Finite Element Model of the Missile, (b) End Model of the Missile [11] 12
Figure 2-5 (a) UAV, (b) Two Different Final Topologies [12] 13
Figure 2-6 Final Topology of the Wing [13] 13
Figure 2-7 (a) Representative Wing, (b) Topology of the First Run, (c) Topology of the Second Run [15] 14
Figure 2-8 (a) A set of F/A-18 bulkheads (b) Initial Topology (c) Final Topology [19] 16
Figure 2-9 Converging Histories of (a) Max. Stress (b) Volume Fraction [19] 16
Figure 2-10 Finite Element Model of Wing Box [24] 18
Figure 2-11 Final Topology of the Wing Box [24] 19
Figure 2-12 Two Different Landing Gear Designs (a) Engineering Principles, (b) Topologically Optimized [25] 20
Figure 2-13 Final Topology of the Engine Mount [25] 20
Figure 2-14 Topologies of Different Cases (a) w$c = 0$, wω =1 (b) w$c = 0.1$, wω =0.9 (c) w$c = 0.3$, wω =0.7 (d) w$c = 0.5$, wω =0.5 (e) w$c = 0.7$, wω =0.3 (f) w$c = 0.9$, wω =0.1 (g) w$c = 1$, wω =0 [26] 22
Figure 3-1 Checkerboard Pattern in ESO [21] 36
Figure 3-2 Minimum Filter Radius and Sub-domain Ωi [21] 38
Figure 3-3 Flowchart of the Constructed Algorithm 43
Figure 4-1 The Folding Wing Structure 47
Figure 4-2 Simplified Wing and Skin Structures 48

Figure 4-3 Simplified Wing and Skin Structures 49
Figure 4-4 Boundary Conditions and Load on the Folding Wing Structure 51
Figure 4-5 Maximum y-Displacement of the Full Design Space Folding Wing by Load 1 53
Figure 4-6 The First Bending Mode for Full Design Space (w1=30.37 Hz) 54
Figure 4-7 The Second Bending Mode for Full Design Space (w2=138.33 Hz) 54
Figure 4-8 The First Torsional Mode for Full Design Space (w3=185.24 Hz) 55
Figure 5-1 Iteration Steps for Load 1 (a) Iter. 15 (b) Iter. 30 (c) Iter. 45 (d) Iter. 59 60
Figure 5-2 Details of the Final Topology at Iteration 59 61
Figure 5-3 Evolution Histories of Mean Compliance and Corresponding Volume Fraction 62
Figure 5-4 Evolution Histories of Maximum Tip Displacement and Corresponding Volume Fraction 62
Figure 5-5 Iteration Steps for $\omega 1$ (a) Iter. 15 (b) Iter. 30 (c) Iter. 45 (d) Iter. 59 64
Figure 5-6 Details of the Final Topology at Iteration 59 65
Figure 5-7 Evolution Histories of the First Natural Frequency and Corresponding Volume Fraction 66
Figure 5-8 Evolution Histories of the Second Natural Frequency and Corresponding Volume Fraction 66
Figure 5-9 Evolution Histories of the Third Natural Frequency and Corresponding Volume Fraction 67
Figure 5-10 Iteration Steps for $\omega 3$ (a) Iter. 15 (b) Iter. 30 (c) Iter. 45 (d) Iter. 59 68
Figure 5-11 Details of the Final Topology at Iteration 59 69
Figure 5-12 Evolution Histories of the Third Natural Frequency and Corresponding Volume Fraction 70
Figure 5-13 Evolution Histories of the First Natural Frequency and Corresponding Volume Fraction 70
Figure 5-14 Evolution Histories of the Second Natural Frequency and Corresponding Volume Fraction 71

Figure 5-15 Iteration Steps for $\omega 3 - \omega 2$ (a) Iter.15 (b) Iter.30 (c) Iter.45 (d) Iter. 62 72
Figure 5-16 Details of the Final Topology at Iteration 62 73
Figure 5-17 Evolution Histories of the First Natural Frequency and Corresponding Volume Fraction 74
Figure 5-18 Evolution Histories of the Second Natural Frequency and Corresponding Volume Fraction 74
Figure 5-19 Evolution Histories of the Third Natural Frequency and Corresponding Volume Fraction 75
Figure 5-20 Evolution Histories of Frequency Separation and Corresponding Volume Fraction 75
Figure 5-21 Evolution Histories of the First Natural Frequency and Corresponding Volume Fraction 76
Figure 5-22 Evolution Histories of the Second Frequency and Corresponding Volume Fraction 77
Figure 5-23 Evolution Histories of the Third Frequency and Corresponding Volume Fraction 77
Figure 5-24 Evolution Histories of Frequency Separation and Corresponding Volume Fraction 78
Figure 5-25 Five Different Multi-objective Topology Optimization Cases with Iterations of 15, 30, 45 and 65 81
Figure 5-26 Evolution Histories of Mean Compliances and Corresponding Volume Fraction 82
Figure 5-27 Evolution Histories of Maximum Tip Displacements and Corresponding Volume Fraction 82
Figure 5-28 Evolution Histories of Frequency Separation and Corresponding Volume Fraction 83
Figure 5-29 Four Different Final Topologies and Elements Near to Tip of the Wing for (a) Case A, (b) Case B, (c) Case C, (d) Case D 84
Figure 8-1 Simple Structure with Two Simple Supports [16] 99

Figure 8-2 Cantilever Beam [21] 101
Figure 8-3 3D Cantilever Beam [21] 103
Figure 8-4 Mesh-independent Solutions of (a) 32x20, (b) 80x50, (c) 160x100, (d) 240x150 [23] 105
Figure 8-5 Iteration Steps for $rmin = 8\ mm$ (a) Iter. 30 (b) Iter. 60 (c) Iter. 90 (d) Iter. 120 107
Figure 8-6 Iteration Steps for $rmin = 4\ mm$ (a) Iter. 30 (b) Iter. 60 (c) Iter. 90 (d) Iter. 120 108
Figure 8-7 Iteration Steps for $rmin = 6\ mm$ (a) Iter. 30 (b) Iter. 60 (c) Iter. 90 (d) Iter. 120 108
Figure 8-8 Evolution Histories of Mean Compliance and Corresponding Volume Fraction 109
Figure 8-9 Evolution Histories of Maximum Tip Displacement and Corresponding Volume Fraction 109
Figure 8-10 Complex Areas of $rmin = 4\ mm$ Case 110
Figure 8-11 Iteration Steps for Load 2 (a) Iter. 30 (b) Iter. 60 (c) Iter. 90 (d) Iter. 120 111
Figure 8-12 Iteration Steps for Load 3 a) Iter. 30 (b) Iter. 60 (c) Iter. 90 (d) Iter. 120 112
Figure 8-13 The First Initial Guess Design of 2D Cantilever Beam 113
Figure 8-14 Iteration Steps for the First Initial Guess Design (a) Iter. 5 (b) Iter. 10 (c) Iter. 15 (d) Iter. 20 114
Figure 8-15 Evolution Histories of Mean Compliance and Corresponding Volume Fraction 114
Figure 8-16 The Final Topology of 2D Cantilever Beam at Iteration 50 115
Figure 8-17 The Second Initial Guess Design of 2D Cantilever Beam 115
Figure 8-18 Iteration Steps for the Second Initial Guess Design (a) Iter. 5 (b) Iter. 10 (c) Iter. 15 (d) Iter. 20 (e) Iter. 25 (f) Iter. 80 116
Figure 8-19 Evolution Histories of Mean Compliance and Corresponding Volume Fraction 117

Figure 8-20 The Final Topology of 2D Cantilever Beam at Iteration 95 118
Figure 8-21 Final Topologies of 2D Cantilever Beam According to Initial Guesses 119
Figure 8-22 The Initial Guess Design of the Folding Wing with the Volume Fraction of 0.3 [38] 120
Figure 8-23 Iteration Steps for the Folding Wing Initial Guess Design (a) Iter. 1 (b) Iter. 15 (c) Iter. 30 (d) Iter. 45 (e) Iter. 60 (f) Iter. 75 (g) Iter. 90 (h) Iter. 105 121
Figure 8-24 Evolution Histories of Mean Compliance and Corresponding Volume Fraction 122
Figure 8-25 Final Topologies for (a) Initial Guess Design (b) Full Design 123

LIST OF ABBREVIATIONS

ABBREVIATIONS

2D	Two dimensional
3D	Three dimensional
BESO	Bi-directional Structural Optimization
ER	Evolutionary Volume Ratio
ESO	Evolutionary Structural Optimization
RR	Rejection Ratio
SIMP	Solid Isotropic Material with Interpolation

LIST OF SYMBOLS

SYMBOLS

AR_{max}	Maximum volume addition ratio
C	Compliance
E	Elastic Modulus
F	Force
K	Stiffness Matrix
M	Mass Matrix
N	Total number of elements
r_{mi}	Minimum filter radius
r_{ij}	Distance between jth node and center of ith element
U	Displacement
V	Volume
V^*	Prescribed total volume
V_i	Total volume of the ith element
x_{min}	Relative density of soft element
α_e	Sensitivity number of the element
ω_j	Natural frequency of the jth mode
$\omega(r_{ij})$	Linear weight factor
ρ	Density

CHAPTER 1

INTRODUCTION

Weight is the most critical parameter for most aerostructures. Aircraft should have lightweight structures like feathers and hollow bones of birds to increase the efficiency and duration of the flight. However, being lightweight is not enough for many times. The structure should be stiff enough to endure loads and be away from resonance and excessive deformation. To lighten aero structures, many methods have been proposed and applied throughout aviation history and among those, material selection is one of the most common methods. The Wright brothers used framed wing structures made of ash wood material for their first vehicle. Lately, the Airbus A380 has been made of mostly aluminum-based alloys due to its low density compared with steel. Composite materials are also quite popular in these times while building an aircraft and as an example, the composite material content of the Boeing 787 Dreamliner is nearly more than half of its weight where the fuselage structure is made of carbon-based composites while there is fiberglass material to support wing-fuselage connections.

Structural optimization is another way to reduce the weight of the system. There are several optimization methods naming as size, shape, and topology. Although topology optimization is the most challenging one among them due to its complexity, this method comes with many benefits. It ensures optimal material distribution over the design space while satisfying various objectives such as stiffness, stress, natural frequency, etc.

In this study, an aluminum missile folding wing of a cruise missile is optimized by using the Bi-directional Evolutionary Structural Optimization (BESO) method for

stiffness and natural frequency criteria. The aim is to reduce the weight of the wing while evolving the structure for improved stiffness and natural frequency values. Stiffness is critical for wing structures because it directly affects the displacement of the wing under the aerodynamic load. Improving the natural frequencies of the wing is also crucial to prevent dynamic instabilities and the phenomenon of flutter. Topology optimization is able to change the natural frequencies of the structure by changing its topology in the desired direction and reducing the weight of the wing simultaneously.

1.1 Background and Motivation of the Study

Missile systems could take different forms depending on their launching platforms. A missile system could be launched by a plane, an open-top launcher, or a sheltered canister platform. Missiles launched from canisters usually have folding wing structures to occupy less volume and get into the canister easily. Figure 1-1 shows the Roketsan Atmaca Cruise Missile whose launching platform is a canister and it has eight folding wings [1].



Figure 1-1 Roketsan Atmaca Cruise Missile [1]

Folding wing structures are activated by torsional springs after launching. These torsional springs could be loaded and ready to launch for up to fifteen years in the canister. At the end of this period, relaxation of the torsional spring occurs and the torque value decreases [2]. Folding wing structures should be as light as possible to be opened up robustly and fast after fifteen years, even with this decreased torque value. In addition to this, aiming for a lightweight design is quite essential for every aerospace structure. Because of these reasons, the folding wing should be optimized to have a lighter design while satisfying necessary structural properties such as stiffness and natural frequency. The outer dimensions of the wing are constant due to aerodynamic performance requirements, and this situation leads to topology optimization on the inner volume of the wing without changing any exterior dimension. Besides this obligation, topology optimization is favorable because it promises better performance in comparison with other optimization types. There are several topology optimization methods, and they are mainly divided into gradient-based and gradient-free methods. While gradient-based methods use gradient information to determine the direction of the optimization, gradient-free methods do not need any gradient information. In this study, the weight of the folding wing and the weight of the entire missile system are reduced by optimizing the folding wing with one of the most known gradient-based methods, "Bi-directional Evolutionary Structural Optimization (BESO)". This iterative method leads the topology of the structure to evolve until the given constraint is satisfied, and the resulting structures in this thesis show that this method provides well-optimized structures with improved mechanical performance.

To implement BESO on the wing structure, an algorithm is constructed in the MATLAB environment that uses MSC NASTRAN as a finite element solver. This algorithm works autonomously after the initial inputs are given, and it is terminated when the given constraint is satisfied. A new contribution to the literature is made by working in the field of multi-component optimization with this algorithm. This algorithm optimizes two different parts of the folding wing at the same time, while most studies in this area focus on single-component optimization. The wing design

obtained at the end of the optimization process would be novel and must be manufacturable by conventional chip removal methods to have a convenient production cycle. Final structures should have uncomplicated topologies without any inner cavities and be suitable for machining with widespread chip removal tools.

1.2 Objectives of the Study

The main objective of this thesis is to design a folding wing with decreased weight and superior structural properties by using BESO.

The followings are the objectives of this thesis:

- Creating a successful algorithm in MATLAB using MSC NASTRAN finite element solver to perform a topology optimization.
- Verifying developed algorithm through case studies from the literature.
- Optimizing baseline wing structure using the created algorithm in MATLAB to have a lighter structure with objectives of stiffness and natural frequency.
- Investigating the contribution of BESO parameters by comparing different topologies.
- Evaluating all possible designs according to mechanical properties of stiffness and natural frequencies.
- Comparing the manufacturability of the final structures by checking the complexity of their topologies

1.3 Limitations of the Study

The folding wing mechanism has inner and outer parts connected with a torsional spring. Following its launch, torsional springs are then activated and they rotate the inner and outer wing parts. Finally, spring-loaded pins lock the system and the wing

gets its final stable shape. Due to its complexity, some assumptions are bringing the following limitations into this thesis study:

- This thesis focuses on the shape of the wing after launching, and therefore, torsional springs are not modeled.
- Spring-loaded pins lock wing parts together after the launching. These elements are neglected and wing parts are assumed as one to make a simpler finite element model.
- Outer skin structures are connected to the wing body by rivets. These rivets are neglected and connections between parts are assumed as a whole.
- Only the first three modes of the folding wing are considered and any mode switching is not taken into account.
- Maneuver loads are out of the scope of this thesis.
- Buckling failure and maximum von Mises stress values are not checked in this thesis.
- Flutter analysis is beyond the scope of this thesis.

1.4 Outline of the Thesis

This thesis primarily consists of six chapters and the organization is as follows.

In Chapter 2, types of structural optimization methods are explained. Topology optimization is selected for this study; thus, the most known topology optimization methods are explained considering their differences, advantages, and disadvantages. The implications of these optimization methods on several aerospace cases are shown to provide insight. The selection of BESO as the main optimizer method is detailed with reasons.

Chapter 3 focuses on BESO by providing the main idea behind it and the formulation of the method. An advanced filter system to avoid the checkerboard pattern problem, which is a well-known problem to indicate the shape of the elements' formation, is examined. The working principles of the created algorithm in the MATLAB

environment are introduced in this chapter. This algorithm uses MSC NASTRAN as a finite element solver and MATLAB as an environment to create a cycle to iterate every topology. Several reference studies are tested to investigate the efficiency of this created algorithm and they are all presented in the related appendices.

In Chapter 4, the folding wing structure is introduced with its specifications, dimensions and properties. Finite element modeling of the baseline structure is demonstrated with its element types and numbers. Besides the model, boundary conditions and loads are also assigned prior to the analyses. After constructing the model, static and modal analyses are performed to obtain the stiffness and the natural frequencies of the baseline wing structure.

Chapter 5 is all about optimizing the folding wing structure. The created and tested MATLAB algorithm works on the main structure, which is modeled and ready for optimization. Different optimization studies on this wing structure are done and explained. The first objective is to obtain the maximum stiffness under the aerodynamic loads, and the second is to obtain the maximum selected natural frequency. Both objectives have a volume constraint, and the optimization goes until this constraint is satisfied. Additionally, a multi-objective study on stiffness and separation of natural frequencies is shared. Several topologies are obtained here due to different objectives and varying parameters of BESO.

In Chapter 6, final conclusions are presented and recommendations for future studies are given.

CHAPTER 2

LITERATURE REVIEW

2.1 Introduction

Dictionary meaning of "optimization" is the act of making something as "good" as possible. This "good" can be several things if the topic is structural optimization. Therefore, structural optimization is the term to describe all efforts throughout finding an optimum structure in terms of stiffness, weight, natural frequency, and so on. There are various methods to optimize structures with different variables and goals in several different areas. One of the main application areas is aerospace, where there is a strong need for optimum structures having lightweight but sufficient designs. After computational developments and improvements in performance of algorithms with time, these optimization methods become more essential in the aerospace industry. There are countless examples of optimizations on aerospace structures in the literature and some of them related to this particular research area are also presented in this chapter.

2.2 Structural Optimization Methods

The origins of mathematical optimization can be traced back to the 17^{th} century, to the days of Pierre de Fermat. In the same century, Newton proposed an iterative method to find the optimum, which laid the foundation for today's optimization methods. The first traceable study on structural optimization is assumed to be from Maxwell in 1869 [3]. However, the most known primitive example of structure optimization was given by Michell in 1904 on the economy of material in truss structures [4]. This work is a significant initial step to structural optimization with an objective of weight, and the frame structure studied (Figure 2-1) is used in many

subsequent studies as a reference structure. This type of structure is also investigated as a case study in this thesis, and the results are shown in Appendix A.

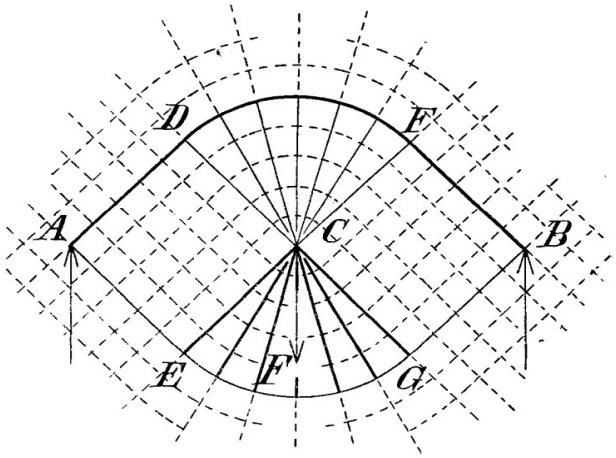


Figure 2-1 Famous Michell Type Structure [4]

The era of modern structural optimization started when Schmit first integrated finite element analysis into structural optimization by using an IBM 653 computer in 1960 [5]. Schmit showed that the lightest design does not always mean that it is fully stressed using a simple three-bar truss (Figure 2-2), two load cases, and a computer program. It comes as no surprise that structural optimization and mathematical programming were merged at that time because of the strong competition for space

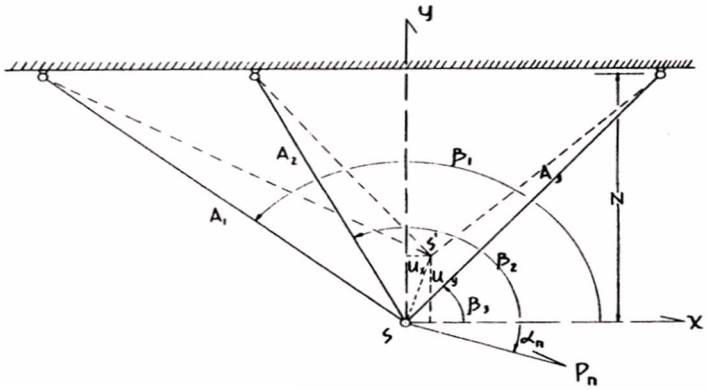


Figure 2-2 Three-bar Truss [5]

and the need for lightweight structures. Research funds were substantial to develop new methods, and digital computers started to be common. Vanderplaats defines that time as “The Magnificent ’60s” due to numerous discussions and progresses on structural optimization [6].

After the “Magnificent ’60s”, developed methods have become diversified due to different needs and different approaches. These methods can be categorized in several ways, and the most accepted categorization is *sizing, shape,* and *topology optimization*. All of these optimization methods iteratively adjust the size, shape, or topology of a design until the structure demonstrates maximum utility, subject to performance restrictions. Figure 2-3 demonstrates the general aspects of these categories [7].

Being the simplest of these three optimization categories, *sizing optimization* works by changing the dimensions of the design while keeping shape and topology constant. Therefore, the optimum is sought by varying dimensions of the design. As an example, these dimensions can be the span, chord, or thickness of the aircraft wing. In the literature, this method is generally used to determine the dimensions of truss structures.

Shape Optimization changes the locations of the nodes through the cross-section shape of the design to find an optimum shape. This optimization generally involves sizing optimization, which means a higher computational cost. This method is commonly used to design the cross-sectional shapes of structural elements, such as beams and columns, to be as lightweight as possible while meeting requirements.

Topology Optimization is the most complex one of these three categories. The complexity of this process is due to the large number of design variables, which refer to the various characteristics of the elements in the design space; and density is the most commonly used one. If the density of the element is 0, this means that the element does not exist anymore. In this way, holes are obtained in the structure, the topology differs, and material distribution over the design is arranged as efficiently as possible. A higher number of elements means a higher number of combinations

while processing for the optimum topology. This search takes considerable computational time but results in structures close to the global optimum and hence, better results for the objective under the constraints. This makes topology optimization the most popular structural optimization category in seeking the best.

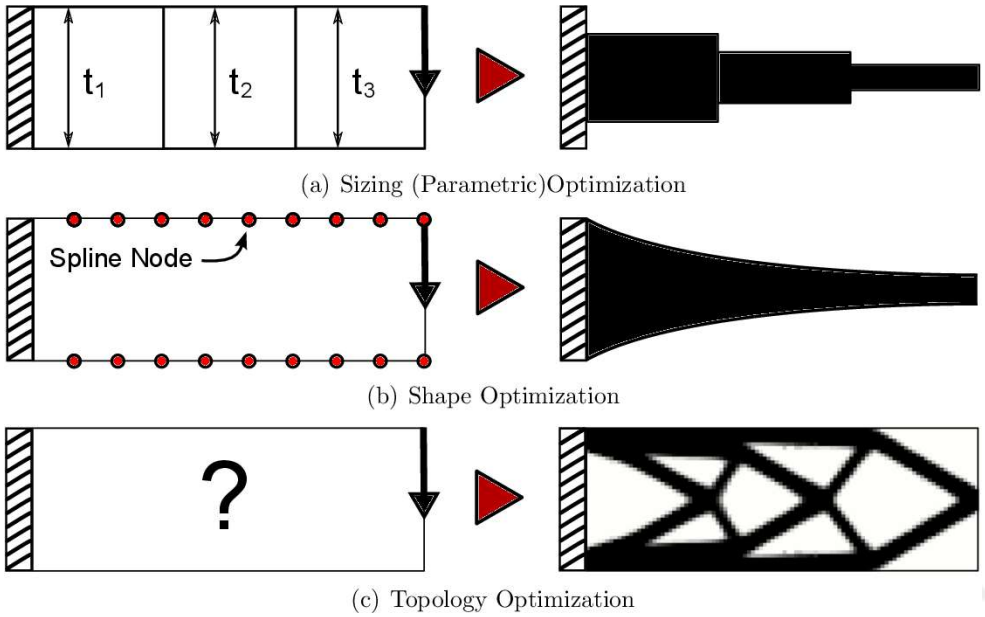


Figure 2-3 Recap of Optimization Categories [7]

Because of the computational complexity and the high computational time of topology optimization, researchers strived to find the most efficient way to apply topology optimization to structures, and thus new mechanisms sprouted. These mechanisms are explained briefly in this chapter with examples.

2.2.1 Solid Isotropic Material with Penalization (SIMP)

The best-known topology optimization method is Solid Isotropic Material with Penalization (SIMP), developed simultaneously by Bendsøe in 1989 [8] and Zhou and Rozvany in 1991 [9]. The term SIMP was first introduced by Rozvany in 1992 [10]. This revolutionary method extended the field of topology optimization and made topology optimization applicable to different engineering topics with diverse objectives. Even though it was one of the early methods, nowadays many commercial optimization software still uses this method for calculations.

Finite elements in the design space initially have discrete densities of 0 or 1. Direct search methods could be computationally expensive because of the discrete black/ white or solid/void topologies. To use continuous variable formulation, there should be some elements with intermediate densities. During the optimization of SIMP, some elements gained densities between 0 and 1. These virtual densities affect the elastic modulus of the elements. The relationship between density and elastic modulus is related to the penalty factor (p), which is exponential and generally selected as 3. The elements with intermediate densities form “grey areas” in the design space, and hence, efficient continuous function between elements is provided. Difficulties of discrete design space with discontinuous objective function are eliminated in this way because the objective function is now continuous and its sensitivity is differentiable.

There are several examples of using SIMP to optimize structures in aerospace. One of them was conducted by Luo et al. in 2006 to optimize the topology of the full missile body with compliance and eigenfrequency-related objectives [11]. This multi-objective study aims to find the optimum topology for minimum compliance and maximum fundamental frequency while performing static and dynamic analyses in a sequence. A multilevel sequence algorithm is employed to do multi-objective optimization with different levels of importance. Level 1 is selected as the maximum fundamental frequency problem, and Level 2 is selected as the compliance problem. First, single objective optimization for frequency is conducted. After receiving the

optimum frequency result from this run, Level 2 is started with the constraint of the optimum frequency value from Level 1. Figure 2-4 shows the resulting topology of this study.

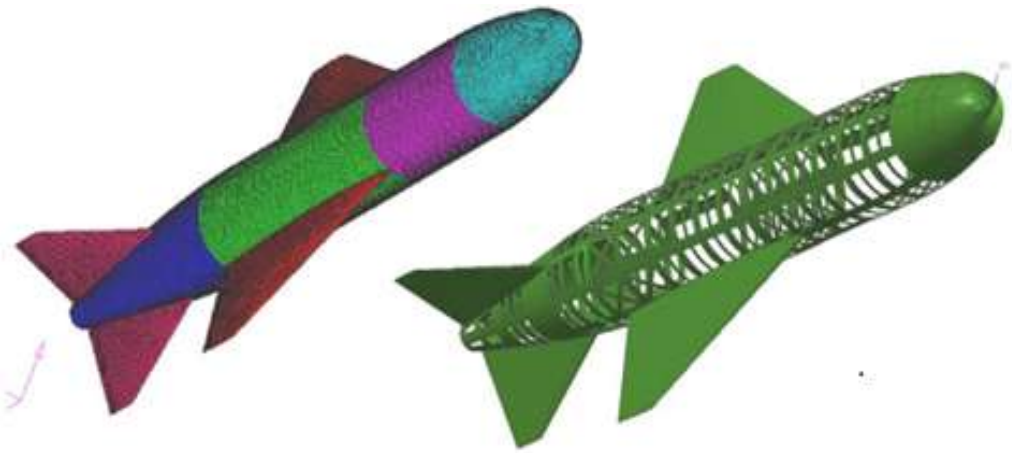


Figure 2-4 Finite Element Model of the Missile, (b) End Model of the Missile [11]

At the end of this successful study, 1107 kg of mass is removed from the structure while the fundamental eigenfrequency is increased to 176% of its initial value. These results show that topology optimization contributes to the design in a drastic way and guides the mechanical designer of the structure to the optimum. Additionally, the authors indicate that the manufacturability of this topology is out of scope and there would be some design changes if prototyping is the case.

In 2009, Eves et al. published a paper on the topology optimization of a UAV Wing [12]. The main aim is to determine the optimum structural layout of the wing with optimum locations of ribs and spars. Minimum compliance is the objective, and there are constraints on local buckling and deflection. Two different topologies are obtained due to different approaches and are shown in Figure 2-5.

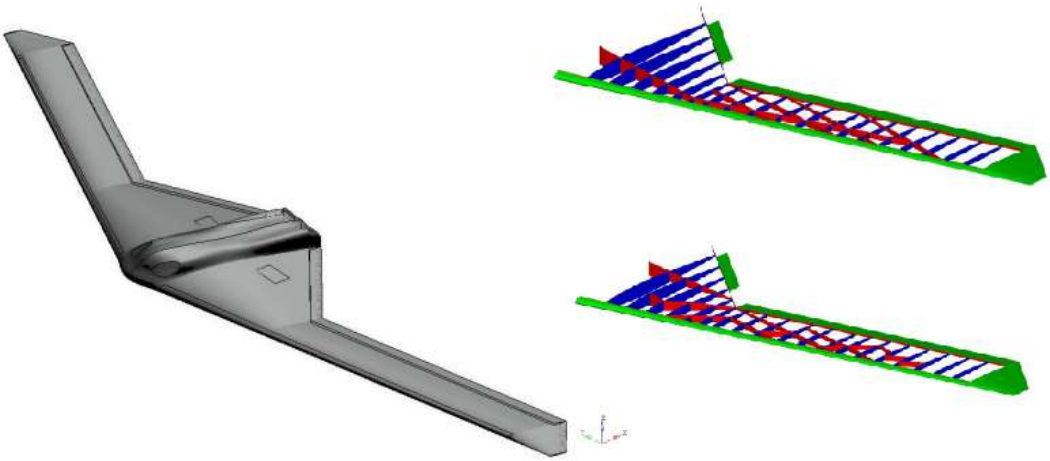


Figure 2-5 (a) UAV, (b) Two Different Final Topologies [12]

Oktay et al. conducted research on 3-D structural topology optimization of an aerial vehicle in 2014 [13]. They used the homogenization method, which is the predecessor of SIMP and was suggested by Bendsøe and Kikuchi in 1988 [14]. Topology optimization is completed with CFD analysis and minimum compliance is aimed. In the end, the structure in Figure 2-6 is obtained and it is 2.19 times stiffer than the conventional design with the same volume.

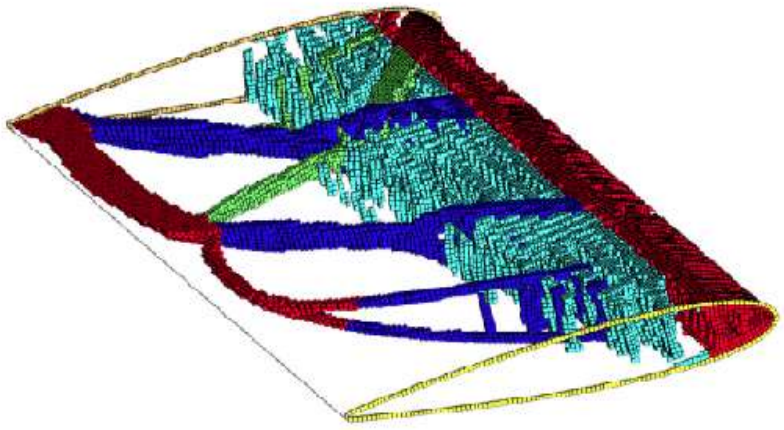


Figure 2-6 Final Topology of the Wing [13]

One of the most important aerospace related problems is flutter, the unwanted phenomenon that occurs when there is a coupling of modes during the flight. This coupling causes self-excited oscillation on the wing where energy is extracted from the flow. Munk and his colleagues worked on a representative aircraft wing to avoid from flutter by changing the topology of the wing in 2017 [15]. The most common dynamic optimization objectives on wing structures are maximizing the fundamental frequency and separating it from the neighboring frequencies. Munk et al. aimed to maximize the difference between the second and the third modes of the wing by decreasing the second mode and holding the third mode the same. The first try ended up with a 42% reduced fundamental frequency, which is undesired due to the tendency of divergence. Therefore, frequency constraint was implemented for the first mode and the analysis was rerun again. Even though frequency separation is less for the last result, it is more convenient because of the higher fundamental natural frequency. Despite the weight is dropped by 15%, the flutter speed is increased with the topology of Figure 2-7 (c). This work shows how capable of topology optimization is for dynamic objectives.

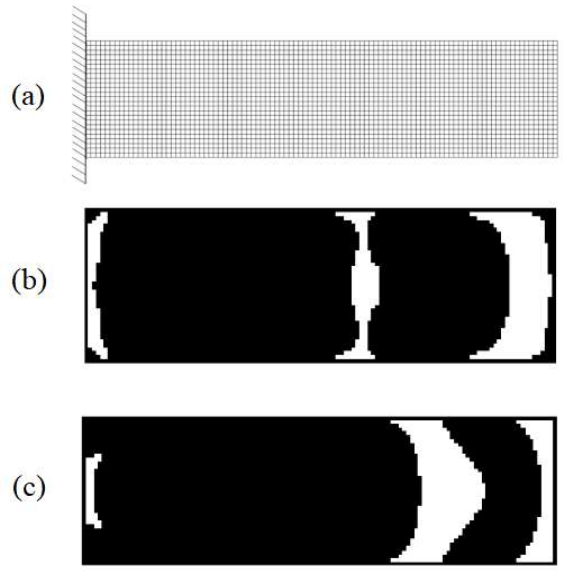


Figure 2-7 (a) Representative Wing, (b) Topology of the First Run, (c) Topology of the Second Run [15]

2.2.2 Evolutionary Structural Optimization (ESO)

Evolutionary Structural Optimization (ESO) was first introduced by Xie and Steven in 1993 [16]. This method promises continuously evolving designs by every iteration as its name suggests. The topology of the design part is slowly improved during the optimization until it reaches the optimum. This method became popular because it is easy to implement and use with any finite element solver. The main idea is quite simple as; noncontributing and inefficient elements are removed from the structure step by step. To determine which element is contributing, the sensitivity number of every element should be calculated. According to objectives, the sensitivity number could be selected as von Mises stress value, strain energy value, or such. During calculating the sensitivity numbers, finite element solvers have an essential role. After removing noncontributing elements from the structure, the next iteration is started with the new topology and this cycle goes on until the objective volume is reached. Even though this method is simple and useful, it does not guarantee that optimum topology is obtained every time. The main reason is that the mechanical links could be broken by removing elements and this situation introduces mechanical instability to the system, where there is no comeback because elements are removed and can not be recovered back.

ESO method was first used for dynamic problems in 1994 by Xie and Steven [17]. This study suggests new sensitivity number calculations to maximize or minimize the natural frequencies of the structure. The authors demonstrated more dynamic problems in 1996 [18] by maximizing selected frequencies, maximizing the gap between two frequencies and optimizing multiple frequencies at the same time. This study showed the capabilities of evolutionary methods on dynamic problems.

In 2011, Das and Jones presented a study on topology optimization of a bulkhead component of a F/A-18 aircraft by ESO [19]. This aircraft is prominent by its maneuverability capability and speed; hence the weight of the aircraft has an important role on the performance of the aircraft and this is the main aim of this

study. The criterion for sensitivity number is selected as von Mises stress and Figure 2-8 shows the initial and final topology of the bulkhead.

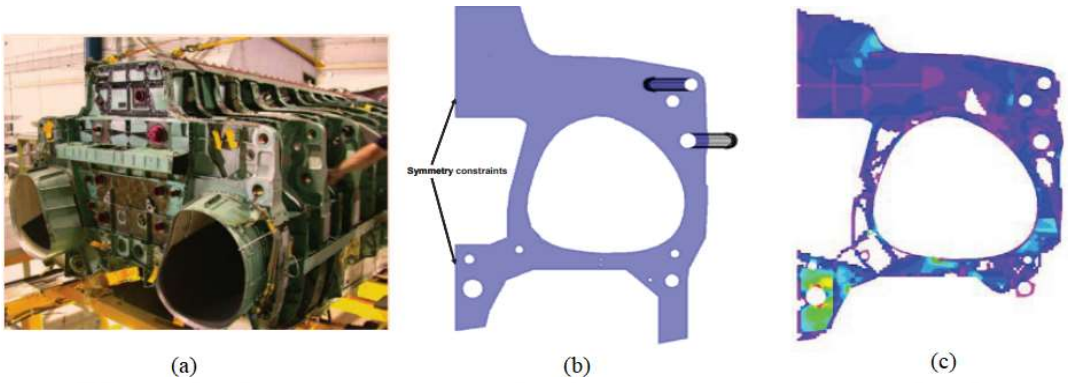


Figure 2-8 (a) A set of F/A-18 bulkheads (b) Initial Topology (c) Final Topology [19]

The algorithm converged after 86 iterations and the volume decreased to 75% of the initial volume. Converging histories of the analysis are demonstrated in Figure 2-9. Since there are several bulkheads in the aircraft, this weight reduction may affect the dynamics of the aircraft drastically.

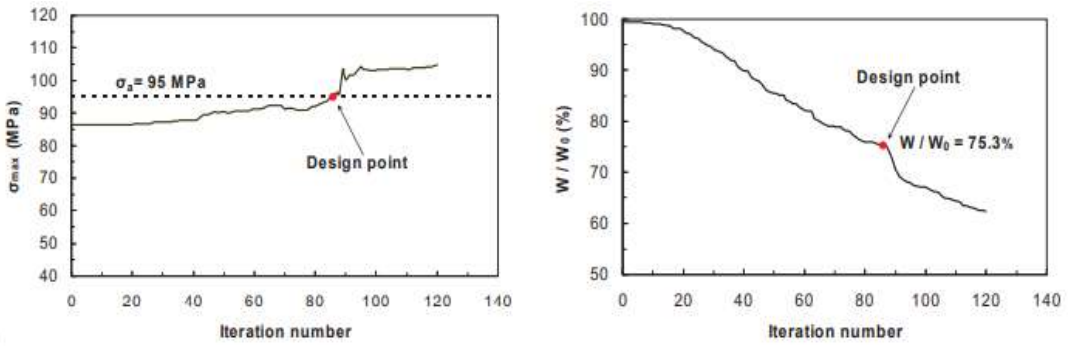


Figure 2-9 Converging Histories of (a) Max. Stress (b) Volume Fraction [19]

Unrecoverable elements limit the scope of the application of ESO and it creates a need for a superior methodology. Querin came up with an improved ESO method which allows recovering removed elements from previous iterations and named this method as Bi-Directional Evolutionary Structural Optimization (BESO) in 1998 [20].

2.2.3 Bi-directional Evolutionary Structural Optimization (BESO)

BESO is the methodology that works in both ways, removing and adding elements. Removed elements are excluded from the topology but they are not totally removed from the calculations. The sensitivity numbers of void elements are still calculated by using an advanced filter scheme that utilizes the sensitivity numbers of adjacent elements. After all sensitivity numbers are calculated, solid elements with lower sensitivity numbers are removed from the topology and void elements with higher sensitivity numbers are recovered back to solid again. Although this filter adds complexity to the calculations, it comes with the benefit of results much closer to the optimum one.

BESO has two main versions, namely; hard-kill BESO and soft-kill BESO. The mechanical properties of void elements in hard-kill BESO are stated as zero. So, they do not contribute to the static or dynamic analysis by any chance but they have again sensitivity numbers by the filter scheme. In every iteration, some elements are removed from the topology and computation time for every step gets lower due to fewer elements involved in the analysis. This is one of the biggest advantages of the hard-kill BESO. On the other hand, the mechanical properties of void elements are not zero but weakened in soft-kill BESO. This means that the mechanical properties of void elements are specified as quite small numbers but they are not completely removed from the topology and still occupy a place in the finite element analysis at every step. Therefore, the computation time of iterations does not decrease with each step, and this creates a major disadvantage for soft-kill BESO. However, this method offers better performance for natural frequency-based optimization than hard-kill BESO could [21].

The initial research for stiffness optimization by BESO was conducted by Yang in 1999 [22]. The improvements were made on this method by Huang and Xie in 2007 by involving historical sensitivity numbers of the elements in the calculations [23]. This upgrade increased the accuracy and reliability of the method in a significant

way. Soft-kill BESO method was detailed in 2010 by Huang and Xie with a comprehensive study [21].

One of the greatest examples of using BESO for an aircraft structure was presented by Munk in 2018 [24]. In this study, Munk showed many topology optimization related problems with different constraints such as buckling, stress and frequency. In the end, the author shared the final study about topology optimization of a wing-box of large transport aircraft under stress and buckling constraints. The aluminum outer skin structure, which is excluded from the optimization to preserve the continuity of the aerodynamic surface, is subjected to the flight conditions listed in Table 2-1. For simplicity, the aerodynamic load is not changed during the optimization with evolving topologies.

Table 2-1 Flight Conditions of the Wing-Box [24]

Altitude (m)	Mach Number	The angle of Attack (°)
10000	0.85	2

The finite element model of the wing box with eight-node polyhedron solid elements is shown in Figure 2-10.



Figure 2-10 Finite Element Model of Wing Box [24]

The analysis is done according to the buckling and stress constraints to minimize the weight. The final topology without outer skins is shown in Figure 2-11. This

topology has a volume that is 35% of the initial design, which means that a 65% reduction in mass is present.



Figure 2-11 Final Topology of the Wing Box [24]

This example demonstrates the strong capabilities of BESO in handling multiple constraints and its usefulness in the aerospace industry, where weight minimization is often a key objective while facing numerous constraints.

Munk and his colleagues again published a study about BESO on aircraft components in 2019 [25]. This study presents two different design problems to illustrate the effectiveness and benefits of topology optimization compared to traditional engineering design approaches. The first case is the aircraft landing gear of a Jabiru J160 and the second case is the engine mount design of a Jabiru 2200cc. For both cases, successful topologies are developed by BESO, and results are discussed. There are two constraints for the landing gear design. The first constraint is the stress because this landing gear should resist load cases of level landing and one-wheel landing. The second constraint is displacement because the landing gear should not exceed 1-inch displacement vertical to guarantee that there is no contact between the landing gear and wing strut. With these two constraints, analysis was conducted to minimize mass, and a successful topology was obtained after 97 iterations. At the same time, different part is designed for the landing gear by using engineering design principles, hand calculations, and CAD tools. Both designs are shown in Figure 2-12 after rendering. For three of four load cases, the stress level is

closer to the maximum limit for the topologically optimized structure, and this shows that material distribution is extremely efficient. Additionally, it is 3.5 kg lighter than the one obtained through engineering principles design. This study is a good example of the benefits of topology optimization over traditionally engineering-based designs.

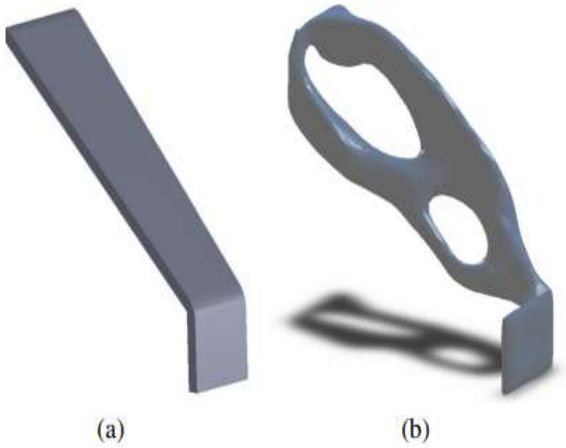


Figure 2-12 Two Different Landing Gear Designs (a) Engineering Principles, (b) Topologically Optimized [25]

For the second case, an engine mount design of a Jabiru 2200cc engine is investigated. This engine mount should resist all loads and buckling of thin members should be avoided during minimum mass optimization. After 98 iterations, topology in Figure 2-13 is obtained, and volume is decreased to 4.35% of the initial volume.

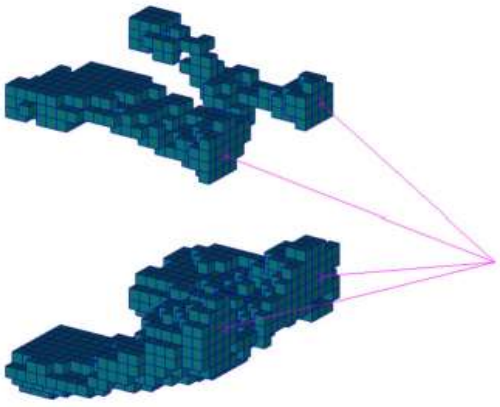


Figure 2-13 Final Topology of the Engine Mount [25]

In 2019, Teimouri and Asgari conducted research on multi-objective BESO topology optimization [26]. They aimed to find different 2-D structures which are obtained by varying weighted coefficients of the objectives, namely; stiffness and natural frequency for this study. These objectives are also used in this thesis, and therefore the findings of this study have great importance.

The objectives are minimizing the compliance and maximizing the fundamental frequency while decreasing the volume to half of the initial volume. There are different cases with different weighted coefficients and they are indicated in Table 2-2. Weighted coefficients are multiplied by the sensitivity numbers of each objective, then they are added together and combined sensitivity numbers are obtained. These new sensitivity numbers are used to determine added or removed elements. When coefficients are 1 and 0, the case is a single-objective case. Table 2-2 also shows the final objective values of compliance and fundamental frequencies of each case. It is clear that the weighted coefficients have a great impact on the objective values. Topologies of each case can also be seen in Figure 2-14.

Table 2-2 Weighted Coefficients and Objective Results [26]

Case	w_c (Weighted Coefficient of Compliance)	w_ω (Weighted Coefficient of Natural Frequency)	C [Nmm] (Mean Compliance)	ω_1 [rad/sec] (Fundamental Frequency)
a	0	1	35	170
b	0.1	0.9	29	167
c	0.3	0.7	22.8	165
d	0.5	0.5	12.4	158
e	0.7	0.3	11	152
f	0.9	0.1	9.8	150
g	1	0	9.8	147

As it can be seen from Figure 2-14, topologies differ with weighted coefficients. When the weighted coefficient of compliance is higher, the mechanical links in the middle take a specific shape that effectively minimizes compliance in the system.

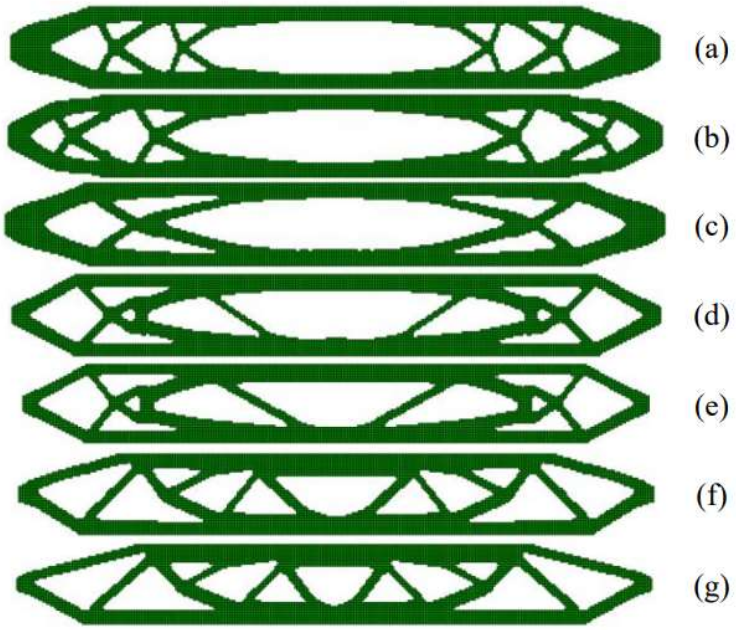


Figure 2-14 Topologies of Different Cases (a) $w_c = 0$, w_ω =1 (b) $w_c = 0.1$, w_ω =0.9 (c) $w_c = 0.3$, w_ω =0.7 (d) $w_c = 0.5$, w_ω =0.5 (e) $w_c = 0.7$, w_ω =0.3 (f) $w_c = 0.9$, w_ω =0.1 (g) $w_c = 1$, w_ω =0 [26]

Optimization of minimum weight for an aero structure usually requires consideration of both compliance and natural frequency, as structures may be vulnerable to resonance or excessive displacement without proper attention to these factors. Thus, topology optimization methods which work simultaneously for multi-objectives are quite beneficial in the aerospace industry. Results obtained by this study using BESO for multi-objective topology optimization are reasonably successful and promise confidence for future works.

2.2.4 Level Set Topology Optimization

Sethian et al. implemented the level set approach for the first time to topology optimization in 2000, capturing the free border of a structure in linear elasticity [27]. Boundaries in the level set method are represented as the zero-level curve of a scalar function which is the level set function. Optimization conditions and controlling the dynamics of the level set function according to the physical problem change the contour of the geometric boundary. The majority of the level-set formulations are dependent on finite elements, hence boundaries are determined by the discrete mesh elements.

2.2.5 Metaheuristic Methods

Metaheuristic methods are stochastic and do not need any gradient information, which makes them unique. There are numerous metaheuristic methods because each of them mimics different features of nature. While Grey Wolf Optimizer tries to assimilate and apply the behavior of a wolf pack [28], Crow Search Algorithm investigates the intelligent behavior of sneaky crows, which search for excess food hiding places of other crows [29]. The best-known meta-heuristic optimization methods are Particle Swarm Optimization (PSO) [30], Genetic Algorithm (GA) [31] and Ant Colony Optimization (ACO) [32]. All these nature-based methods have similar searching techniques: exploration and exploitation. Randomly new designs are generated to find the optimum in a huge design space with the guidance of these methods. These methods are straightforward, highly adaptable, and do not rely on derivative information, making them applicable to a wide range of engineering problems and valuable in situations where derivative information is costly to obtain. Most importantly, the ability of these methods to avoid local optimum is better than the gradient-based methods.

In 2010, Luh investigated a metaheuristic method of binary particle swarm optimization on topologies [33]. Several cases of minimum compliance and

minimum weight are shown in this study. Jaafer et al. showed the capabilities of the Binary Bat Algorithm on topology optimization in 2020 [34]. They investigated new filtering and penalty algorithm on well-known topology problems and discussed the results. These two studies show that metaheuristics methods can work well with topology optimization as well as they work with shape and size optimization.

2.3 Comparison of the Topology Optimization Methods

SIMP method is one of the prior and most-known topology optimization methods. It is a comparatively simple method and can be applied to many different engineering topics with variable loads and boundary conditions. This is the main reason why most topology optimization software uses this method for calculations. In the literature, there are numerous studies about this method, and one of them is from Rozvany in 2009 [35]. He investigated the SIMP method in a detailed way and compared it with ESO. Even though he generally mentioned about advantages of SIMP, he also stated several defects of SIMP. The most important defect of SIMP is having difficulties with complex non-convex problems. As the other gradient-based methods do, SIMP does not guarantee global optimum when the structure is highly non-convex, and there are many local optimums. This methodology tends to stick with one of the local minimums because of its gradient background, and this sometimes leads to the wrong solution. One other disadvantage of SIMP is having grey areas, where densities of elements are between 0 and 1. These areas are essential for SIMP mechanism, but they lead to the manufacturability problem of the final topology. Rozvany states that these areas can be removed by some new studies on SIMP, but even these studies do not promise to remove all of these grey areas. This is an important problem if the final topology should be manufactured.

Contrary to SIMP, the geometry of the structure is defined by discrete elements in the level set topology methods. These methods are promising for the future developments of topology optimization with a strong mathematical background and the ability to handle highly complicated shapes and topologies. In 2013, Sigmund

and Maute conducted deep research on nearly all topology optimization methods by comparing them with advantages and disadvantages [36]. One of the biggest drawbacks of level-set methods is the dependency on the initial guess of the topology. This stems from the Hamilton-Jacobi equation, which updates level set functions. This equation does not allow forming of new holes in the topology. To integrate new holes, there should be an additional step that can be costly and effects the convergence of this method.

Metaheuristics methods are fascinating algorithms that show how nature and engineering can be similar and work together. Besides their attractive backgrounds, they can present nice solutions to structural optimization problems. These methods are not just common for structural optimization; they are also used for computational software-based problems. In 2011, Sigmund criticized metaheuristic methods heavily and stated that these methods are useless if the subject is topology optimization [37]. The main idea of this criticism stems from the possible number of combinations. Elements in the design can be solid or void and there can be more than 100,000 elements in the topology optimization problem easily. This creates 10 to the power of 30100 different combinations. Certainly, metaheuristics methodologies decrease the number of combinations with search algorithms, but again the size of the design space is intimidating. This makes these methods incredibly expensive for the sense of computation if the problem is to design the topology of any structure. Sigmund commented in the same study as graduate students should not spend any year researching these methods, which are definitely inferior to existing topology optimization methods. However, it should not be forgotten that metaheuristic methods are the best match for parallel computing with supercomputers by their nature. There is a still chance for these methods to be popular and efficient with the developed, cheaper, and more common supercomputers in the future on topology optimization.

BESO is one of the most advanced heuristic methods and it is investigated by many authors in different studies. All these studies show that implementing BESO to any topology related engineering problem is quite simple and not cumbersome. This

method ranks the sensitivity numbers of the elements and determines added or removed elements. This feature provides flexibility to use this method with any commercial finite element solvers. Sensitivity numbers of all elements can be calculated by finite element solvers and values can be implemented into BESO calculations. In addition, it can work with different objectives and constraints while eliminating the mesh dependency by the filter scheme. Rozvany criticizes this method in 2009 as being computationally ineffective due to its fully heuristic structure [35]. Even though it is correct, this method is more prone to avoid local optimums than other gradient-based methods because of its heuristic structure. This makes this method more applicable for highly complex non-convex structures, such as the main topic of this thesis. Huang and Xie discussed Rozvany's criticism in 2010, and they emphasized the advantages of BESO with its application areas [21]. Soft-kill BESO is highly recommended for natural frequency-orientated topology optimization in this study because local artificial modes can be avoided, and effective results are found by this method.

2.4 Conclusion

This chapter focuses on structural optimization methods, with a particular emphasis on topology optimization techniques and their applications in the aerospace industry. It is demonstrated that topology optimization is a game changer approach to achieve highly effective structures with minimal weight. In addition to weight, there may be other constraints of stress, stiffness and natural frequency. After comparing different topology optimization methodologies, soft-kill BESO is selected for this thesis study due to its compatibility with finite element solvers and its ability to generate satisfactory results for non-convex geometries.

CHAPTER 3

OPTIMIZATION METHODOLOGY

3.1 Introduction

To optimize structures, there should be a tool to implement a rigid strategy according to objectives and constraints. This strategy is about selecting legitimate constraints and objectives which are beneficial in the related engineering area. Stiffness, stress and natural frequency are the main examples of objectives in aerospace optimization studies. In this thesis, three main strategies are selected to optimize the folding wing structure. The first strategy is decreasing the weight of the wing while keeping its stiffness at the maximum level and minimum compliance is selected as the objective to accomplish it. Compliance simply means the product of applied load and displacement and minimizing it results in maximizing stiffness. The change of the mean compliance of the topology is equal to the strain energy value of added or removed element. The second strategy is maximizing the selected natural frequency value of the wing while decreasing its weight. Optimizing natural frequencies have great importance for many engineering areas and it is possible to implement it with topology optimization. This type of optimization is more cumbersome than compliance optimization, but it can be more beneficial for some special cases. The last strategy is a multi-objective optimization with the objectives of stiffness and natural frequency at the same time. Topologies evolve according to two different objectives with the constraint of weight and this advanced multi-objective approach can present results that are feasible for stiffness and frequency criteria simultaneously.

Generally, commercial software tools are used for topology optimization studies. In this study, an in-house generated code in MATLAB environment with MSC NASTRAN finite element solver is used. The central objectives of constructing an algorithm in this thesis include the ability to customize and control the design. The resulting algorithm is adaptable, reliable and provides the user a greater control. Additionally, the creation of such an algorithm affords the opportunity for intellectual property protection. Intellectual property has significant importance in the aerospace and defense industry and the protection of it can prevent potential issues in the face of global crises. This difficult situation is always avoided and prevented by having genuine and independent engineering tools and facilities. Even though the constructed algorithm in this study uses MSC NASTRAN as a finite elemental solver, there is no future risk for intellectual property problems because every finite element solver can be implemented easily into this algorithm which turns out to be one of the best aspects of it.

In this chapter, applied strategies and the constructed algorithm are explained in detail. ESO and BESO are used as solver optimization methods, and they are both implemented into the generated algorithm. Although they are similar, there are main differences such as filter scheme, addition of elements and selection of input parameters. The formulations of these optimization methods in the algorithm are provided in this chapter. Reference studies to investigate the accuracy of the constructed algorithm are also shown in the related appendices.

3.2 Calculations of Evolutionary Structural Optimization (ESO) Method

ESO is a simple yet effective topology optimization method that has gained popularity due to its simplicity. While it may not always provide the optimal solution, it is a useful tool for having ideas about optimized structures. ESO method involves gradually removing elements from the structure, leading the structure to evolve and eventually reach its final topology through this process of element removal. Finite element analysis is used to identify elements for removal,

specifically targeting those with lower stress or strain energy values in order to increase the structure's efficiency where the stress or strain values of all elements should be within a narrow, safe range. In this study, ESO is chosen for testing the constructed algorithm due to its simplicity and speed in producing results. Von Mises stress is used as the criterion and a related reference study is shared in Appendix A.

There are two main parameters of ESO, namely, rejection ratio (RR) and evolutionary rate (ER). After performing the finite element analysis, von Mises stress of every element is divided by the maximum von Mises stress value of the whole structure individually and the ratio found is compared with RR. This comparison determines whether an element is removed or not, as shown in Equation (3-1).

$$\frac{\alpha_e}{\alpha_{max}} < RR_i \tag{3-1}$$

α_e is the von Mises stress of the element and α_{max} is the maximum von Mises stress. RR_i is the rejection ratio of i^{th} iteration, because it is updated every iteration by ER. This is shown in Equation (3-2).

$$RR_{i+1} = RR_i + ER \tag{3-2}$$

The elements are removed according to Equation (3-1), then, RR is updated by Equation (3-2) and a new iteration is started with this RR value. The process of removing inefficient elements according to von Mises stress values in each iteration continues until the optimal structure is obtained. Steps of the whole procedure are listed as follows:

1. Dividing the structure into finite elements
2. Conducting finite element analysis to find out stress or strain energy level

3. Removing elements according to Equation (3-1)
4. Updating RR according to Equation (3-2)
5. Repeating steps between 2 and 4 until the optimum solution is obtained

3.3 Calculations of Bi-directional Evolutionary Structural Optimization (BESO) Method

BESO is the superior method with adding/removing capabilities and a filter scheme. Elements are gradually removed and added to the topology until the optimum is reached. Filter scheme ensures mesh-independency andsolves checkerboard problem whichis detailed in this chapter. BESO promises more successful results which are closer to the optimum topology than ESO [20]. However, it is computationally more expensive and more complicated than ESO due to the filter scheme. The first and the second steps are again discretizing the structure to finite elements and conducting finite element analysis. After performing a finite element analysis, the sensitivity numbers of every element are calculated. These sensitivity numbers are then used to determine the added or removed elements, and calculations differ from objective to objective. In this study, sensitivity number calculations of stiffness and natural frequency are presented.

Stiffness is one of the major aspects of nearly all aerospace structures. Inversion of the stiffness is compliance and mean compliance of the structure can be expressed by the total strain energy value under external loads. It is calculated as below:

$$C = \frac{1}{2} f^T u \tag{3-3}$$

where f is the external load vector, and u is the displacement vector. When the i_{th} element is removed from the structure, the mean compliance, C, is changed as

$$\alpha_i^e = \Delta C = \frac{1}{2} f^T \Delta u = -\frac{1}{2} f^T K^{-1} \Delta K u = \frac{1}{2} u_i^T K_i u_i \tag{3-4}$$

where u_i is the displacement vector of i_{th} element, K is the global stiffness matrix, and ΔK is the change of stiffness matrix after removal of i_{th} element, which equals to K_i, the stiffness matrix of the i_{th} element. This change in mean compliance is stated as an "elemental sensitivity number" and it is shown as α_i^e. This equation indicates that the change in mean compliance after removing the i_{th} element equals the elemental strain energy of the i_{th} element. In that way, the most inefficient elements are the ones with low strain energies, and they should be eliminated to minimize compliance or maximize the stiffness, which are the same.

For most BESO applications, the aim is minimizing compliance given in Equation (3-5), while decreasing volume according to Equation (3-6).

$$\text{Minimize } C = \frac{1}{2} f^T u \tag{3-5}$$

$$\text{Subject to } V^* - \sum_{i=1}^{N} V_i x_i = 0 \tag{3-6}$$

$$x_i = 0 \text{ or } 1 \tag{3-7}$$

V^* and V_i are prescribed total volume and total volume of the i_{th} element. N indicates the total number of elements in the design space. Equation (3-7) shows the binary design variable of x_i and it means whether element is solid or void. When the element is void, it is removed from the structure and analysis goes on. This is valid only for the hard-kill BESO and this binary design variable is different for soft-kill BESO, which distinguishes the main difference between the two methods.

Volume constraint in Equation (3-6) is expressed as equality in the BESO calculations [21], while volume constraint is less than or equal to zero for SIMP calculations as exemplified in the study of Luo [11]. Therefore, most of the BESO studies start from unfeasible full-design domain, and analysis continues until the volume constraint and convergence criterion in Equation (3-8) are satisfied.

$$\text{convergence criterion} = \frac{\left|\sum_{i=1}^{N} C_{k-i-1} - \sum_{i=1}^{N} C_{k-N-i-1}\right|}{\sum_{i=1}^{N} C_{k-i-1}} \leq \tau \tag{3-8}$$

Where τ is allowable convergence tolerance, N is the integer number which is generally selected as 5 [21] and k is the current iteration number. This equation is satisfied when the change in the mean compliance over the selected number of iterations is acceptably small.

Directly removing elements from the structure creates difficulties in topology optimization. The most common problem is having irrational topologies with discontinuities. To overcome this problem, soft-kill BESO utilizing the material interpolation scheme was suggested by Huang and Xie [38].

Equations (3-5) and (3-6) are still valid for soft-kill BESO but there is a need for a new design variable set in order to define weak mechanical properties of the soft elements and this variable set can be stated as

$$x_i = x_{min} \text{ or } 1 \tag{3-9}$$

where x_{min} is quite a small number, in most of cases it is 0.001 [21]. This equation shows that elements with lower sensitivity numbers are not removed from the structure totally. Instead, their mechanical properties are weakened by the material interpolation scheme through penalization, which was first proposed by Bendsøe to

have nearly solid-void designs of SIMP in 1989 [8]. Young's modulus of the elements which are selected to be weakened should be interpolated as,

$$E(x_i) = E_1 x_i^p \tag{3-10}$$

where E_1 is the Young's modulus of solid elements and p is the penalty component, which is generally selected as 3 [21]. In this way, elements with lower sensitivity numbers are not removed from the structure but they do not contribute to the structure in a mechanical sense anymore.

After some derivations and using the material interpolation scheme, Huang and Xie [21] calculated the sensitivity number of solid or soft elements such as

$$\alpha_i = -\frac{1}{p}\frac{\partial C}{\partial x_i} = \begin{cases} \frac{1}{2} u_i^T K_i^0 u_i, & \text{if } x_i = 1 \\ \frac{1}{2} x_{min}^{p-1} u_i^T K_i^0 u_i, & \text{if } x_i = x_{min} \end{cases} \tag{3-11}$$

where K_i^0 is the elemental stiffness matrix of the solid element. It is clear that the sensitivity numbers of soft elements depend on the penalty component. When the penalty component diverges to infinity, this sensitivity number becomes zero, which is basically the same as hard-kill BESO. This shows that soft-kill BESO is a sub-type of hard-kill BESO.

When the design variable is zero, it is not included in the finite element analysis, and it saves a lot of computational time. This is why hard-kill BESO is the most preferred and the fastest BESO method among the others. However, the risk of having permanent damage in the topology is higher with this method [21]. In addition, there are some special material interpolation schemes of soft elements to avoid from localized vibration modes in the soft-kill BESO method. This benefit can be very

crucial if the objective is selected as maximizing any natural frequency of the structure. Because of all these reasons, soft-kill BESO is selected as the main method to use in this thesis, and it is aimed to be implemented into the algorithm successfully.

Apart from stiffness, natural frequency of a structure is also one of the most popular objectives in aerospace. The primary objectives of this type of topology optimization method include maximizing the selected natural frequency or the gap between two natural frequencies. Huang provided how to calculate sensitivity numbers for frequency optimization with soft-kill BESO in 2009 [38]. He explained a new way of finding the sensitivity numbers of the elements and suggested a new alternative material interpolation scheme to avoid from artificial localized vibration modes in soft zones. This new scheme aims to solve the extremely high ratio between mass and stiffness in soft regions. To keep this ratio at a reasonable level, density and Young's modulus should be penalized as

$$\begin{aligned} \rho(x_{min}) &= x_{min}\rho^0 \\ E(x_{min}) &= x_{min}E^0 \end{aligned} \tag{3-12}$$

where ρ^0 and E^0 are the density and Young's modulus of the solid material, respectively.After some derivations and implementing a new material interpolation scheme into elemental sensitivity number calculations as Huang and Xie stated [21], the sensitivity number for maximizing j_{th} natural frequency can be found as

$$\alpha_i = \frac{1}{p}\frac{\partial \omega_j}{\partial x_i} = \begin{cases} \dfrac{1}{2\omega_j} u_j^T \left(\dfrac{1-x_{min}}{1-x_{min}^p} K_i^0 - \dfrac{\omega_j^2}{p} M_i^0\right) u_j, & \text{if } x_i = 1 \\ \dfrac{1}{2\omega_j} u_j^T \left(\dfrac{x_{min}^{p-1}-x_{min}^p}{1-x_{min}^p} K_i^0 - \dfrac{\omega_j^2}{p} M_i^0\right) u_j, & \text{if } x_i = x_{min} \end{cases} \tag{3-13}$$

where M_i^0 and K_i^0 are mass and stiffness matrices of the i_{th} solid element. ω_j is the j_{th} natural frequency and u_j is the eigenvector of j_{th} natural frequency.

Until now, three different sensitivity number calculations are shown. Equations (3-4) and (3-11) are the ones with the objective of maximizing stiffness and they are for hard-kill BESO and soft-kill BESO, respectively. Equation (3-13) is to maximize ω_j by using the soft-kill BESO method. After calculating the sensitivity numbers, the remaining sequences to evolve for optimal structure are the same for all approaches. The next important step is implementation of the filter scheme into the algorithm.

3.4 Filter Scheme

Inclusion of filter scheme is one of the biggest differences between ESO and BESO. The main aims of this scheme are solving the checkerboard problem, calculating the sensitivity numbers of void/soft elements and creating mesh-independent solutions. When the structure is discretized using low-order bilinear or trilinear finite elements, optimization by ESO method may result in a checkerboard pattern due to discontinuities along element boundaries. This unwanted pattern shown in Figure 3-1 decreases the manufacturability of the structure which is an important problem for many industrial engineering problems. The second important problem of ESO is the mesh-dependency. This method is highly dependent on the initial meshing hence different topologies can be achieved by changing initial mesh sizes or types. This variation decreases the trustworthiness of ESO method and it is undesired. The filter scheme prevents dependency on the initial mesh and ensures mesh-independent solutions. One final benefit of the filter scheme is its ability to calculate sensitivity numbers of void or soft elements. Because these elements are typically removed from the structure or weakened through penalization, their sensitivity numbers are usually quite low or zero. This causes them to fall behind in the ranking and be unable to be recovered through the BESO adding scheme. However, with the filter scheme, the sensitivity numbers of void or soft elements are calculated by including the

surrounding elements. This means that if the sensitivity numbers of neighboring elements are increased, the sensitivity number of void/soft elements will also increase, allowing them to rise in the ranking. As a result, void/soft elements can be recovered back and contribute to the structure by taking on some of the mechanical burden of the neighboring elements.

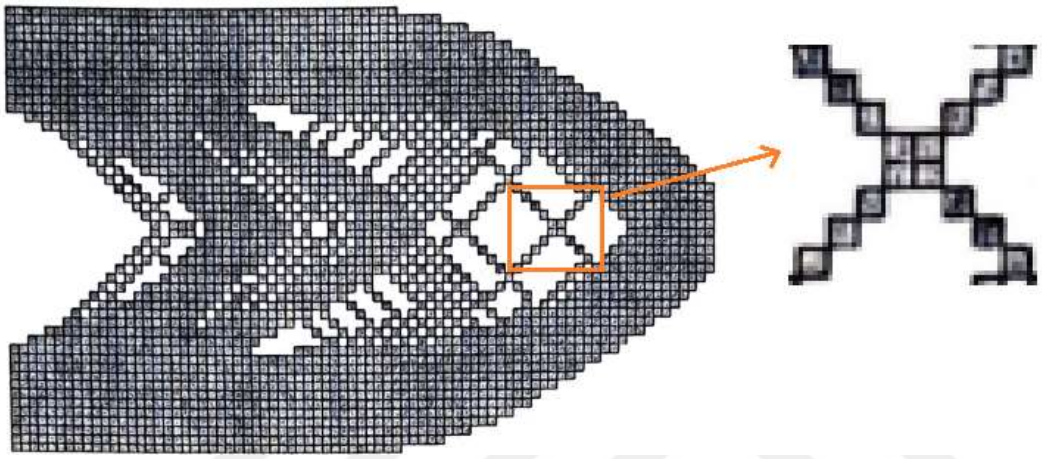


Figure 3-1 Checkerboard Pattern in ESO [21]

Several filter schemes are offered during the development of BESO and the investigated scheme in this thesis was offered by Huang and Xie in 2010 [21]. Before implementing the filter scheme, elemental sensitivity numbers should be distributed to nodes by using weight factors and it is shown as,

$$\alpha_j^n = \sum_{i=1}^{M} \omega_i \alpha_i^e \tag{3-14}$$

where α_j^n and α_i^n are sensitivity numbers of the j_{th} node and i_{th} element, respectively. M is the total number of nodes which are connected to the i_{th} element. ω_i is the weight factor of the i_{th} element and can be calculated as,

$$\omega_i = \frac{1}{M-1}\left(1 - \frac{r_{ij}}{\sum_{i=1}^{M} r_{ij}}\right) \tag{3-15}$$

where r_{ij} is the distance between the center of the i_{th} element and the j_{th} node. Therefore, if a node is near to the center of the element, it has more nodal sensitivity number. After distributing the sensitivity number of elements to nodes, new elemental sensitivity numbers should be calculated using self and neighbor nodes. Minimum filter radius, r_{min} , is introduced for this purpose and it is shown in Figure 3-2. In 2D problems, the circle from the center of the i_{th} element is created with the radius of r_{min}. This circle would be a sphere for 3D problems. For both cases, the inner area of the circle or inner volume of the sphere is called as sub-domain Ω_i and all nodes in this domain are included in the sensitivity number calculation of the i_{th} element as,

$$\alpha_i = \frac{\sum_{j=1}^{K} \omega(r_{ij}) * \alpha_j^n}{\sum_{j=1}^{K} \omega(r_{ij})} \tag{3-16}$$

where K is the total number of nodes in the sub-domain and $\omega(r_{ij})$ is the linear weight factor calculated as

$$\omega(r_{ij}) = r_{min} - r_{ij} \qquad (j = 1,2,\dots\dots,K) \tag{3-17}$$

It is clearly seen that the above filter scheme smoothens the topology and adds the capability of calculating sensitivity numbers of void/soft elements. If the nodes in the sub-domain Ω_i have great sensitivity numbers, it affects the sensitivity number

of the i_{th} element even though it is void/soft. It is ranked with this newly calculated value and this process makes BESO method works smoothly.

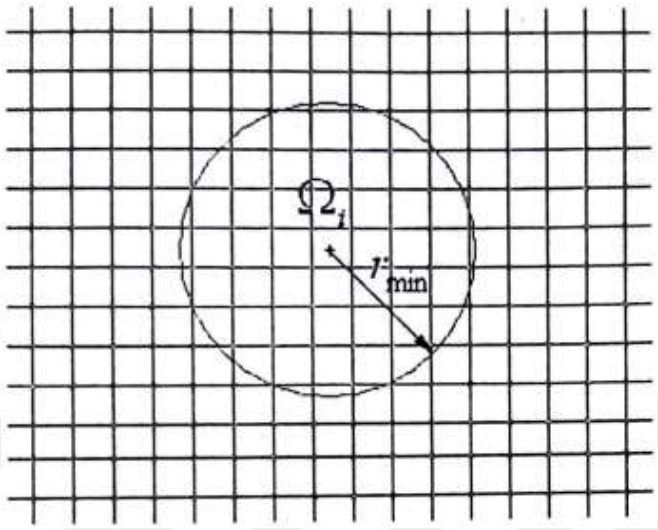


Figure 3-2 Minimum Filter Radius and Sub-domain Ω_i [21]

Besides the filter scheme, Huang and Xie offered an extra step for smoother topology and prevented chaotic oscillations by using historical sensitivity numbers in 2007 [23]. They suggested to average sensitivity numbers of elements with the previous iteration. This simple averaging scheme contributes effectively to increase the chance of converging. This scheme does not affect the final topology in a significant way, but it helps optimization to converge.

After calculating the sensitivity number for the desired objective by using a filter and averaging scheme to smooth topology, elements should be ranked with their sensitivity numbers to determine which one is to add or remove from the structure.

Before adding or removing elements, the target volume for the next iteration should be calculated as,

$$V_{k+1} = V_k(1 \pm ER) \quad (k = 1,2, \dots \dots \dots) \qquad (3\text{-}18)$$

where V_{k+1} is the target volume of the next iteration, V_k is the current volume of the structure and k is the iteration number. Evolutionary Rate, ER, helps to decrease or increase the target volume until the final volume is reached. It affects directly the number of total iterations and therefore the whole computational time. If ER is selected as too small, the number of iterations becomes unnecessarily high. Similarly, the structure can not be converged to the optimum if ER is selected as a quite big number. Target volume calculations with ER continues until the predetermined final volume is reached. Even the final volume is reached, optimization may continue until the objective values become stable.

There are two main comparison equations to add or remove elements and they are indicated as,

$$\alpha_i \leq \alpha_{del}^{th} \qquad (3\text{-}19)$$

$$\alpha_i > \alpha_{add}^{th} \qquad (3\text{-}20)$$

where α_{add}^{th} and α_{del}^{th} are threshold sensitivity numbers for adding and removing, where α_{add}^{th} is always bigger than or equal to α_{del}^{th}. If the sensitivity number of a solid element satisfies Equation (3-19), it becomes void/soft. Similarly, if any void/soft element has a sensitivity number bigger than α_{add}^{th}, it transforms to a solid element. An important point here is determining these threshold sensitivity numbers. There are some basic selection rules for these numbers:

1. The number of elements corresponding to the next targeted volume is calculated. For example, if there are 1000 elements and the next target volume is 0.5, then 500 elements correspond to this volume (assuming all elements are identical). All elements are then sorted based on their sensitivity

numbers. The sensitivity number of the 500th element is assigned as α_{th} and threshold numbers are considered as $\alpha_{del}^{th} = \alpha_{add}^{th} = \alpha_{th}$.

2. The number of elements added in the iteration is proportional to the total number of elements and this ratio is called as the volume addition ratio (AR). If this ratio is less than the predetermined AR_{max} , the third step is ignored. If it is larger, the third step must be executed.
3. The α_{add}^{th} value is calculated as the ratio of the number of added elements to the total number of elements that should be present according to AR_{max}. This adding threshold value should be just slightly below the sensitivity value of the last added element. α_{del}^{th} is found by adding the volume of the added elements to the current volume and subtracting the volume required by the next iteration from the last answer.

The term AR_{max} is introduced in these steps. Its goal is to ensure that an excessive number of void/soft elements are not transformed into solid elements, as this can adversely affect the structure's integrity.

To sum up the whole BESO procedure in steps:

1. Discretizing the structure with finite elements and assigning mechanical properties of the material to elements.
2. Conducting finite element analysis, obtaining necessary values such as strain energy or von Mises stress to calculate sensitivity number according to the objective of the study. Equation (3-4) is for minimum compliance by hard-kill BESO, Equation (3-11) is for minimum compliance by soft-kill BESO and finally, Equation (3-13) is for maximizing the first frequency by soft-kill BESO.
3. Applying the filter scheme to distribute sensitivity numbers to nodes and collecting them again to elements with minimum filter radius by using Equations (3-14), (3-15), (3-16), and (3-17).
4. Averaging sensitivity numbers with historical data.
5. Selecting target volume for next iteration by Equation (3-18).

6. Adding or removing elements according to Equations (3-19) and (3-20).
7. Repeating steps between 2 and 6 until the volume constraint (Equation (3-6)) and the convergence criterion (Equation (3-8)) are satisfied, which happens when difference between objective values of the last iterations becomes less than the allowable convergence tolerance value.

3.5 Constructed Algorithm in MATLAB

To optimize the folding wing structure for natural frequency and/or stiffness, there is a need for an optimization tool. In this study, an algorithm is constructed in MATLAB environment to optimize structures by using ESO or BESO with the objectives of stiffness and/or natural frequency. This algorithm uses MSC NASTRAN as a finite element solver.

Firstly, finite element modeling software is used to discretize the structure with finite elements. This is a non-recurring step because there is no need to model the structure during the optimization process. Any finite element modeling and analysis software can be used for this purpose and MSC PATRAN is selected in this study. Finite elements, boundary conditions and loads should be documented in the Bulk Data Format (BDF) file for the algorithm interface. Then, a finite element solver should be executed to find necessary information such as strain energy or von Mises stress value. These values are written in the result text file of "f06" by MSC NASTRAN and stored for future sensitivity number calculations. MATLAB reads the f06 file and takes all necessary information. Then, the algorithm evaluates all the values and calculates sensitivity numbers according to the selected objective. Filter scheme and averaging are applied to smoothen the desired topology. Elements to be added or removed are determined by ranking elements according to their sensitivity numbers. The material properties of removed elements are weakened by the material interpolation scheme and new information about elements is written to a new BDF

file. After this step, MSC NASTRAN analyzes the structure again and these iterations continue until the target volume is reached. This algorithm works automatically until it reaches to the final topology, but it needs some initial inputs such as the first finite element model of the structure, evolutionary rate (ER), maximum volume addition ratio (AR_{max}), minimum filter radius (r_{min}), penalty component (p) and the final target volume. The whole process is detailed and shown in Figure 3-3 and reference studies of this algorithm using BESO are demonstrated in Appendix A.

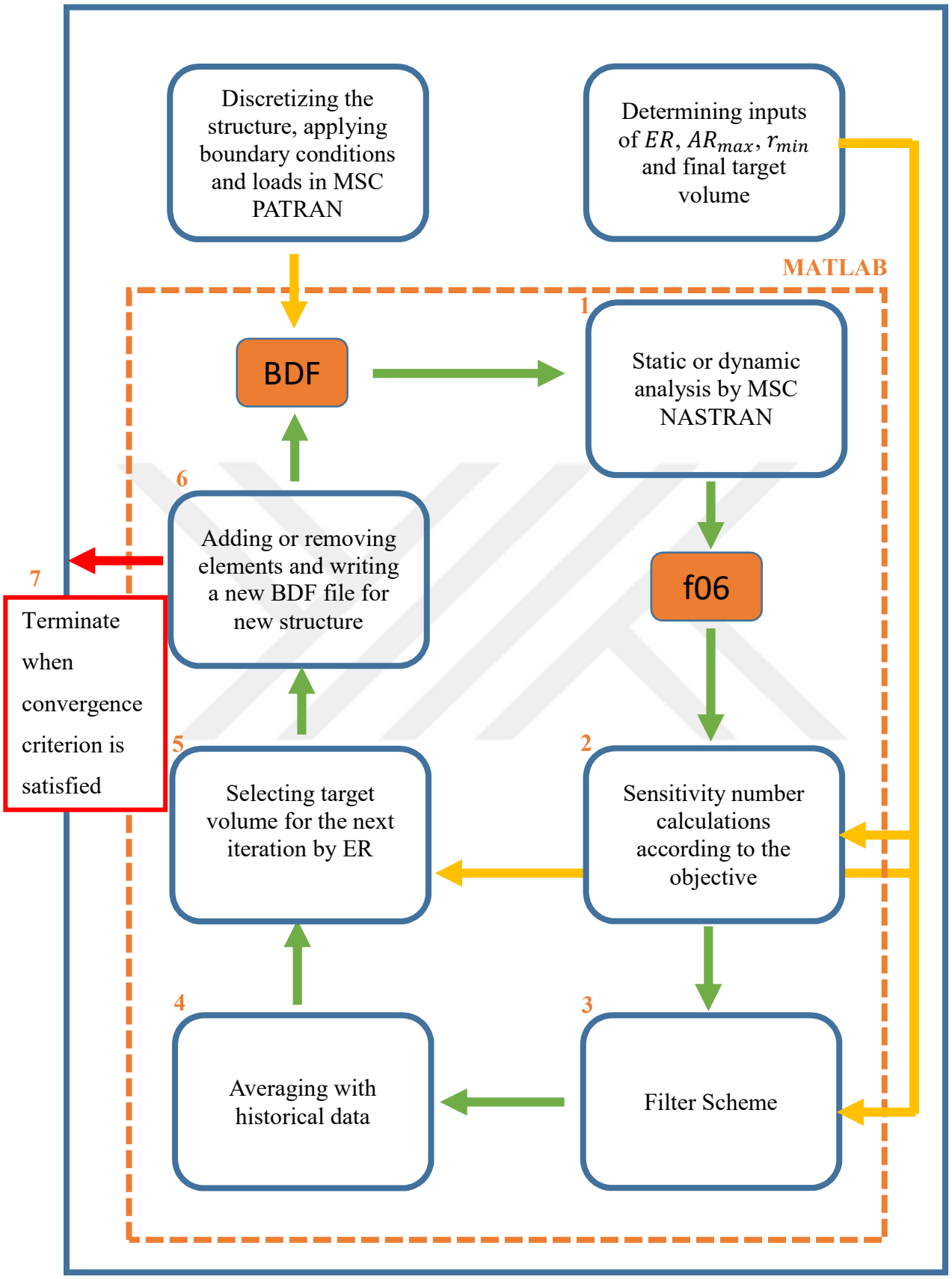


Figure 3-3 Flowchart of the Constructed Algorithm

3.6 Conclusion

In this chapter, BESO and ESO formulations have been described in detail, as they serve as the foundation for the algorithm created in this thesis. Details about this algorithm which is constructed in order to optimize the folding wing structure have been shared. It has been determined that the competence of the algorithm in optimizing the folding wing structure is evident as it consistently produces final topologies that are comparable and nearly equivalent to the final reference topologies which are presented in Appendix A.

CHAPTER 4

STRUCTURAL FINITE ELEMENT MODELLING AND PRELIMINARY ANALYSES OF THE FOLDING WING

4.1 Introduction

Before starting the topology optimization, the folding wing structure should be discretized with finite elements. The type and size of the elements have great importance in static and dynamic analysis. Because evolutionary optimization methods are iterative methods to find optimum structure by evolving, the computational time of every single iteration is crucial. Besides the computational time, the mesh is important for the performance of the analysis and the success of the final topology. Even though BESO promises mesh-independent solutions, the study in Appendix B shows that it is not "fully" mesh-independent for 3D structures and using finer mesh may provide better objective results and better insight into the topology with more details. In addition to mesh, boundary conditions and loads are also critical considerations in topology optimization. Therefore, boundary conditions and loads should be specified carefully before topology optimization takes place. In this chapter, the general characteristics of the folding wing structure, its finite element model, boundary conditions, and loads are demonstrated. Results of preliminarily static and modal analyses on the folding wing are also shown.

4.2 Mechanical Specifications of the Folding Wing Structure

Most of the mechanical properties of the folding wing structure are certain and known. This wing is made of aluminum 7075-T6, which is quite popular in the

aerospace industry due to its high strength and good corrosion resistance. The mechanical properties of this material are shown in Table 4-1 .

Table 4-1 Mechanical Properties of AL 7075-T6

Density	2.81 g/cm^3
Elastic Modulus	71.7 GPa
Ultimate Tensile Strength (UTS)	572 MPa
Yield Tensile Strength	503 MPa

The cruise missile system is equipped with four foldable wings on its middle section, which are used to provide lift and stability during flight. The folding wing structure (Figure 4-1) consists of several parts: the inner wing, the outer wing, the inner spring, the outer spring, skin structures, and mechanical fasteners. Springs and mechanical fasteners are excluded from the optimization because their effects in static and modal analyses are neglected. The custom-machined torsional springs generate torque to launch the wings into position, and spring-loaded pins lock the mechanical parts in place after deployment. The inner spring is between the whole folding wing structure and the missile fuselage, while the outer one is between the outer and inner wing structures. In addition to springs, skin structures are also excluded from the design space of optimization, but they are in the structural finite element model due to their mechanical support to the wing. The aim of these skin structures is to close the wing's outer surfaces and provide a continuous aerodynamic surface. They are attached to wing structures by rivets, which are also excluded in the optimization. The primary objective of this thesis is to optimize the inner and outer wing structures while certain regions on these wings are excluded from the design space due to their role in the aerodynamic performance of the wings. The internal volume of the wing structures are optimized through the use of the constructed algorithm. It is worth noting that the excluded regions of the wings and skin structures should still be present in both static and dynamic analyses as they contribute significantly to the overall mechanical performance of the wing.

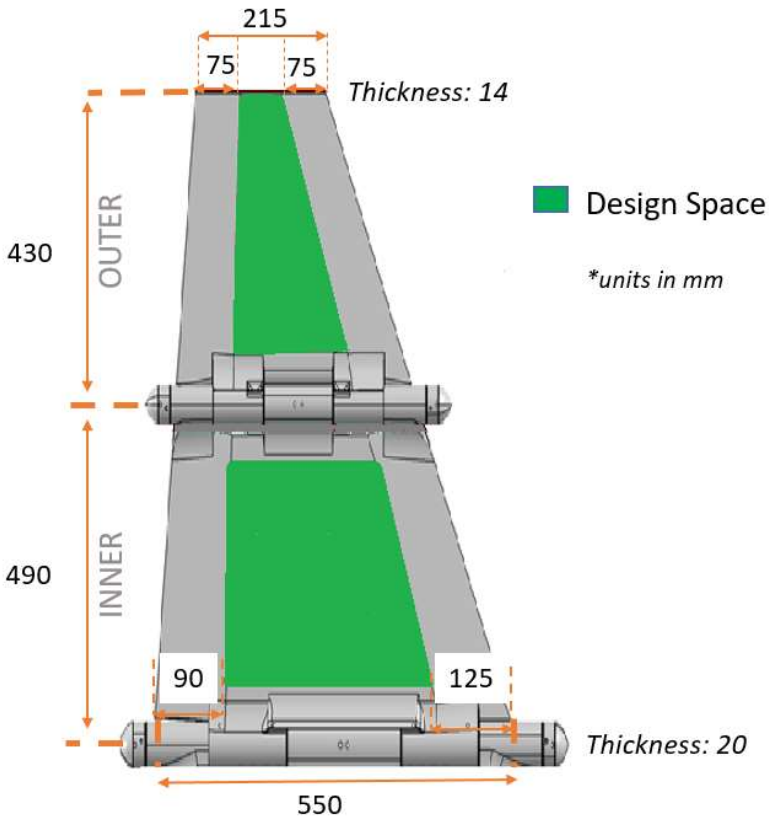


Figure 4-1 The Folding Wing Structure

There should be some assumptions on the folding wing structure to facilitate the optimization process. Firstly, the springs are removed because the system is locked after they function. After this step, springs do not significantly contribute to the structure, and this study aims to find the optimum topology after wings are launched. Secondly, mechanical fasteners are removed, and parts are treated as a whole to decrease the complexity of the mesh. Every additional fastener to structure comes with a computational cost. Lastly, distorted and ineffective surfaces on the wing are corrected in a proper way. The quality of the mesh is particularly important in the design space. With these assumptions, a new model is created, which is shown in Figure 4-2. The skin structures indicated in this figure are sheet metal covers, and they prevent the wing from the aerodynamic effects of changing topologies.

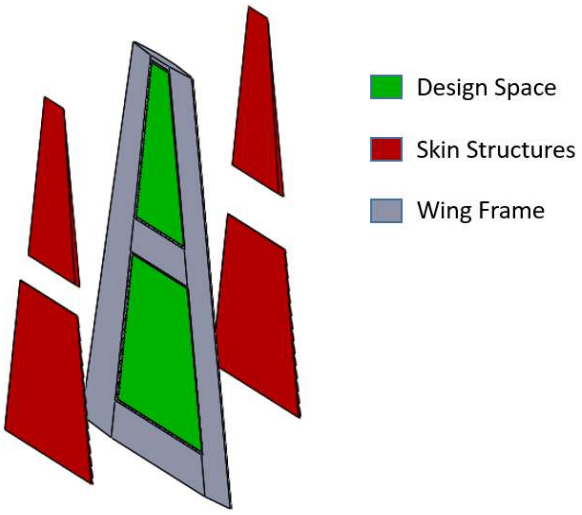


Figure 4-2 Simplified Wing and Skin Structures

The finite element model of the folding wing has a great impact on the computational time, so it should be determined wisely. In this study, design spaces are modelled with a fine mesh, while excluded regions are modelled with a coarse mesh to decrease the size of the model and the computational time. One other aspect of meshing is the filter scheme in BESO calculations. During this filter scheme, virtual spheres around element centers are formed to select neighbor nodes, and these nodes are included in sensitivity number calculations. Due to this step, using isoparametric elements in the design space eases the algorithm in a significant way and decreases the computational complexity. Therefore, all elements in the design space are selected as 8-noded isoparametric hexahedron brick elements (HEX8). 4-noded tetrahedron brick elements (TET4) are selected for the remaining non-design areas because this type of element is a suitable choice for convenience if the quality of the mesh is not the priority. Figure 4-3 exhibits the finite element model of the structure with two different element types. In addition, used element types are given in Table 4-2 with the number of elements and nodes.

Table 4-2 Mesh Information

Type	Number of elements	Number of nodes
HEX8	74825	93126
TET4	179764	20912

4.3 Boundary Conditions and Loads on the Folding Wing Structure

After creating the finite element model of the folding missile wing, the next step is to determine the boundary conditions and loads that will be used in static and dynamic analyses. Once the missile has been launched, the folding wings are locked together by spring-loaded pins, causing the wings to act as a single unit. As a result, the wings are treated as a cantilever beam during the topology optimization process. They are fixed at the bottom surface and free at the other end.

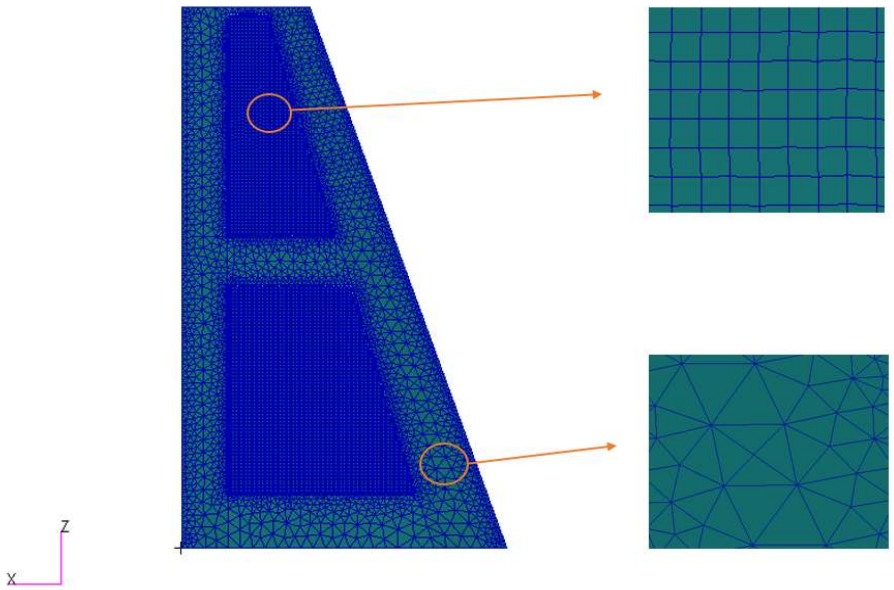


Figure 4-3 Finite Element Model of the Folding Wing

There are several load cases for this wing and its operation. Because there are four folding wings on the missile, loads differ from wing to wing. The worst load condition is considered during the optimization, and it is named Load 1. The aerodynamic pressure is distributed along the surfaces of the inner and outer wings. These outward surfaces are non-design areas, so they do not change with iterations and transmit these loads to internal design spaces. Besides these distributed loads, there is also a hinge moment on the combined wing. Table 4-3 shows the loads used in the optimization. This table expresses distributed loads with their resultant forces and locations. Because the surface area of the inner wing is bigger than the surface area of the outer wing, the resultant force of the inner wing is much higher than the resultant force of the outer wing. Figure 4-4 shows the boundary conditions and load distribution on the wing with a given coordinate system.

Table 4-3 Loads on the Folding Wing

Load Cases	**Outer Wing**			**Inner Wing**			**Hinge Moment**
	Resultant Force (N)	**X (mm)**	**Z (mm)**	**Resultant Force (N)**	**X (mm)**	**Z (mm)**	**M_z (Nmm)**
Load 1	2400	-116	673	5200	-231	263	105000
Load 2	2400	-116	673	5200	-231	263	-
Load 3	-	-	-	-	-	-	105000

There are also different load cases named as Load 2 and Load 3. They are not actual load cases but they are performed during the topology optimization to see what is the effect of the hinge moment on the final topology and results are shared in Appendix D.

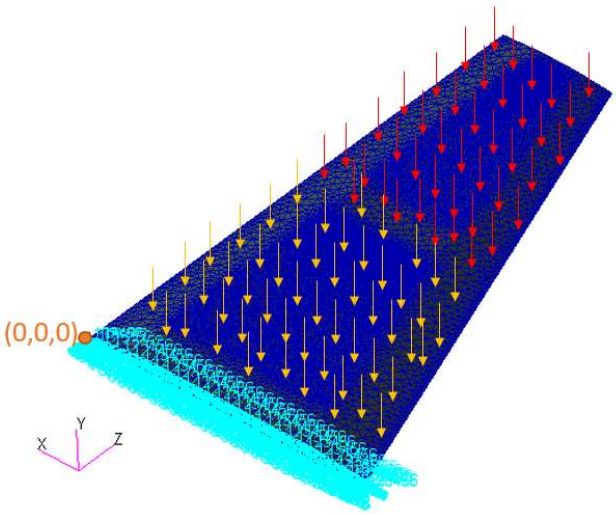


Figure 4-4 Boundary Conditions and Loads on the Folding Wing Structure

4.4 Preliminary Static Analysis of the Folding Wing Structure

Before starting the topology optimization process, it is sensible to conduct preliminary analyses to establish a baseline for the full design space and empty design space. The full design space refers to the structure which has all design elements, while the empty design space represents the wing in its lightest possible condition with all elements removed. These analyses provide a reference point for comparing the performance of the topology optimization. Furthermore, these analyses reveal the initial mechanical performance of the folding wing before any topology optimization is applied.

Three different load cases are used for static analysis, and results of mean compliance and maximum displacement in the y direction are obtained. Mean compliance equals the total strain energy of all elements in the structure and minimizing it means maximizing the stiffness, which is one of the main objectives of this thesis. Therefore, it is important to have this value to compare structures with each other to

see performance differences. All of the obtained results are shown in Table 4-4. Figure 4-5 depicts the static displacement of Load Case 1.

Table 4-4 Mean Compliance and Maximum y Displacement Values of Three Different Load Cases

	Mean Compliance (Nmm)		
	Load 1	**Load 2**	**Load 3**
Full Design Space	3.065×10^4	3.083×10^4	3.438×10^2
Empty Design Space	4.853×10^4	4.899×10^4	4.463×10^2
	Maximum Displacement in y Direction (mm)		
Structures	**Load 1**	**Load 2**	**Load 3**
Full Design Space	30.110	30.430	1.240
Empty Design Space	43.438	46.850	1.640

As expected, the compliance values for the full design space are lower than those for the empty design space because the full design structure has greater stiffness. This basic finding is also reflected in the maximum displacements in the y direction. It is anticipated that structures after topology optimization will have mean compliance values that fall between those of the full and empty designs. The aim is to create a structure with a lighter weight, more efficient material distribution and adequate stiffness, but the mean compliance of the final topology cannot be as low as that of the full design structure. Additionally, it is clear that Load 3 has little effect on the maximum y displacement.

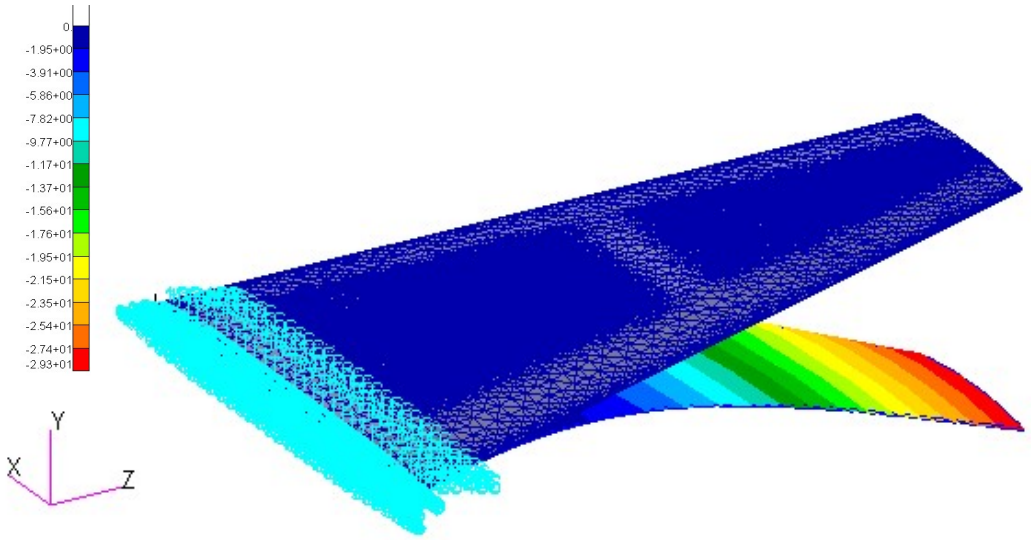


Figure 4-5 Maximum y- Displacement of the Full Design Space Folding Wing by Load 1

4.5 Preliminary Modal Analysis of the Folding Wing Structure

Dynamic characteristics of the wing shall be investigated by preliminary modal analysis because one of the objectives of the algorithm in this thesis is to maximize selected natural frequencies of the folding wing structure. Therefore, there is a need for preliminary modal analyses of both full and empty design spaces similar to static analyses. The first three natural frequencies ($\omega_1, \omega_2, \omega_3$) are reported in Table 4-5, and mode shapes corresponding to the full design space are demonstrated in Figure 4-6, Figure 4-7, and Figure 4-8.

Table 4-5 First Three Natural Frequency Values of the Folding Wing Structure

	Natural Frequencies (Hz)		
	$\boldsymbol{\omega_1}$	$\boldsymbol{\omega_2}$	$\boldsymbol{\omega_3}$
Full Design Space	30.37	138.33	185.24
Empty Design Space	31.11	137.22	165.44

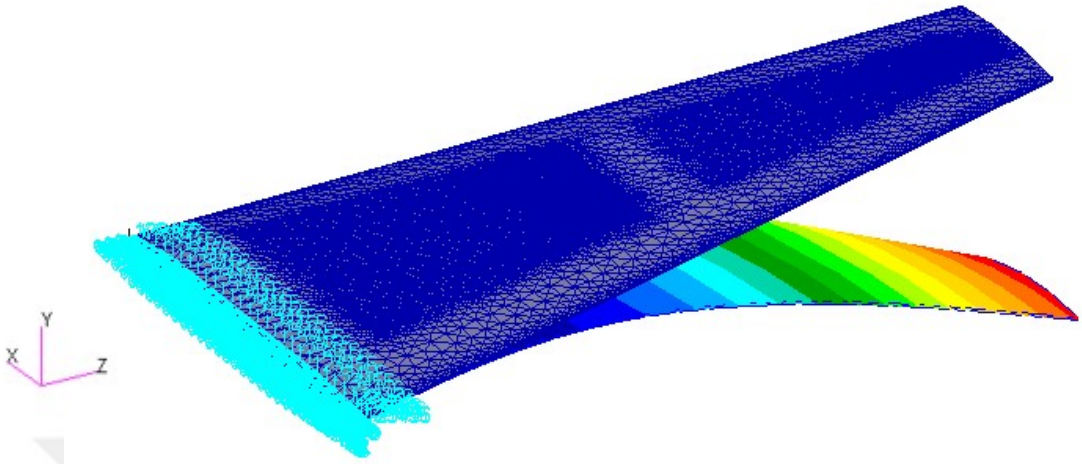


Figure 4-6 The First Bending Mode for Full Design Space (ω_1=30.37 Hz)

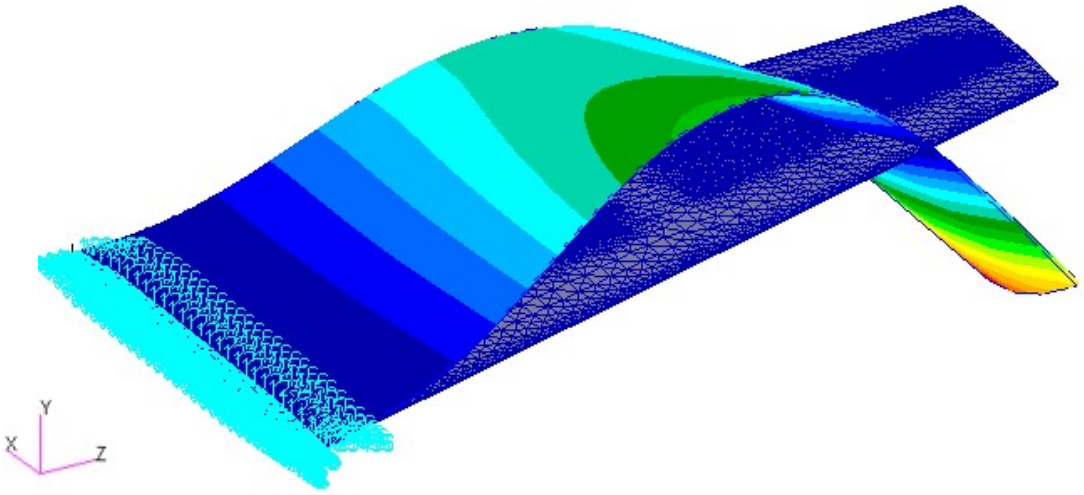


Figure 4-7 The Second Bending Mode for Full Design Space (ω_2=138.33 Hz)

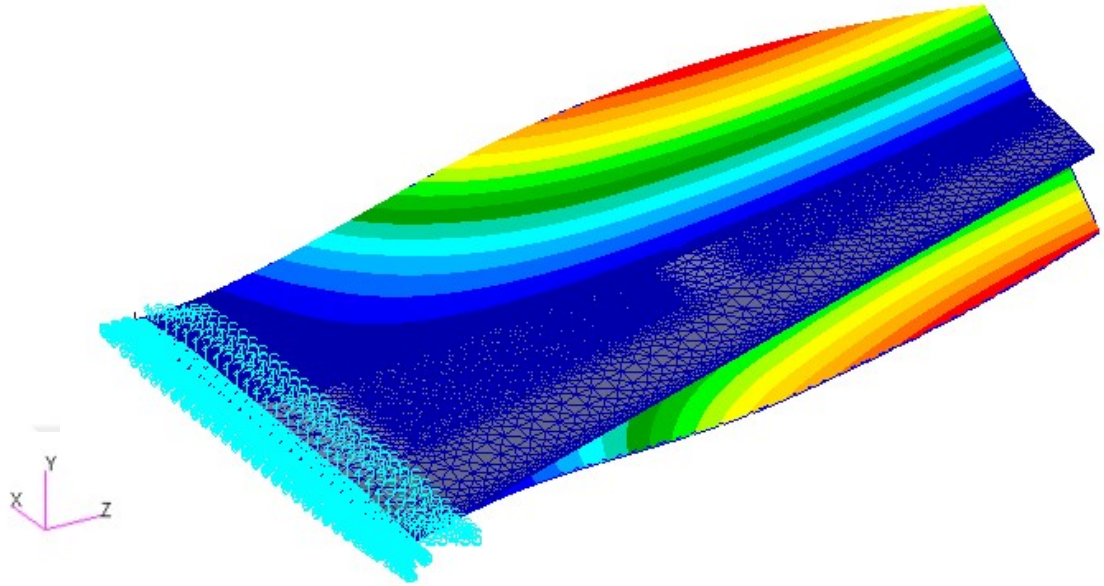


Figure 4-8 The First Torsional Mode for Full Design Space (ω_3=185.24 Hz)

As already demonstrates, there is not any remarkable difference between the first and second natural frequencies of the full and empty design spaces. There are several reasons behind this outcome. Firstly, there is a wing frame (Figure 4-2), which is a non-design area and it contributes to the structure in a significant way. Even when the design space is empty of material, this frame provides primary structural stability. Secondly, the natural frequency is basically the square root of stiffness divided by mass. Both of these variables decrease at the same time when a material is removed from the structure. Therefore, it is understandable that there are no important differences between the first two natural frequencies. However, the difference for the third natural frequency is noteworthy. It means that material in the design space dramatically contributes to the torsional mode and the removal of material results in a more serious reduction in torsional stiffness.

One of the major objectives of this thesis is to alter the natural frequencies of a system through changes to its topology. This can be accomplished through the

application of the topology optimization technique, which can be used to minimize or maximize natural frequencies, or to maximize the difference between two natural frequencies. These kinds of objectives can be necessary for the design of the aerospace structure and some studies on these objectives are shared in the next chapter.

4.6 Conclusion

This chapter presents the initial static and modal analyses conducted on the structure in two configurations: one with the full design space and one with the empty design space. These analyses provide an initial understanding of the mechanical performance of the folding wing before starting the topology optimization process and they showed that there is a significant compliance change between the full and empty designs, as expected. Furthermore, it is found that the natural frequencies of the full and empty design spaces do not significantly differ, except for the torsional mode. This is due to the fact that materials within the design space significantly contribute to torsional stiffness and the lack of them causes 10.8% decrease for the third natural frequency. This value can be manipulated by the contribution of the topology optimization and the related study is shared in Chapter 5.

CHAPTER 5

TOPOLOGY OPTIMIZATION OF THE FOLDING WING STRUCTURE

5.1 Introduction

This chapter is about the topology optimization process of the folding wing structure which is introduced in Chapter 4 with all of its mechanical properties, finite element model, boundary conditions and application of loads. The constructed algorithm detailed in Chapter 3 is used to optimize this wing structure. This algorithm proves its effectiveness with benchmark problems and it has the capability to do successful topology optimization on complex 3D structures. The primary aims of the study are to optimize the stiffness of the structure under applied loads and/or to maximize the chosen natural frequency. Both single-objective and multi-objective analyses are conducted to address these objectives and successful final topologies are obtained.

5.2 Design Variables

The constructed algorithm is based on BESO method, which has several parameters that must be specified prior to initiating the topology optimization process. Some of these variables only influence the convergence of the optimization while others can also affect the final topology. Therefore, it is crucial to properly select these variables in order to obtain succeeded final topologies.

One of the most important variables is r_{min}, minimum filter radius (Figure 3-2) and it eliminates the mesh-dependency and checkerboard pattern by determining the number of nodes to calculate the sensitivity numbers of each element. Increasing this parameter involves more nodes in the calculations resulting in a smoother transition of sensitivity values between elements. For 2D problems, circles, and for 3D problems, spheres with this radius are formed around the element centers. The radius

of these circles/spheres must be chosen such that they enclose more than one element. As a case study, several r_{min} values are selected as 4 mm, 6 mm, 8 mm for the stiffness objective, and different topologies are found with changing r_{min} values. The main finding of this study is that lower values of r_{min} result in more optimally designed topologies but they are too complex to use conventional chip removal manufacturing methods while higher values of r_{min} yield smoother, more easily manufactural topologies with lower stiffness values. As a result, 6 mm radius is selected for all optimization processes because the obtained topology with 6 mm radius promises smaller compliance than the topology with 8 mm radius. Although topologies with 4 mm radius have the minimum compliance, these topologies have many checkerboard pattern zones and these zones cannot be manufactured. This selection is detailed in Appendix C.

Another variable is the final volume constraint which determines the ratio of the final volume to the initial volume of the design space. When the topology reaches the final volume, optimization continues until the converging criterion is satisfied and then it stops. Determining this value is up to the designer and the requirements of the study. In this thesis, this ratio is selected as 30% to have quite a light structure without significant loss of mechanical properties.

The evolutionary volume ratio, ER, is the common variable of ESO and BESO. It determines the volume difference between adjacent iterations. A larger ER value results in a greater volume being removed from the structure between iterations which reduces the total number of iterations and the computational time required. However, it is important to note that excessive values of ER may lead to convergence issues. Huang and Xie presented several works on BESO with different structures and ER was selected as 1%, 2%, 3% and 5% for most of them [21]. For the 3D cantilever beam which is symmetric and a much simpler structure compared to the folding wing structure, 3% was selected. Therefore, ER is selected as 2% for this thesis and in the end, all topologies are converged, and it shows that the selected ER value is sufficient.

Maximum volume addition ratio, AR_{max}, is a variable to prevent the structure from adding excessive numbers of elements in one iteration because it can affect the convergence of the optimization. Huang and Xie selected AR_{max} as 50% for the 3D cantilever beam problem and they suggested large AR_{max} for 3D structures [21]. At the same time, they used $AR_{max} = 2\%$ for four different natural frequency studies. As a result, this variable is selected as 5% in this thesis as the folding wing structure is a 3D structure while natural frequency is one of the main objectives. All topologies are converged and it shows that the selected AR_{max} is a proper one.

While using the soft-kill BESO method, there are two parameters, x_{min} and p, which are the relative density of the soft element and penalty exponent, respectively. These parameters determine the contribution of the soft elements to the main structure. Huang and Xie stated that the penalty exponent has almost no effect if it is selected greater than 1.5. They also used x_{min} values of 10^{-3} for static cases and 10^{-6} for dynamic cases. Because of these selections, x_{min} is selected as 10^{-6} and p is selected as 3 during the optimization processes of this thesis.

5.3 Optimization for Stiffness Criteria

The folding wing structure should be optimized to be lightweight while still able to withstand aerodynamic loads. Therefore, the stiffness value of the wing has significant importance. Three different loads are introduced in Chapter 4 and different topologies are found for every different load case using the BESO algorithm. Results of Load 2 (only bending load) and Load 3 (only hinge moment) are shown in Appendix D. Load 1 represents the worst-case load, and the primary focus of stiffness optimization is on this load. Mean compliance and maximum tip deflection in the y direction of every iteration are shown to provide insight about the optimization direction. Maximum tip deflection is the product of mean compliance and the load but it is shared because it directly represents the visual mechanical effect of the load on the structure. $ER = 2\%, r_{min} = 6\ mm, AR_{max} = 5\%,\ p = 3$ and $x_{min} = 10^{-6}$ are selected as the main parameters. Iterations steps and the optimized

structure are shown in Figure 5-1 and Figure 5-2, respectively. Although outer skin structures are not shown in these figures, they are included in the analysis. Optimization took a total of 59 iterations and 1.6 hours by the computer with 16 GB RAM. Mean compliance and maximum tip displacement in the y direction are then presented in Figure 5-3 and Figure 5-4. This optimization is started from the full design space and different initial guess design studies are investigated in Appendix E and F.

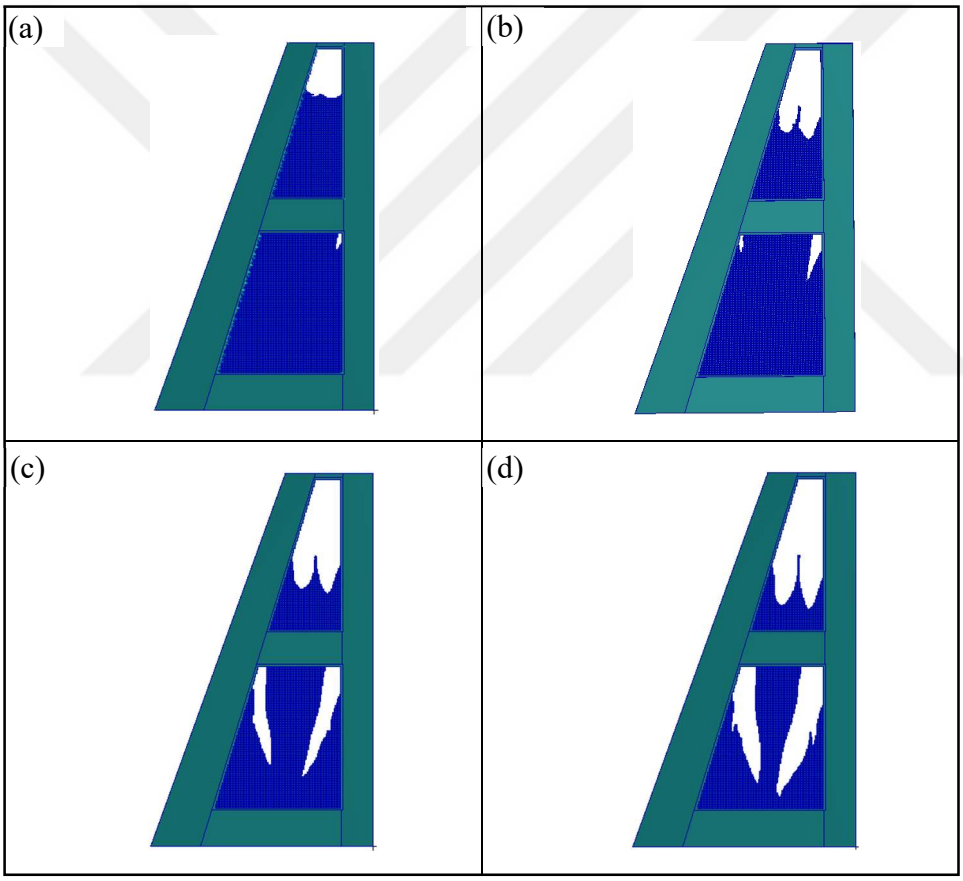


Figure 5-1 Iteration Steps for Load 1 (a) Iter. 15 (b) Iter. 30 (c) Iter. 45 (d) Iter. 59

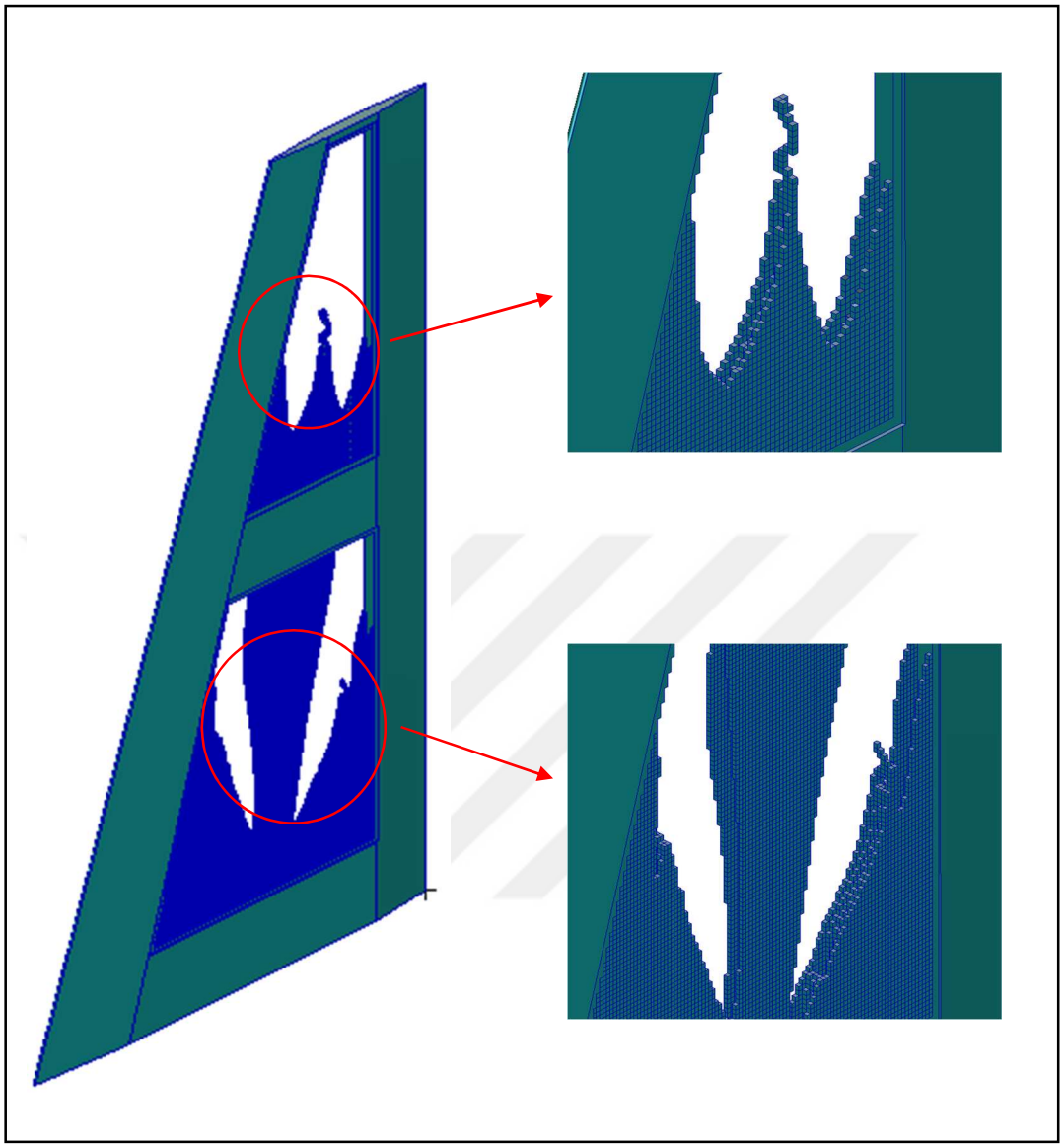


Figure 5-2 Details of the Final Topology at Iteration 59

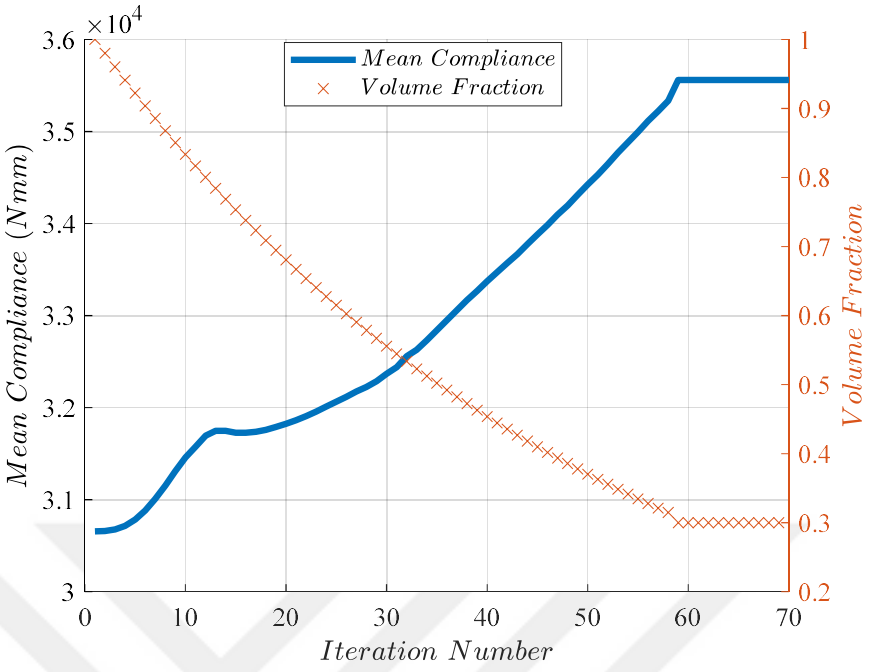


Figure 5-3 Evolution Histories of Mean Compliance and Corresponding Volume Fraction

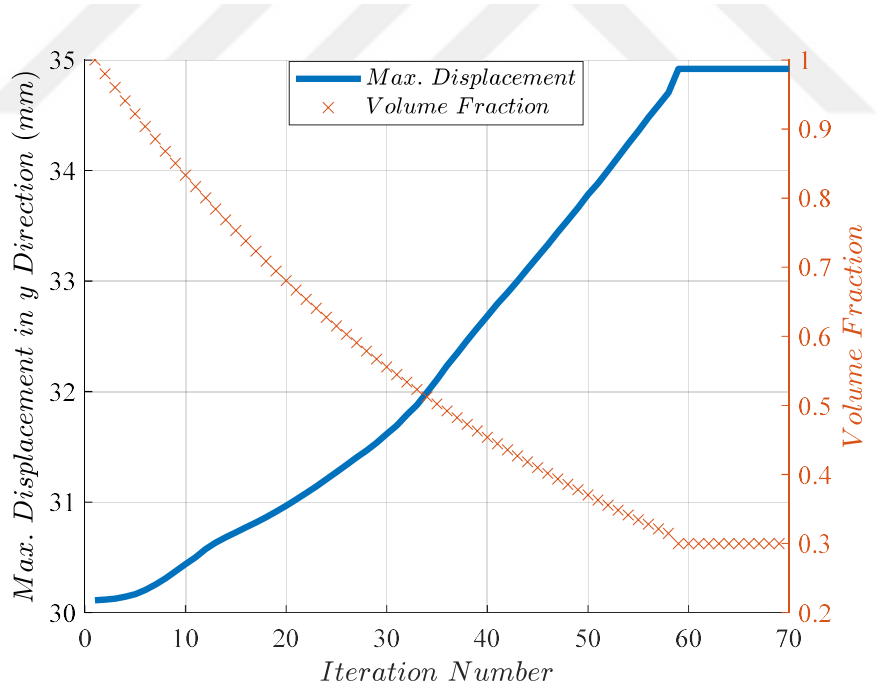


Figure 5-4 Evolution Histories of Maximum Tip Displacement and Corresponding Volume Fraction

Mean compliance and maximum tip displacement values are increased by every iteration as expected because it is not possible to have the stiffness of the wing with full design space while removing materials. However, these values are kept at minimum during the optimization by the algorithm and the volume of the design space is decreased to 30% of its initial volume. Here are the main remarks from the optimized structure:

- The final topology indicates that the strain energy values in the inner regions (which are closer to the missile fuselage) of the outer and inner wings are greater than those in the outer regions.
- Under the load, the outside surface elements of the wings experience higher displacement and thus have higher strain energy values compared to the internal elements. As a result, most of the elements in the middle layer (which is the farthest from the aerodynamic surface) are removed due to their lower strain energy values.
- As it can be seen from Figure 5-3 and Figure 5-4, the analysis does not stop when the final volume ratio is achieved and it continues in the same volume ratio until the convergence criterion in Equation 3-8 is satisfied. This criterion is the main reason of the horizontal lines at the end of those iterations.

5.4 Optimization for Natural Frequency Criteria

Several investigations are done in this study on the objective of natural frequency. ER =2%, r_{min} = 6 mm, $AR_{max} = 5\%$, $p = 3$, and $x_{min} = 10^{-6}$ are selected as the main parameters for all frequency related cases. The first case involves maximizing the first natural frequency (ω_1), which may lead to a reduction in vibration amplitudes and potentially prevent divergence. The second case involves maximizing the third frequency (ω_3) corresponding to the first torsional mode. Preliminary analyses in Chapter 4 demonstrates that this frequency is significantly impacted by the removal of material within the design space. The third case is maximizing the gap between the second and the third natural frequencies

(ω_2, ω_3) because as materials are removed from the structure, these natural frequencies may become close to each other. When these modes interact with each other, the wing can start to oscillate which may lead to flutter. Maximizing the gap between the modes may help to reduce the likelihood of flutter, as the modes are less likely to interact with each other. However, it is important to note that the gap between the static wind-off modes is just one factor that can affect the likelihood of flutter and other factors can be listed as structural damping of the wing and the airspeed. Therefore, one must perform a detailed flutter analysis to detect modes causing the instability and this is beyond the scope of this thesis.

5.4.1 Maximizing The First Natural Frequency

This study aims to maximize the first natural frequency of the folding wing while its volume is decreasing to 30% of the initial volume. Iteration steps and the optimized structure are shown in Figure 5-5 and Figure 5-6, respectively. Optimization took a

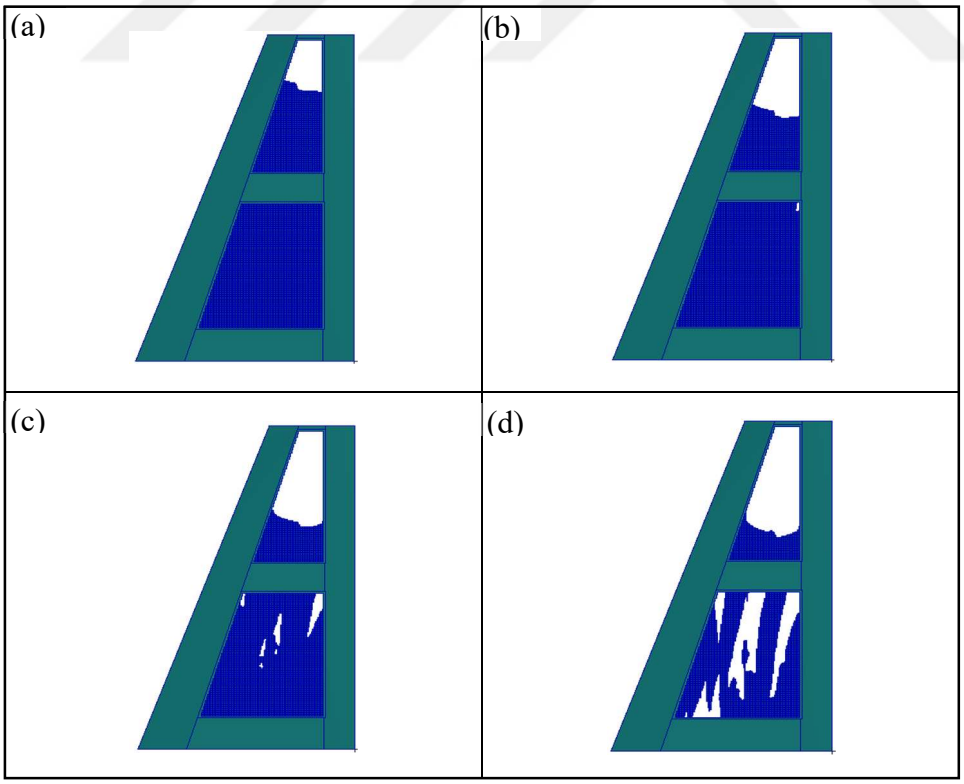


Figure 5-5 Iteration Steps for ω_1 (a) Iter. 15 (b) Iter. 30 (c) Iter. 45 (d) Iter. 59

total of 59 iterations and 3.1 hours to complete. The first natural frequency history is shown in Figure 5-7. The second and the third natural frequencies are also calculated and given in Figure 5-8 and Figure 5-9.

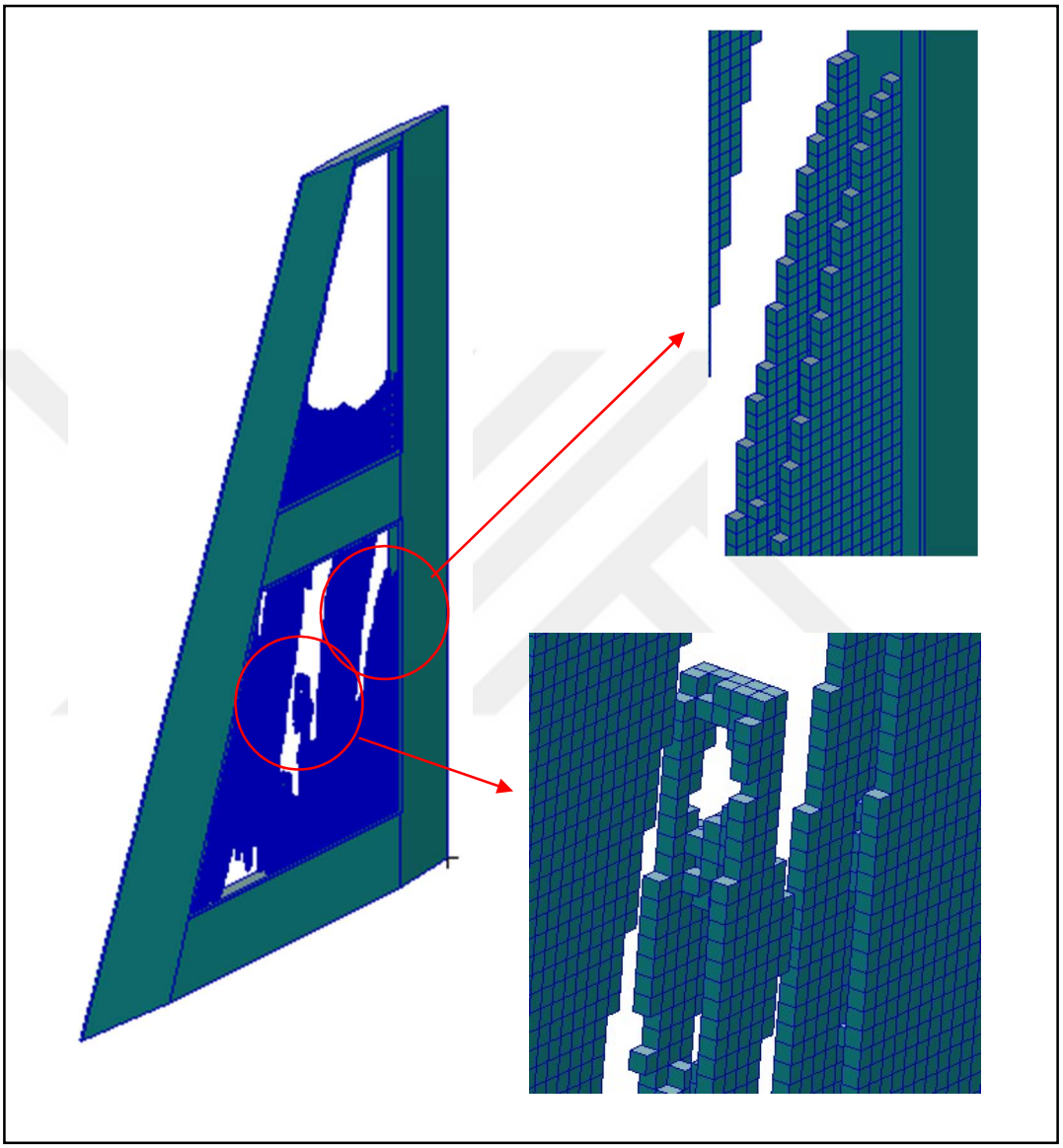


Figure 5-6 Details of the Final Topology at Iteration 59

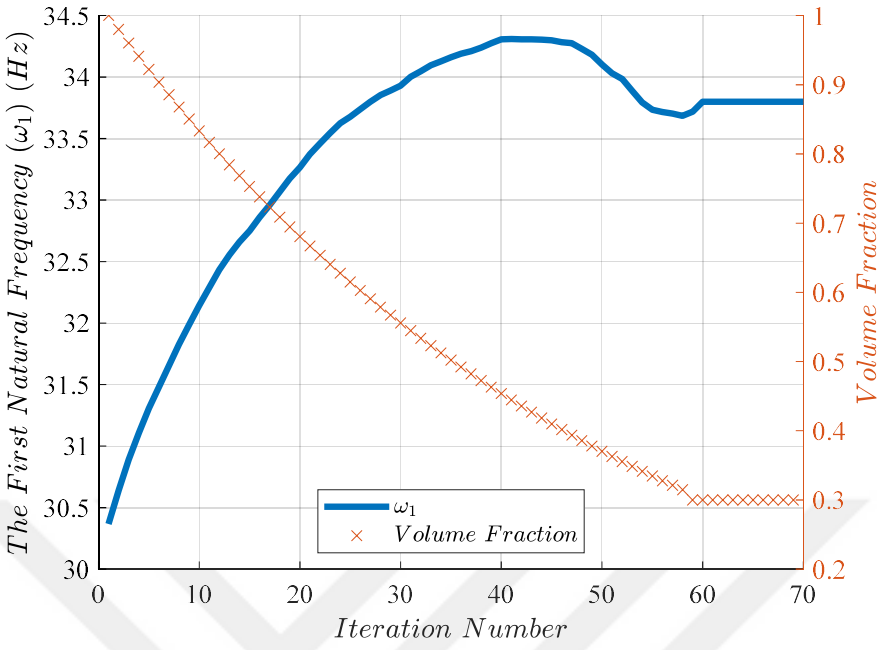


Figure 5-7 Evolution Histories of the First Natural Frequency and Corresponding Volume Fraction

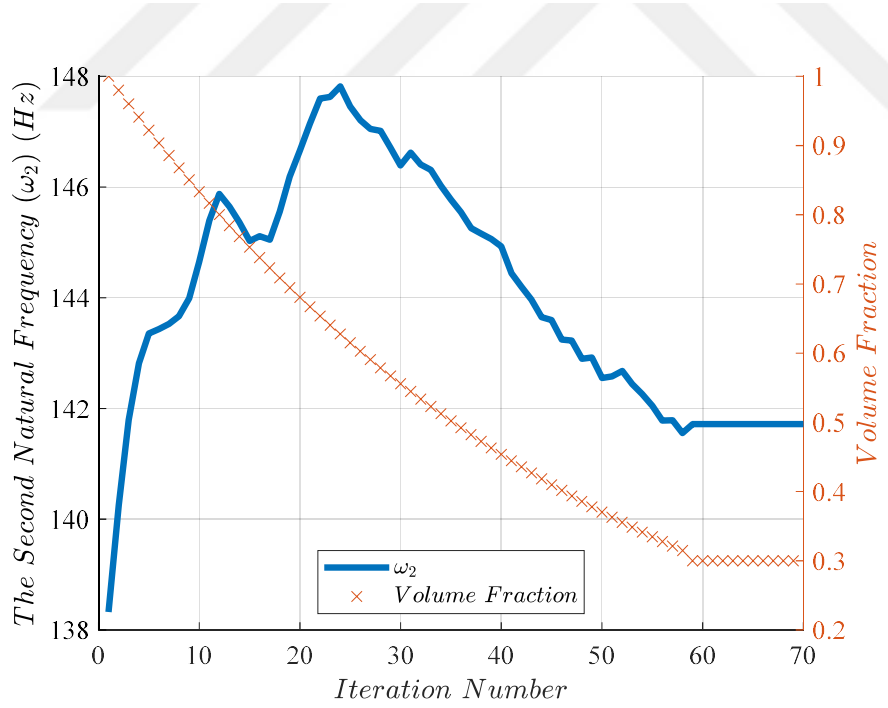


Figure 5-8 Evolution Histories of the Second Natural Frequency and Corresponding Volume Fraction

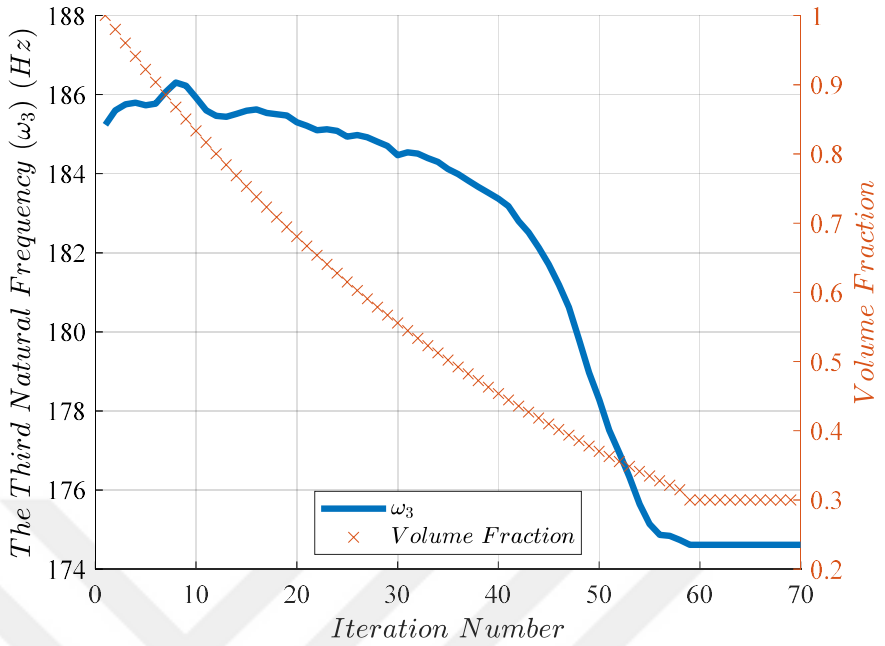


Figure 5-9 Evolution Histories of the Third Natural Frequency and Corresponding Volume Fraction

The results of this study indicate that the application of BESO has a significant impact on the natural frequencies of the system. Specifically, the first natural frequency is increased by 11% as aimed while the second natural frequency is increased by 2.5%, and the third natural frequency is decreased by 6%. The maximum first natural frequency is observed at iteration 41 with a volume fraction of 0.45 and it represents an increase of 11.5% over the full design space frequency. These findings reveal that BESO enhances the first natural frequency remarkably by also offering the advantage of a lighter weight design.

5.4.2 Maximizing the Third Natural Frequency

The third natural frequency is 185 Hz for the full design space structure, and it becomes 165.5 Hz when all elements in the design space are removed from the structure. This decrease of 10,8% shows that the elements in the design space contribute to the torsional stiffness significantly and in order to eliminate this critical drop, BESO is applied to the folding wing structure. Iteration steps and the optimized structure are shown in Figure 5-10 and Figure 5-11, respectively. Optimization took a total of 59 iterations and 3.1 hours.

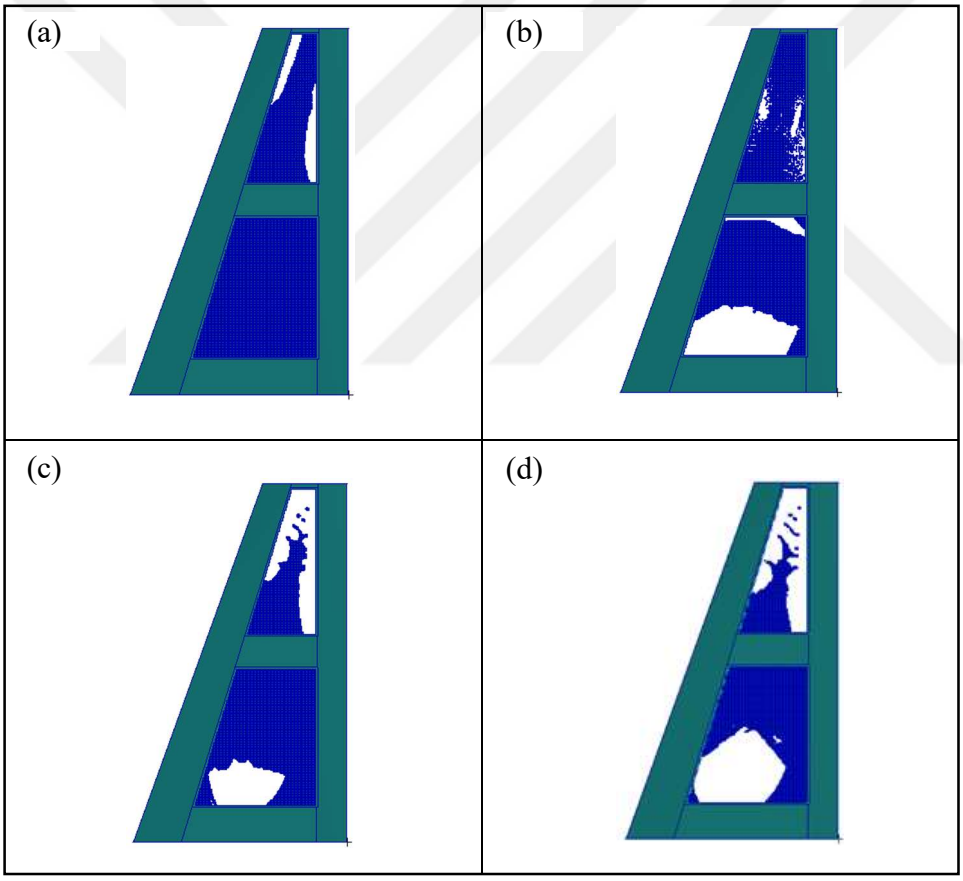


Figure 5-10 Iteration Steps for ω_3 (a) Iter. 15 (b) Iter. 30 (c) Iter. 45 (d) Iter. 59

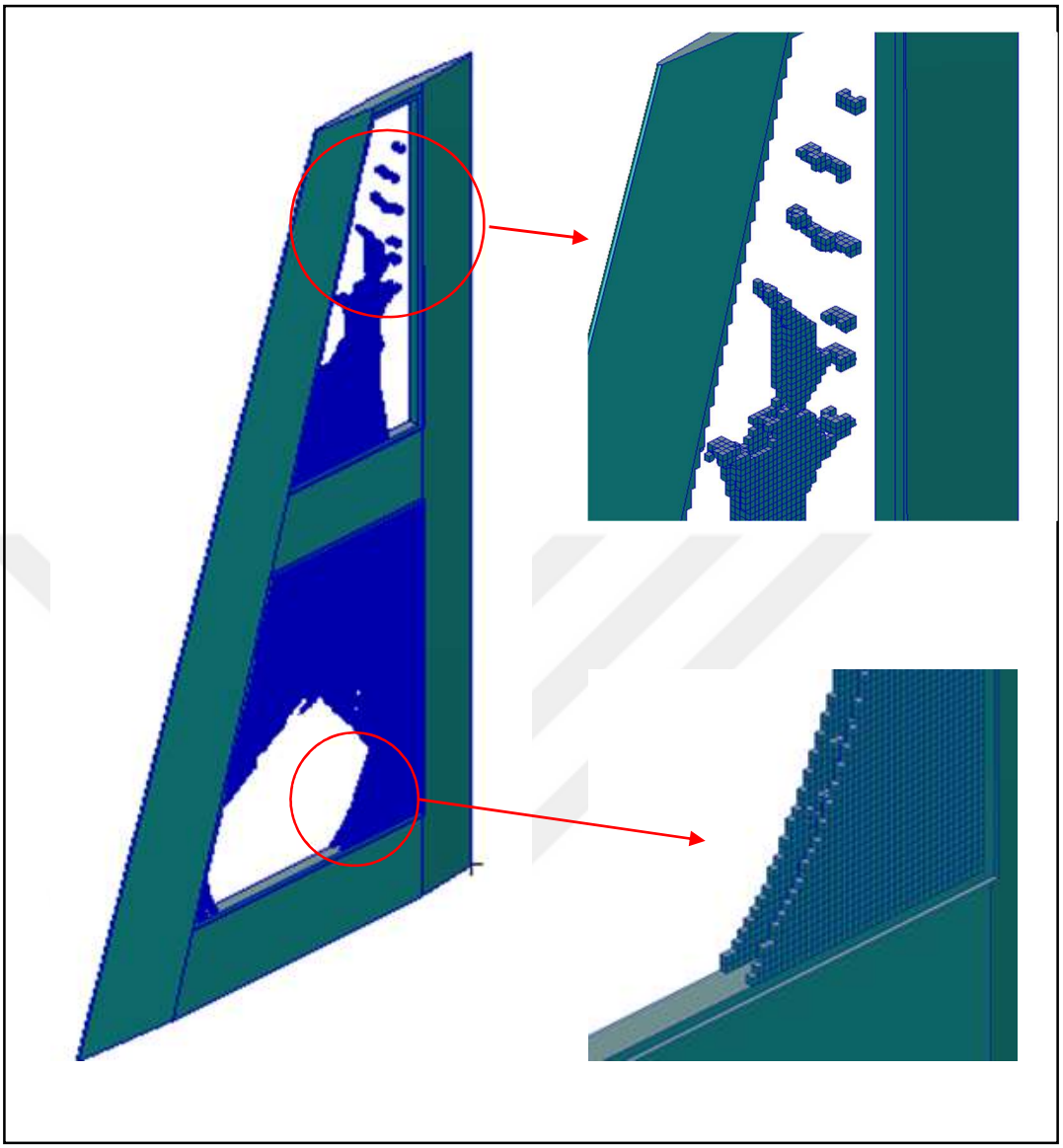


Figure 5-11 Details of the Final Topology at Iteration 59

It should be reminded that outside skin structures are not shown in the figures. The element islets on the outer wing shown in Figure 5-11 are to connect two skin structures. The third natural frequency history is shown in Figure 5-12 while the first and the second natural frequencies which are also calculated for this optimization are given in Figure 5-13 and Figure 5-14.

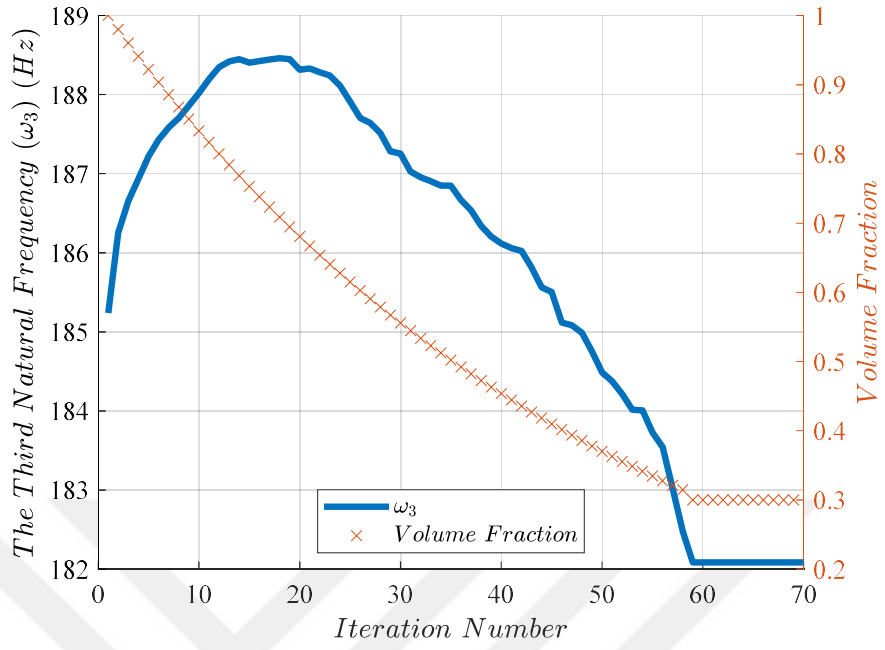


Figure 5-12 Evolution Histories of the Third Natural Frequency and Corresponding Volume Fraction

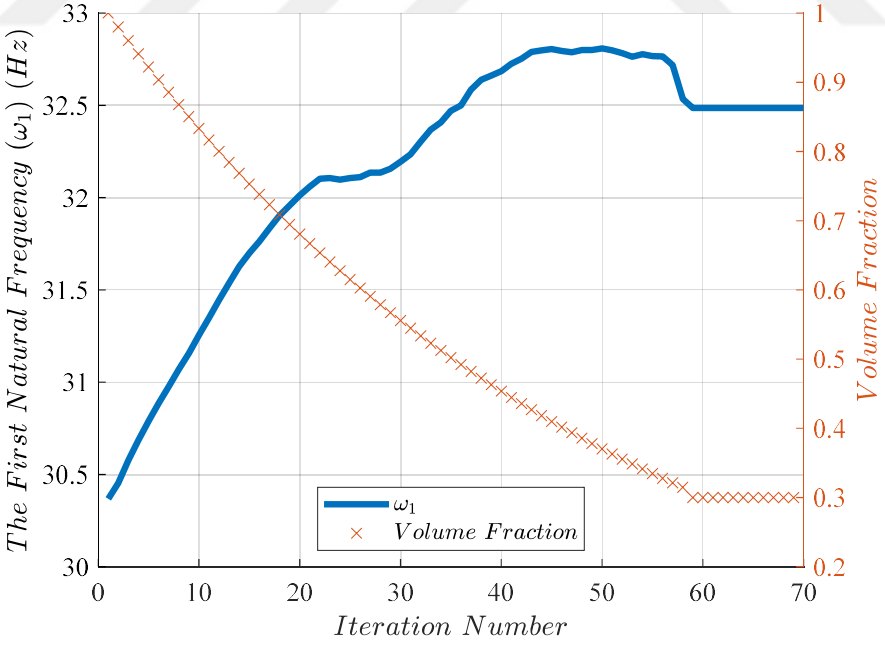


Figure 5-13 Evolution Histories of the First Natural Frequency and Corresponding Volume Fraction

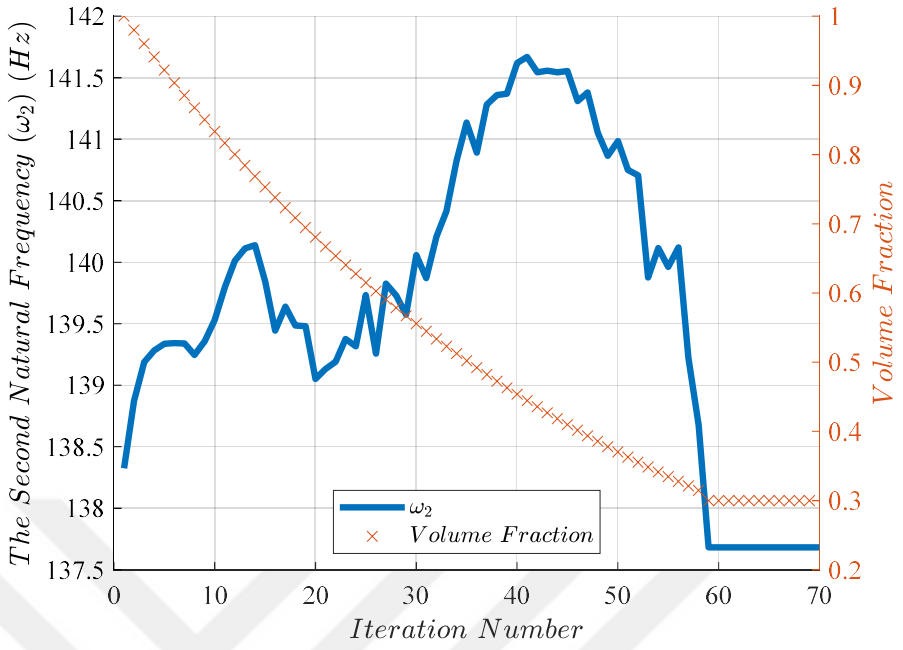


Figure 5-14 Evolution Histories of the Second Natural Frequency and Corresponding Volume Fraction

Although the aim of this study is to maximize the third natural frequency through BESO, there is a 1.7% decrease in the third natural frequency between the full design structure and final structure with a volume fraction of 0.3. However, this decrease does not represent any failure of the algorithm as the third frequency at the end is the highest that can be achieved with a volume fraction of 0.3. This achievement is more evident when a 1.7% decrease is compared with the drop of 10,8% in the third natural frequencies of the full and the empty design space structures. The maximum third natural frequency is observed at iteration 19 with a volume fraction of 0.7 and it represents an increase of 1.7% over the full design space frequency. As a result, the structure is modified in a way to lose 70% of the elements in the design space and has the highest possible third natural frequency. At the same time, the first natural frequency is increased by 7% and the second natural frequency has the relatively same value.

5.4.3 Separation of the Second and the Third Natural Frequencies

Previous studies show that the third frequency tends to decrease and the second frequency to stay the same or increase during the topology optimization with different objectives. This leads these natural frequencies to come closer and it is generally an unwanted situation due to the coupling of modes. To prevent this, a new objective of separating these natural frequencies is identified in this thesis. Iteration steps and the optimized structure are shown in Figure 5-15 and Figure 5-16, respectively. Optimization took a total of 62 iterations and 3.2 hours.

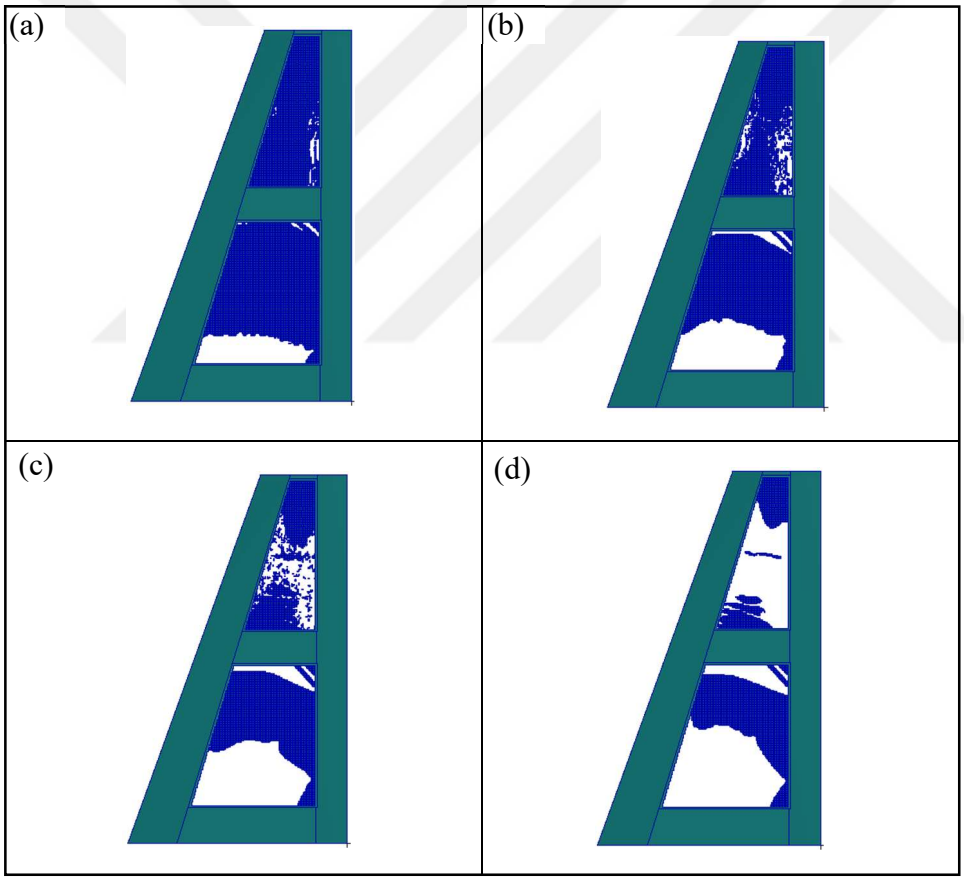


Figure 5-15 Iteration Steps for $\omega_3 - \omega_2$ (a) Iter.15 (b) Iter.30 (c) Iter.45 (d) Iter. 62

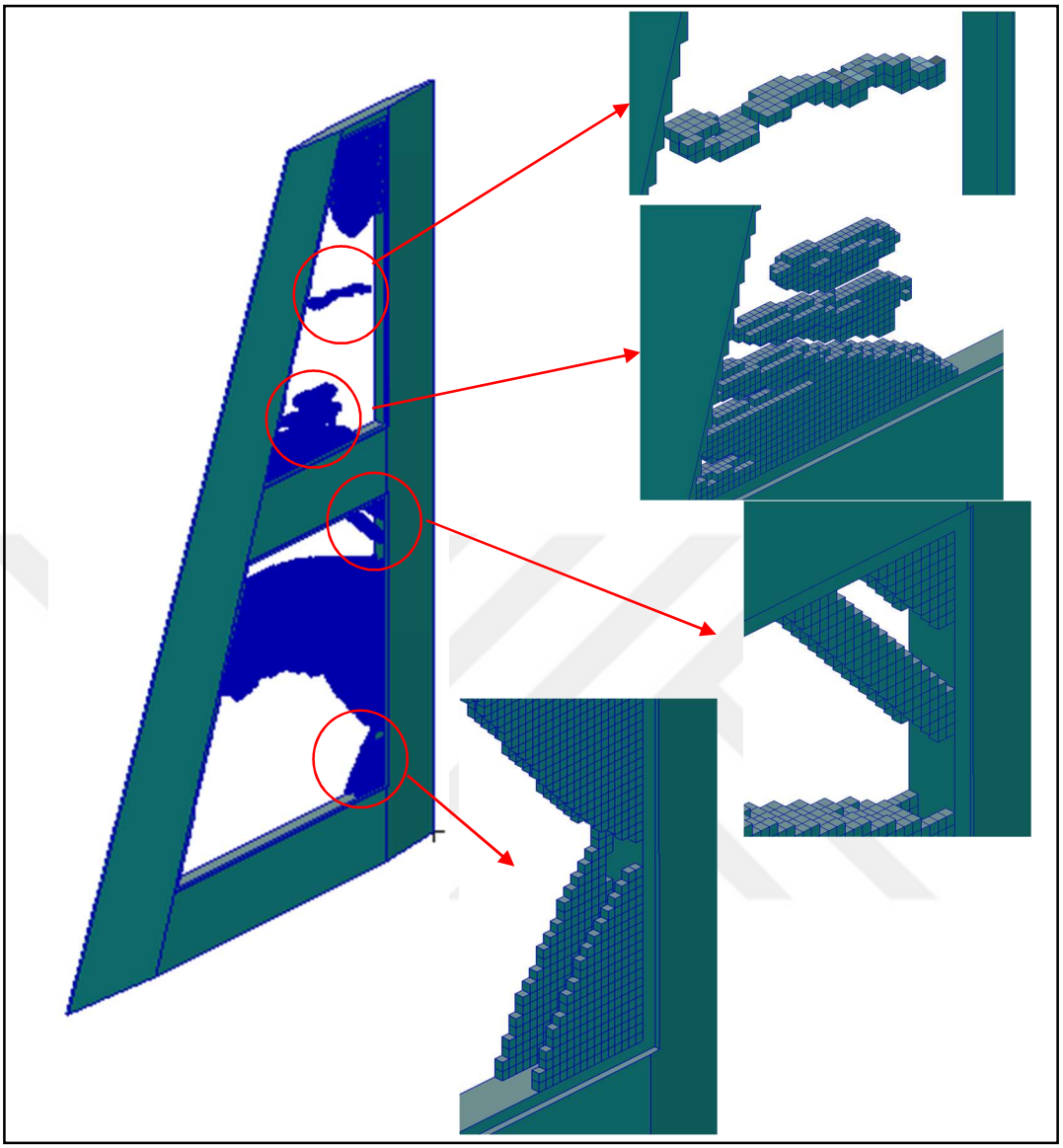


Figure 5-16 Details of the Final Topology at Iteration 62

Similar to the final structure the one before, this topology also has element islets, and these islets connect two skin structures to each other. Evolving histories of the first, second, and third natural frequencies are presented in Figure 5-17, Figure 5-18, and Figure 5-19, respectively. There is an additional plot, Figure 5-20, which shows the frequency separation between the third and the second natural frequencies.

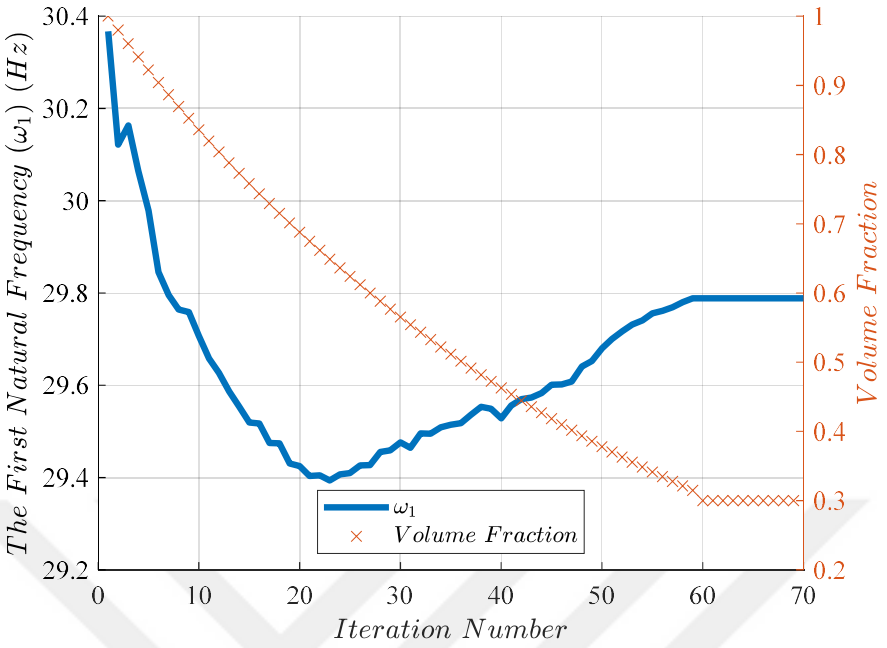


Figure 5-17 Evolution Histories of the First Natural Frequency and Corresponding Volume Fraction

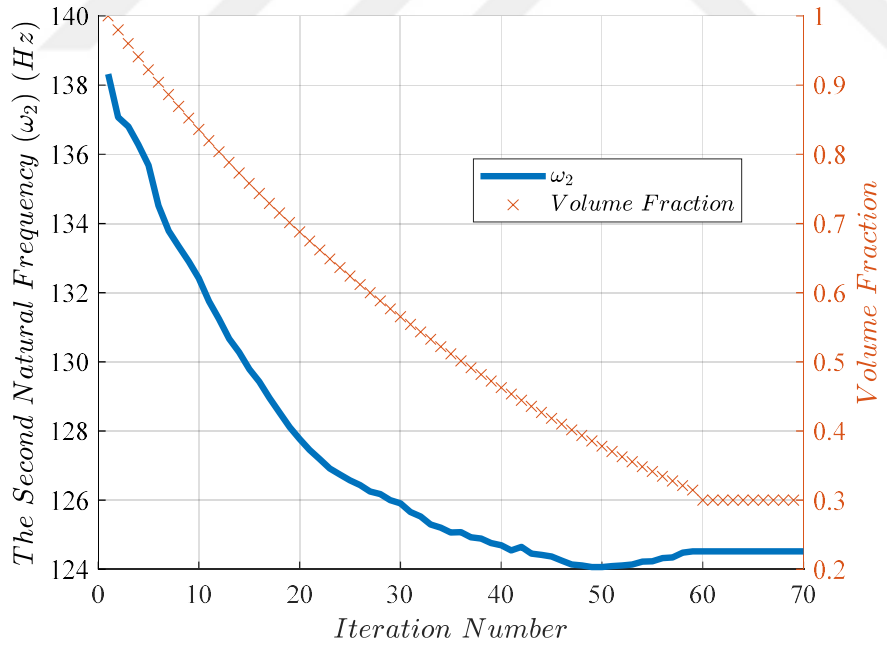


Figure 5-18 Evolution Histories of the Second Natural Frequency and Corresponding Volume Fraction

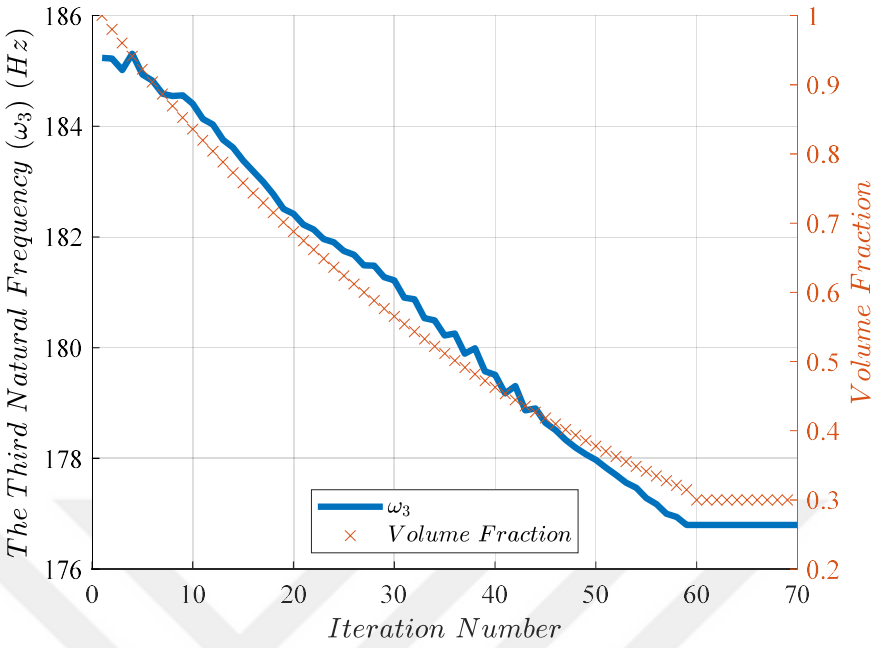


Figure 5-19 Evolution Histories of the Third Natural Frequency and Corresponding Volume Fraction

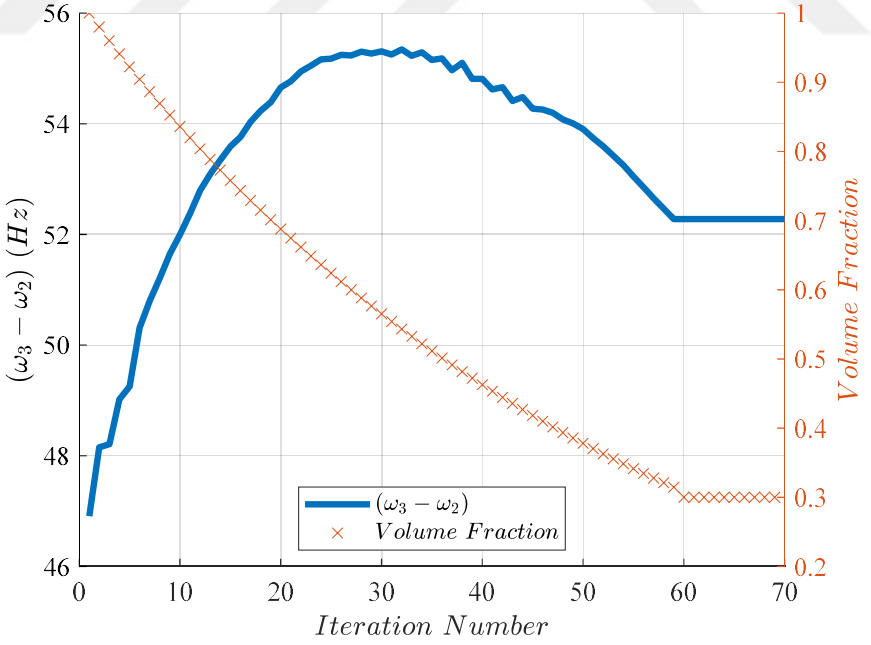


Figure 5-20 Evolution Histories of Frequency Separation and Corresponding Volume Fraction

This study aims to maximize ω_3 while decreasing ω_2 in order to maximize the gap between these frequencies. As desired, ω_2 is decreased by 10% but ω_3 is not increased and in fact, it is also decreased by 5%. Since the decreasing rate of ω_3 is slower than that of ω_2, the gap between them is increased as shown in Figure 5-20 by 12%. One drawback of this study is the decrease of 2% in the first natural frequency which is undesired due to the divergence problem. To prevent this, an extra frequency constraint may be defined in the optimization, or a multi-objective study may then be conducted.

In order to compare the results of all dynamic analyses, including results of maximizing the first natural frequency (Max. (ω_1)), maximizing the third natural frequency (Max. (ω_3)) and maximizing the separation between the third and the second natural frequencies (Max. $(\omega_3 - \omega_2)$), all natural frequencies and the frequency separation are shared in Figure 5-21, Figure 5-22, Figure 5-23, and Figure 5-24.

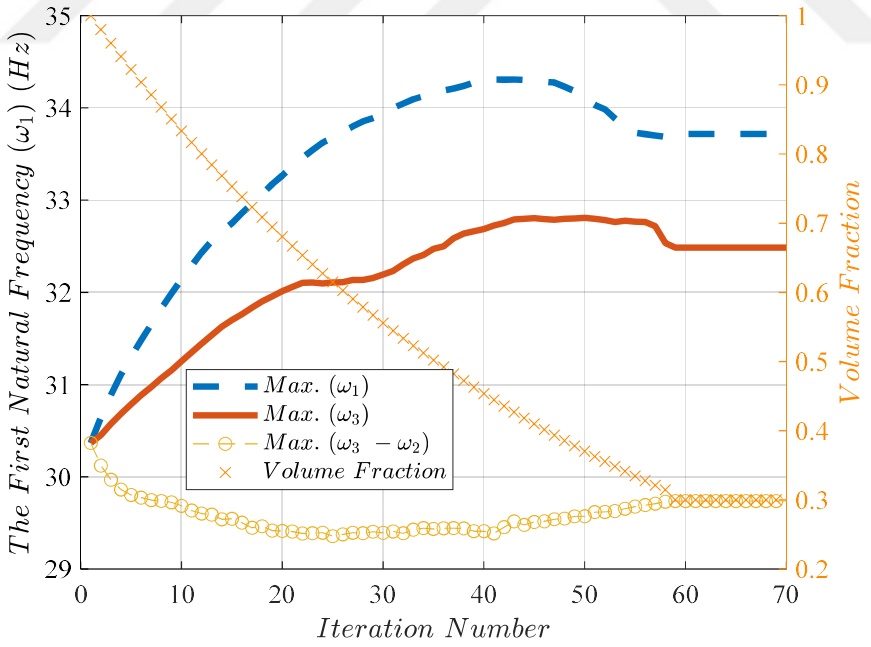


Figure 5-21 Evolution Histories of the First Natural Frequency and Corresponding Volume Fraction

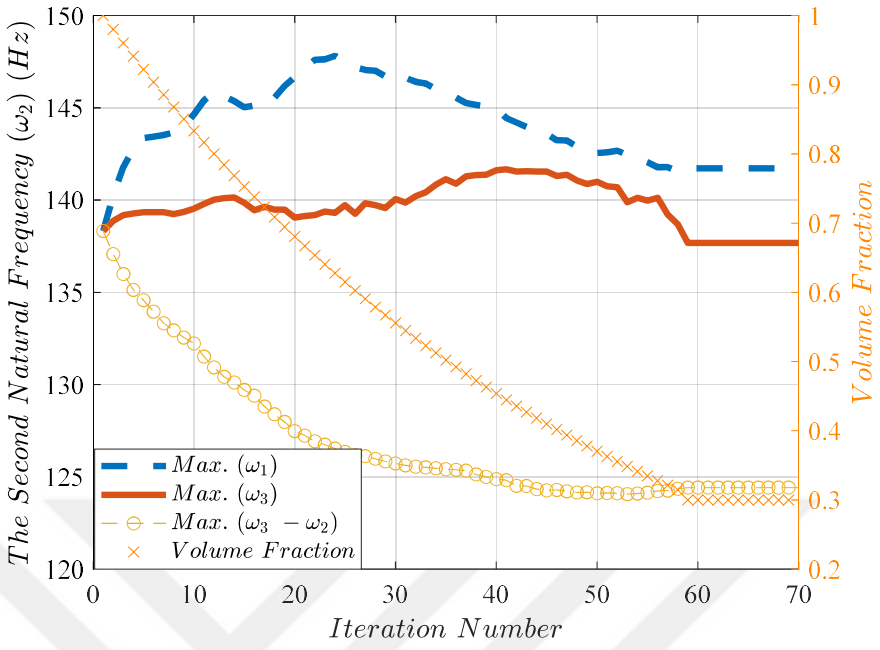


Figure 5-22 Evolution Histories of the Second Frequency and Corresponding Volume Fraction

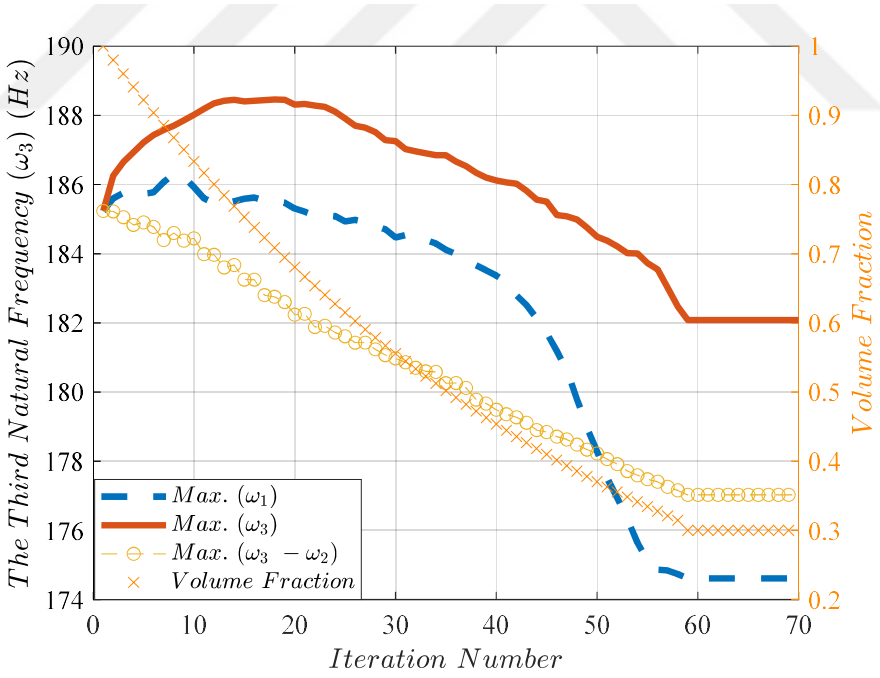


Figure 5-23 Evolution Histories of the Third Frequency and Corresponding Volume Fraction

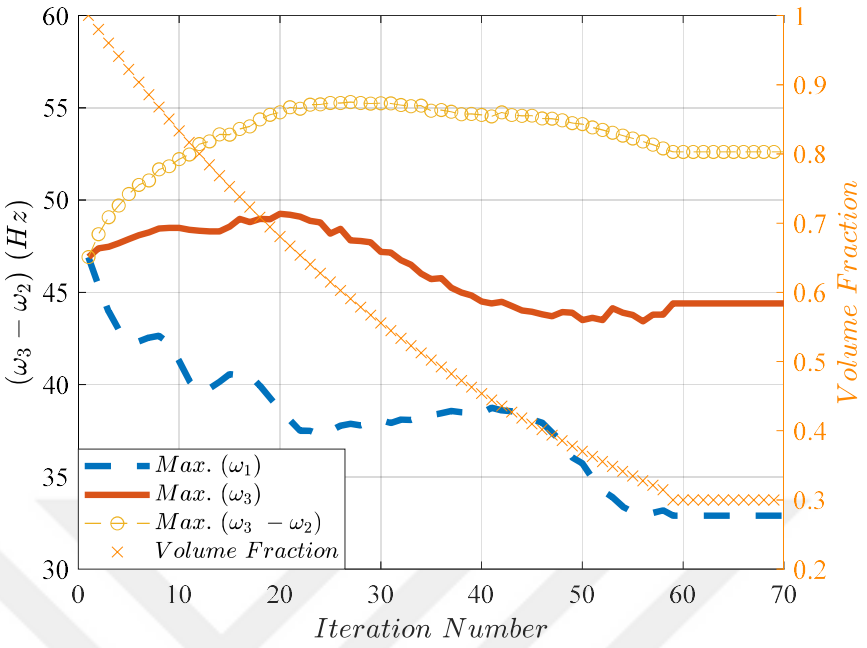


Figure 5-24 Evolution Histories of Frequency Separation and Corresponding Volume Fraction

All of these figures reveal the fact that every case is comparably successful to achieve their objectives by proving that BESO has the effective capability to change the dynamic characteristics of the structure while decreasing its weight. Main remarks from these optimized structures and their converging histories are as follows:

- Similar to the stiffness optimization, the final structures obtained by natural frequency objectives have less number of elements in the middle layer. This trend suggests that elements in the central region contribute less to the calculation of the sensitivity number for all natural frequency objectives and rib-like structures are formed on outer layers as shown in Figure 5-6, Figure 5-11 and Figure 5-16.
- There are some element islets on the outer wing connecting the skin structures (as shown in Figure 5-11 and Figure 5-16) and their presence demonstrates that there is a need for these kinds of connections between skin

structures for the structural integrity. Besides, these islets may provide convenient mechanical interfaces for the attachment of skin structures through fasteners such as bolts or rivets.

- Figure 5-21, Figure 5-22, Figure 5-23 and Figure 5-24 show that Case Max. (ω_1) yield the most favorable results for the first and the second frequencies with the values of $\omega_1 = 33.8$ Hz and $\omega_2 = 141.7$ Hz, while providing comparably lower results for the third natural frequency and the frequency separation.
- On the other hand, Case Max. (ω_3) presents relatively stable performance because there is not any drastic decrease in any frequencies including the frequency separation case.
- Case Max. (ω_3-ω_2) produces the lowest natural frequency values of $\omega_1 = 29.8$ Hz, $\omega_2 = 124.9$ Hz and $\omega_3 = 176.4$ Hz. This situation indicates that this objective shall be selected wisely and all the potential frequency decreases shall be considered.
- When the only aim is maximizing any selected natural frequency or the separation, the given volume fraction constraint shall be considered because final topologies do not provide any maximum objective values. The topologies that provide maximum objective values often require more material than the volume fraction of 0.3 allowed as is clearly seen in Figure 5-21, Figure 5-22, Figure 5-23 and Figure 5-24.

5.5 Multi-objective Study with Stiffness and Separation of Natural Frequencies

In engineering, it is often necessary to consider multiple objectives in the design process and aircraft structures which must be lightweight and able to withstand aerodynamic loads or mechanical components of supersonic missile systems which must withstand manoeuvre loads while minimizing heat transfer, are not the exceptions. In order to address these multi-objective design challenges, multi-

objective topology optimization has emerged as a powerful tool for simultaneously satisfying multiple objectives. This thesis also presents a study of multi-objective optimization with the objectives of maximizing stiffness under Load 1 (the exact worst case) and maximizing the separation between the third and the second natural frequencies.

Teimouri and Asgari presented an informatory study on multi-objective topology optimization for stiffness and frequency with BESO in 2019 which has been already shared in Chapter 2 [26]. They conducted both static and dynamic analyses on the case structure and calculated sensitivity numbers for both objectives separately. Then, they combined these numbers to calculate the total sensitivity number as:

$$\alpha_T^i = c_s * \alpha_s^i + c_w * \alpha_w^i \tag{5-1}$$

where α_T^i is the combined total sensitivity number of the i_{th} element, α_s^i and α_w^i are sensitivity numbers of stiffness and natural frequency of the i_{th} element, respectively.

It is important to note that these single sensitivity numbers should be normalized before combining together due to the magnitude differences between sensitivity numbers of different objectives. c_s and c_s are the weighted coefficients for the stiffness and natural frequency of a system respectively and the sum of these coefficients is equal to 1. When one of these coefficients becomes 1 and the other one becomes 0, the optimization reduces to single-objective. The several topologies with varying coefficients are shared in Figure 2-14 and the same methodology is used in this thesis to find optimum topologies of the folding wing with the stiffness and the natural frequency objectives. Single-objective sensitivity numbers are normalized between 0 and 1 by MATLAB function before calculating the total sensitivity number. ER =2%, $r_{min} = 6$ mm, $AR_{max} = 5\%$, $p = 3$, and $x_{min} = 10^{-6}$ are selected as the main parameters. Optimization took a total of 65 iterations and 7

hours. The main reason for the excessive optimization time stems from dualistic analyses of static and dynamic for every iteration. Five different final topologies are found by changing the values of the weighted coefficient from 0 to 1 with a step size of 0.25. All final results are demonstrated in Figure 5-25.

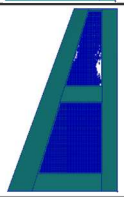
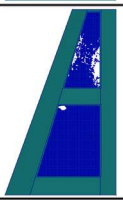
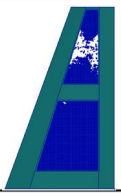
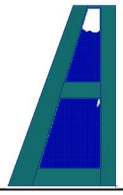
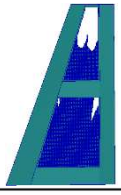
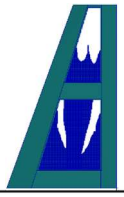
Case		15	30	45	65
A	$c_s = 0,$ $c_w = 1$				
B	$c_s = 0.25,$ $c_w = 0.75$				
C	$c_s = 0.5,$ $c_w = 0.5$				
D	$c_s = 0.75,$ $c_w = 0.25$				
E	$c_s = 1,$ $c_w = 0$				

Figure 5-25 Five Different Multi-objective Topology Optimization Cases with Iterations of 15, 30, 45 and 65

Evolution histories for mean compliance, maximum tip displacement in the y direction and the frequency separation of all cases are shown in Figure 5-26, Figure 5-27 and Figure 5-28.

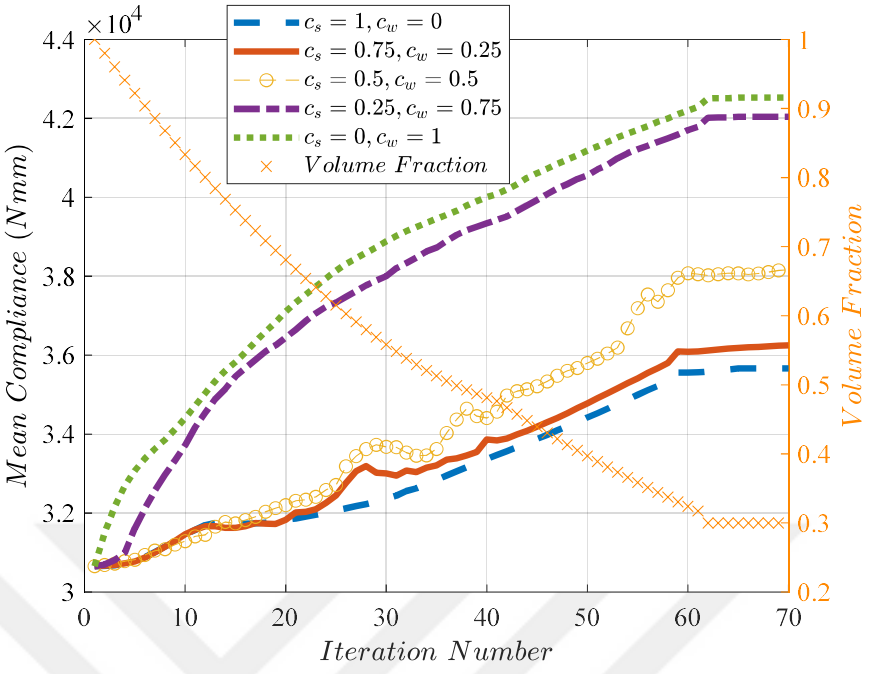


Figure 5-26 Evolution Histories of Mean Compliances and Corresponding Volume Fraction

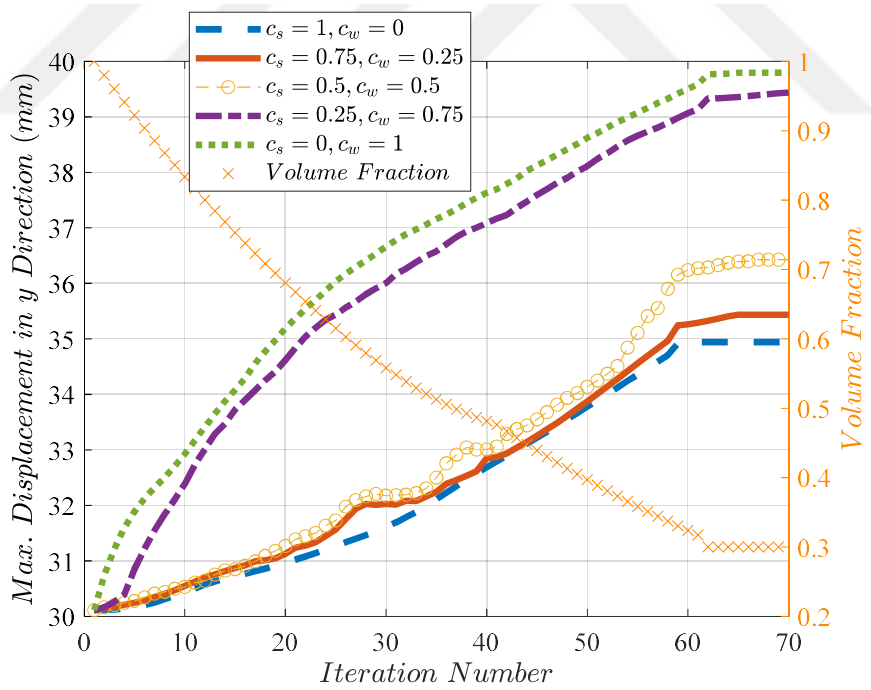


Figure 5-27 Evolution Histories of Maximum Tip Displacements and Corresponding Volume Fraction

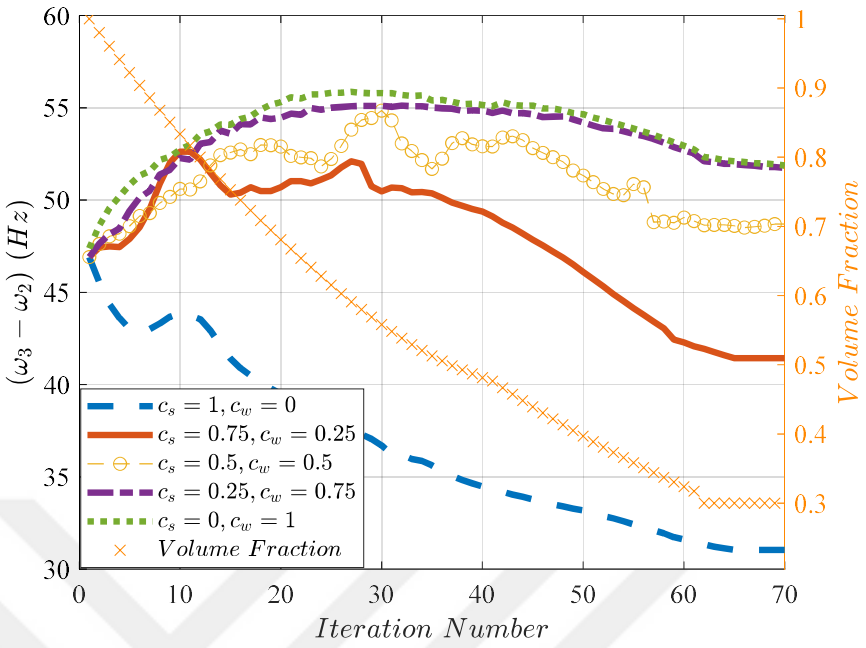


Figure 5-28 Evolution Histories of Frequency Separation and Corresponding Volume Fraction

Mean compliance and the maximum displacement values are resulted as expected. Single-objective stiffness case (Case E) has the minimum compliance (3.57×10^4 Nmm) while the single-objective frequency case (Case A) provides 19% higher mean compliance value (4.25×10^4 N.mm), which is also the maximum mean compliance value compared to other cases. The remaining ones are ordered in the rank of their stiffness coefficients. Similarly, the natural frequencies of all cases are sorted in order except Case B. This case surprisingly provides results which are almost as good as the results of the single-objective frequency case. In addition to these basic outcomes, these figures present rewarding other outcomes such as;

- Case C at the iteration 30 with a volume fraction of 0.56 has superior performance regarding both mean compliance and the natural frequency. Its frequency separation value is just 1.7% below the value of the single-objective frequency case (Case A). At the same time, its compliance is higher than that of the single-objective stiffness case (Case E), by 3.9% percent,

which is a relatively small number compared with the differences between other cases in that particular iteration.

- While all of the cases move in a monotonous way without many fluctuations, Case C has a trend that fluctuates more because it has equal weighted coefficients and these coefficients make this case unstable, unlike the other cases.
- As indicated before, Case A and Case B have almost the same frequency separation at the end (a difference of 0.2%) while the mean compliance of the final topology of Case B is 1.2 % smaller than that of Case A, which means that final topology of Case B has higher stiffness. Figure 5-25 also states that the final topologies of these cases are nearly the same and the difference stems from the inside elements and their orientation.
- Figure 5-29 distinctly exhibits that every final topology except Case E has elements near the tip of the outer wing. Therefore, it is evident that putting material on the tip of the wing increases frequency separation.

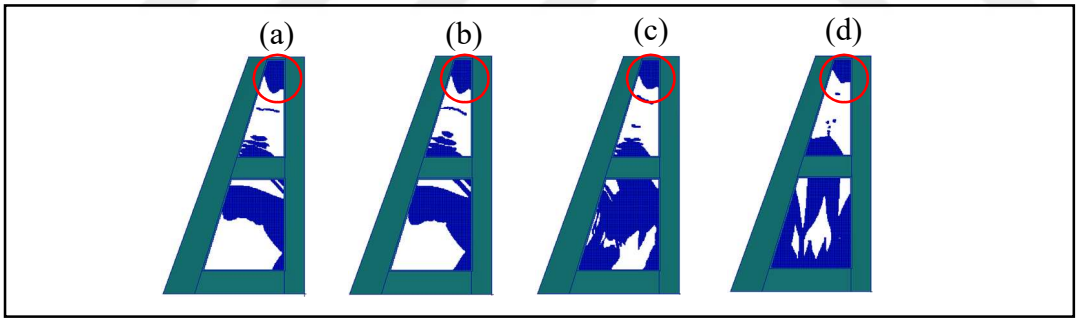


Figure 5-29 Four Different Final Topologies and Elements Near to Tip of the Wing for (a) Case A, (b) Case B, (c) Case C, (d) Case D

To conclude, multi-objective topology optimization presents multiple solutions that can effectively address objectives such as stiffness and frequency concurrently, making it a valuable tool for many engineering challenges aiming for a reduction on the weight of the structures. While the total computation time for multi-objective

optimization may be excessive, the resulting topologies can guide mechanical designers toward optimal design solutions. The versatility of this approach is further enhanced by the ability to adjust the weighted coefficients of sensitivity numbers according to the designer's specific design needs.

5.6 Comparison of All Final Topologies

At the end of this thesis, there are 7 different final topologies with different objectives or different weighted coefficients. Every topology is unique and has its own characteristic, advantages and disadvantages. To compare the mechanical performance of the final topologies, initial full design space structure, empty design space structure, and all the final topologies with natural frequencies and mean compliance values are shown in Table 5-1.

Table 5-1 Summary of All Final Results with Natural Frequency and Mean Compliance Values

	ω_1 (Hz)	ω_2 (Hz)	ω_3 (Hz)	$\omega_3 - \omega_2$ (Hz)	Mean Compliance (N.mm)	Mass (kg)
Full Design Space	30.4	138.3	185.2	46.9	3.07×10^4	12,5
Case A	29.8	124.9	176.4	51.6	4.25×10^4	8,8
Case B	30.0	125.6	177.1	51.5	4.20×10^4	8,8
Case C	31.2	129.7	178.3	48.6	3.80×10^4	8,8
Case D	32.1	135.6	177.0	41.4	3.62×10^4	8,8
Case E	33.7	143.8	174.8	31.0	3.57×10^4	8,8
Case Max. ω_1	33.8	141.7	174.6	32.9	3.61×10^4	8,8
Case Max. ω_3	32.5	137.7	182.1	44.4	3.96×10^4	8,8
Empty Design Space	31.1	137.2	165.4	28.2	4.85×10^4	7,2

There are several conclusions to be drawn from this table. Firstly, it is clear that ω_3 decreases for all cases, even with the objective of maximum ω_3. This means that this particular natural frequency is significantly affected by the removal of the materials. The second remark is about the first natural frequencies of Case E and Case Max. ω_1 as the values are almost the same. Case E is optimized under Load 1 and static deflection under this load closely resembles the first mode shape. This is the main reason for nearly the same first natural frequency values. The last remark is about Case A which is a single-objective case focused on maximizing the gap between the third and the second natural frequencies. It has the highest mean compliance among

all optimization results aside from the empty design space case and this means that the stiffness of Case A is the lowest among all optimization results.

5.7 Conclusion

This chapter presents mainly three different sub-studies which are maximizing the stiffness, manipulating natural frequencies and combining both objectives with a multi-objective topology optimization. In the end, 7 different novel topologies having superior mechanical properties and lightweight designs are achieved. These final results demonstrate that it is possible to have structures which perform effectively under more than one objective. The findings of the multi-objective study contribute to the literature in an important way that there has been a lack of investigation on the 3D structures with several design spaces.

CHAPTER 6

CONCLUSION

6.1 General Conclusions

The main objective of this thesis is to construct an algorithm for topology optimization of a missile folding wing and to demonstrate that the improved mechanical performance of the wing can be achieved through the use of the optimization technique of BESO. The results indicate that the constructed BESO algorithm is able to generate optimized wing designs that exhibit improved structural efficiency compared to the initial topology in the sense of stiffness and natural frequency. As a result, efficient material distributions are obtained by the optimization process, then final topologies are compared with each other via their mechanical performances, and final conclusions concerning the effectiveness of every single optimization study in this thesis are made.

One of the most important achievements of this thesis is to show the potential of BESO for future topology optimization studies in the aerospace industry by demonstrating the effectiveness of this algorithm through the optimization of a folding wing having single and/or multi-objectives. This research is open to other future research on topology optimization of aerospace components in the areas of flutter and advanced topology optimization methods with additional constraints. One of the other contributions of this thesis is to provide results in the area of multi-component design spaces by BESO. The constructed algorithm in this thesis would allow simultaneous optimization of different design spaces such as topologies of inner and outer wing parts. This contribution could represent a significant advancement over existing BESO studies typically focusing on the optimization of single design space.

The accomplishments achieved in this thesis are;

- increasing the first natural frequency of the wing by 11% while the volume of the design space is reduced to 30% of its initial volume,
- increasing the gap between the third and the second natural frequencies by 12% while the volume of the design space is reduced to 30% of its initial volume, and
- presenting a multi-objective study with the objectives of stiffness and natural frequency resulting to several topologies which perform efficiently for both objectives simultaneously.

6.2 Recommendations for Future Work

This thesis provides a valuable insight about the full potential of BESO method and offers promising directions for future work in this particular area. These possible further studies can be listed as:

- Performing flutter analysis: Static frequency separation can be done by BESO and it can be beneficial to avoid flutter. The current constructed algorithm by BESO can be upgraded to a new version including flutter analysis in every iteration and the final topology with the highest flutter speed can also be achieved.
- Including von Mises stress and buckling failure: To ensure the suitability of the structures for use in various aerospace applications, it is crucial to consider both von Mises stress and buckling failure. This study, however, does not take these parameters into account. Future research may include these factors as constraints to seek more realistic outcomes.
- Adopting different mesh types: The current algorithm just works with structured hex-type elements. This algorithm can be upgraded to work with

different mesh types such as unstructured or tetrahedron in order to make the optimization process more versatile.

- Creating complex geometries: The wing structure in this thesis is a simplified version of the real wing by removing springs and mechanical fasteners. They can be implemented to the structure to have more complex but realistic results.
- Introducing different load cases: The folding wing can be studied during the first opening sequence before locking by the spring-loaded pins or with different manoeuvre loads of the missile. This work can increase the reliability of this folding wing since it would be optimized for many load cases and conditions.
- Utilizing additive manufacturing techniques: One of the constraints of this thesis is manufacturability by conventional methods. This restricts the manufacturing of complex topologies with higher mechanical properties. Recently developed many additive manufacturing methods promise to produce complex geometries by using metals and additive layers. Although constructed BESO algorithm is able to generate complex topologies with higher mechanical performance, they are all neglected during this thesis due to manufacturability constraints. These neglected topologies can be used in different studies by using any additive manufacturing methods.

REFERENCES

[1] https://www.roketsan.com.tr/tr/urunler/atmaca-gemisavar-fuzesi

[2] Chang, D. J. (1995). Prediction of Stress Relaxation for Compression and Torsion Springs. Aerospace Corp El Segundo CA Technology Operations

[3] Maxwell, C. (1869), Scientific Papers, Vol. 2, , Dover Publications, New York, 1952, pp. 175-177.

[4] Michell, A. G. M., (1904) "The Limits of Economy of Material in Frame Structures," Philosophical Magazine, Series 6, Vol. 8

[5] Schmit, L.A. (1960) Structural design by systematic synthesis, Proc. 2nd Conference on Electronic Computation, ASCE, New York, pp. 105-122.

[6] Vanderplaats, G. N. (1982). Structural optimization-past, present and future. AIAA journal, 20(7), 992-1000

[7] Boyle, C. (2010). Computational Study of Wolff's Law Utilizing Design Space Topology Optimization: A New Method for Hip Prosthesis Design.

[8] Bendsoe M.P. (1989) Optimal shape design as a material distribution problem. Structural Optimization 1(4):193–202

[9] Rozvany G.I.N. and Zhou M. (1991) "Applications of COC method in layout optimization". In: Eschenauer H, Mattheck C and Olhoff N (Eds.) Proc. Conf. "Eng. Opt. in Design Processes" (Karlsruhe 1990), Berlin, Springer-Verlag, , pp. 59-70.

[10] Rozvany, G.I.N., Zhou, M. & Birker, T. (1992) Generalized shape optimization without homogenization. Structural Optimization 4, 250–252

[11] Z. Luo, J. Yang, L. Chen (2006). A New Procedure for Aerodynamic Missile Designs Using Topological Optimization Approach of Continuum Structures. Aerospace Science and Technology (vol. 10, pp. 364-373).

[12] Eves, J., Toropov, V., Thompson, H.M., Gaskell, P.H., Doherty, J.J., & Harris, J. (2009). Topology optimization of aircraft with non-conventional configurations.

[13] Oktay, E., Akay, H. U., & Sehitoglu, O. T. (2014). Three-dimensional structural topology optimization of aerial vehicles under aerodynamic loads. Computers Fluids, 92, 225–232.

[14] Bendsøe, M.P., & Kikuchi, N. (1988). Generating optimal topologies in structural design using a homogenization method. Applied Mechanics and Engineering, 71, 197-224.

[15] Munk, D.J., Vio, G.A., & Cooper, J.E. (2017). Optimisation of representative aircraft wing geometries with an experimental validation.

[16] Xie Y.M., Steven G.P. (1993) A simple evolutionary procedure for structural optimisation. Computers & Structures 49:885–896

[17] Xie Y.M., Steven G.P. (1994) A simple approach to structural frequency optimization. Computers & Structures 53:1487–1491

[18] Xie Y.M., Steven G.P. (1996) Evolutionary structural optimization for dynamic problems. Computers & Structures 58:1067–1073

[19] Das, R., & Jones, R. (2011). Topology optimisation of a bulkhead component used in aircrafts using an evolutionary algorithm. In L. Vergani,

& M. Guagliano (Eds.), Proceedings of the 11th International Conference on the Mechanical Behavior of Materials

[20] Querin, O.M., Steven, G.P., & Xie, Y.M. (1998). Evolutionary structural optimisation (ESO) using a bidirectional algorithm. Engineering Computations, 15, pp. 1031-1048.

[21] Huang X, Xie Y.M. (2010) Evolutionary topology optimization of continuum structures. Wiley

[22] Yang X.Y., Xie Y. M., Steven G. P., and Querin O. M. (1999). Bi-directional evolutionary method for stiffness and displacement optimisation. AIAA Journal 1999 37:11, 1483-1488

[23] Huang, X. and Xie, Y.M. (2007) Convergent and Mesh-Independent Solutions for the Bi-Directional Evolutionary Structural Optimization Method. Finite Elements in Analysis and Design, 43, 1039-1049.

[24] Munk, D.J (2018). A bi-directional evolutionary structural optimization algorithm for mass minimization with multiple structural constraints. International Journal for Numerical Methods in Engineering. 118.

[25] Munk, D.J & Auld, D. & Steven, G.P. & Vio, G. (2019). On the benefits of applying topology optimization to structural design of aircraft components. Structural and Multidisciplinary Optimization. 60.

[26] Teimouri, M. & Asgari, M.. (2019). Multi-Objective BESO Topology Optimization Algorithm of Continuum Structures for Stiffness and Fundamental Natural Frequency. Structural Engineering & Mechanics. 72. 181-190.

[27] Sethian J.A., Wiegmann A. (2000) Structural boundary design via level set and immersed interface methods. J Comput Phys 163(2):489

[28] Mirjalili, S. & Lewis, A. (2014). Grey Wolf Optimizer. Advances in Engineering Software. 69. 46–61.

[29] Askarzadeh, A. (2016). A novel metaheuristic method for solving constrained engineering optimization problems: Crow search algorithm. Computers & Structures. 169. 1-12.

[30] Kennedy J., Eberhart R. (1995) Particle swarm optimization, in Neural Networks. In: Proceedings, IEEE international conference on; 1942–1948, 1995. p.

[31] Bonabeau E, Dorigo M, Theraulaz G. (1999.) Swarm intelligence: from natural to artificial systems: OUP USA;

[32] Dorigo, M., Birattari, M., & Stutzle, T. (2006). Ant colony optimization. IEEE computational intelligence magazine, 1(4), 28-39.

[33] Luh, Guan-Chun & Lin, Chun-Yi. (2010). A Binary Particle Swarm Optimization for Structural Topology Optimization. 2012 Fifth International Joint Conference on Computational Sciences and Optimization.

[34] Jaafer, A. & Al-Bazoon, M. & Dawood, A. (2020). Structural Topology Design Optimization Using the Binary Bat Algorithm.

[35] Rozvany, G.I.N. (2009) A critical review of established methods of structural topology optimization. Structural and Multidisciplinary Optimization. 37, 217–237.

[36] Sigmund, O., Maute, K. (2013) Topology optimization approaches. Structural and Multidisciplinary Optimization. 48, 1031–1055.

[37] Sigmund, Ole. (2011). On the usefulness of non-gradient approaches in topology optimization. Structural and Multidisciplinary Optimization. 43. 589-596.

[38] Huang, X., Xie, Y.M. (2009) Bi-directional evolutionary topology optimization of continuum structures with one or multiple materials. Computational Mechanics 43, 393–401.

[39] Ürün A., Şahin M. ve Gürses E. (2022), Katlanabilir Füze Kanadının Direngenlik Kıstasına Göre Yapısal Eniyilemesi, UHUK 2022 (*in Turkish*)

APPENDICES

A. Reference Studies

Several benchmark studies are conducted in order to test the constructed algorithm in this thesis.

A.1 Michell Type Structure

Xie and Steven used Michell Type Structure to exemplify the capability of ESO Method in 1993 [16]. They modeled the structure in Figure 8-1 by 50 x 25 four node elements, Young's Modulus and Poisson's ratio are given as 100GPa and 0.3, respectively. This structure is supported by two simple supports and its thickness is 10 mm. The initial rejection ratio (*RR*) is selected as 1% and the evolutionary rate (*ER*) is selected as 0.5%. 1000 N is applied from the middle and the structure is stressed. Elements are ranked according to their von Mises stress values. The aim of this study is to optimize this structure under the specified load until it reaches *RR*s of 5%, 10%, 15%, 20% and 25%, which means the ratio of the stress value of any element to maximum stress in the structure. When *RR* is higher, the stress values of elements are close to the maximum level, which provides more efficient topologies.

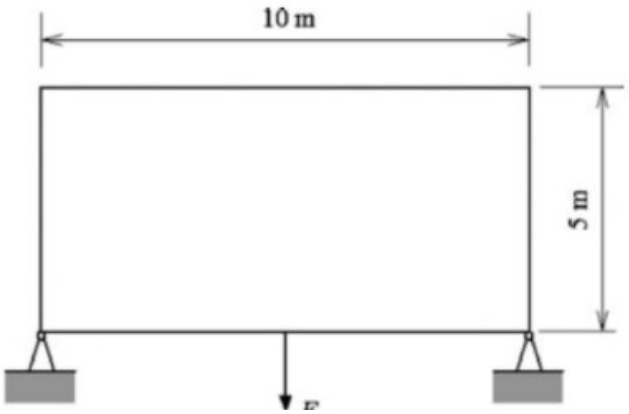
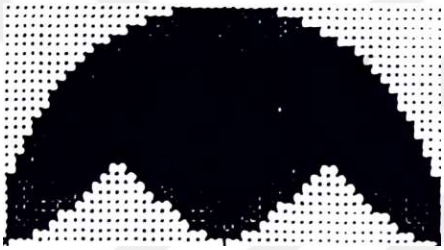
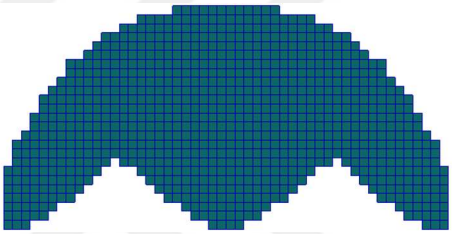
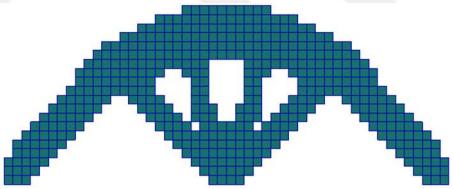
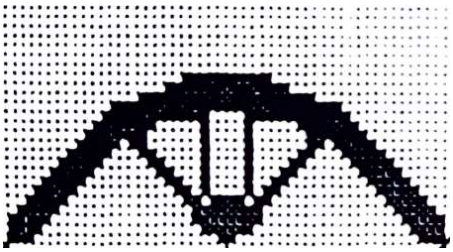
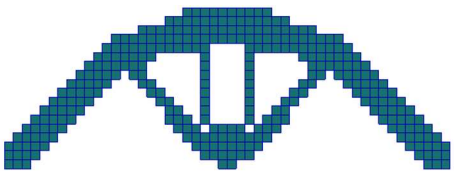
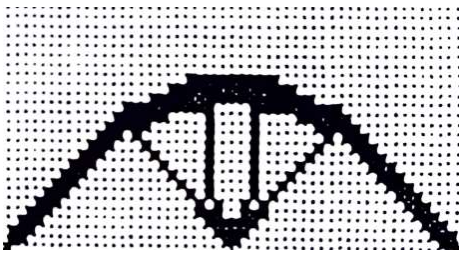
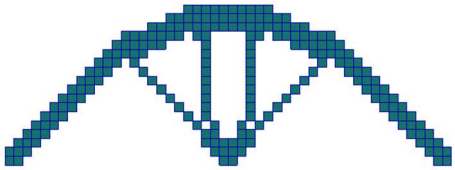


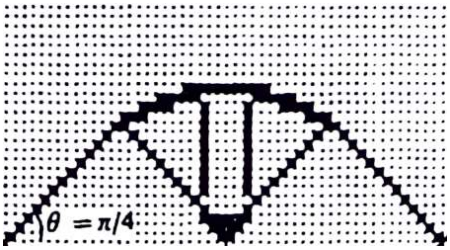
Figure 8-1 Simple Structure with Two Simple Supports [16]

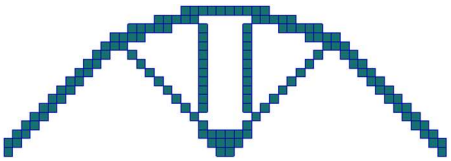
Table 8-1 shows the comparison between the resulting topologies of Xie and Steven's study and the constructed algorithm used in this thesis. It clearly indicates that this algorithm performs efficiently on 2D structures with ESO method. The whole optimization process took 171 iterations and 43 minutes.

Table 8-1 Comparison between reference study [16] and constructed algorithm for ESO

RR	**Xie and Steven** [16]	**Algorithm used in this thesis**
5%		
10%		
15%		
20%		

25%





A.2 2D Cantilever Beam

Huang and Xie conducted a BESO analysis on a cantilever beam which is fixed from one end (Figure 8-2) and 100 N downward force is applied on the center of the other end [21]. The aim is decreasing the volume of the structure to half of the initial volume while preserving its stiffness as much as possible using strain energy values of the elements. The structure is discretized to 160 x 100 four node stress elements and its thickness is 1 mm. BESO parameters are selected as $\mathrm{ER} = 1\%,\ \mathrm{p} = 3,\ r_{min} = 3\ mm$ and $AR_{max} = 5\%$. Young's modulus and Poisson's ratio are 100 GPa and 0.3, respectively.

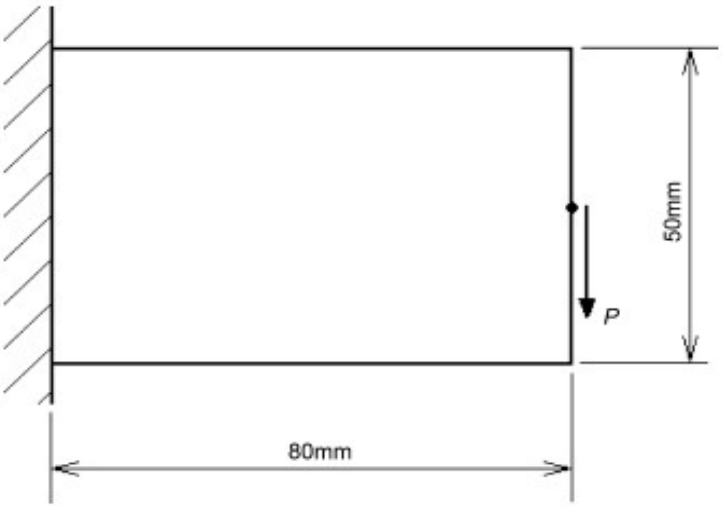


Figure 8-2 Cantilever Beam [21]

Table 8-2 Comparison between reference study [21] and constructed algorithm for BESO

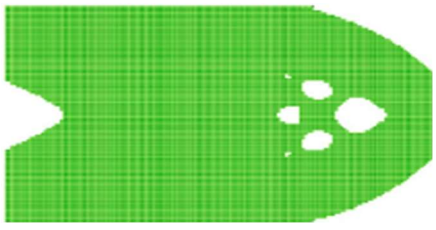
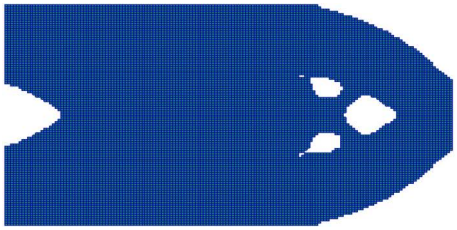
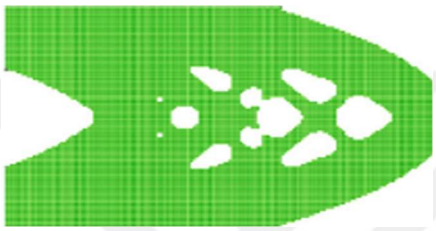
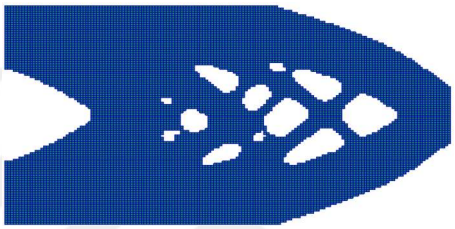
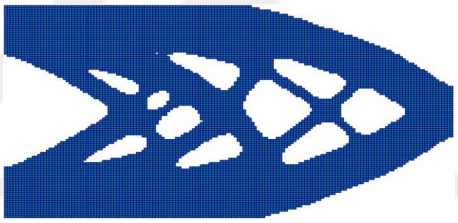
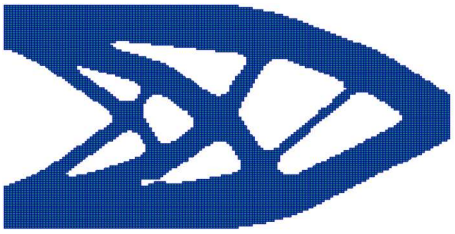
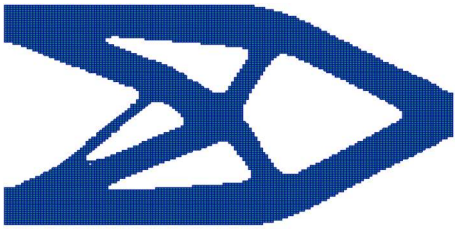
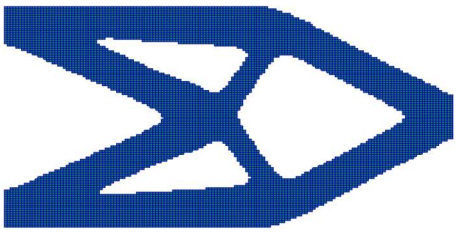
Iter. No.	Huang and Xie [21]	Algorithm in this thesis
15		
30		
45		
60		
79		
100		

Table 8-2 shows the results from both the mentioned study and the algorithm used in this thesis. The main differences are iteration numbers and evolving histories. The reason for these differences is that Huang and Xie used hard-kill BESO while the constructed algorithm used soft-kill BESO. In the end, the final topologies are the same with the same mean compliance of 1.87 N.mm. The total iteration number is 102 and the total computational time is 1.5 hours. This case study demonstrates that the algorithm provides results that are the same with the literature using soft-kill BESO for stiffness optimization.

A.3 3D Cantilever Beam

The algorithm must be tested on 3D structures as the target structure in this thesis is designed and optimized as a 3D. However, optimizing 3D structures can be more challenging due to constructing a proper filter scheme by creating a sphere with a radius of r_{min}. To test the 3D optimizing capability of the algorithm, the structure in Figure 8-3 is optimized until its final volume is 10% of the initial volume while minimizing its compliance. The material properties are given as E=10 GPa and ν=0.3. The half of the structure is modeled solely by using 40000 eight node elements since it is a symmetric structure and computational time is less by this way. BESO parameters are determined as ER $= 3\%$, p $= 3$, $r_{min} = 3\ mm$ and $AR_{max} = 50\%$.

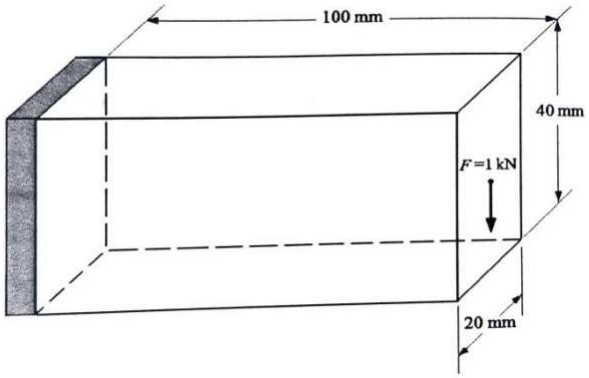


Figure 8-3 3D Cantilever Beam [21]

Table 8-3 Comparison between reference study [21] and constructed algorithm for 3D BESO

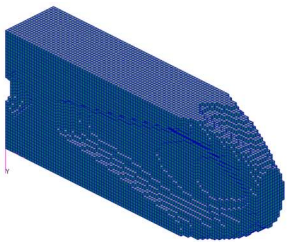
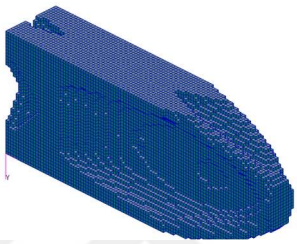
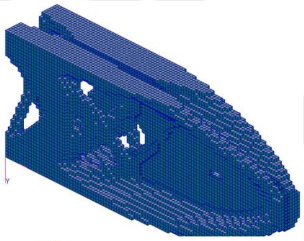
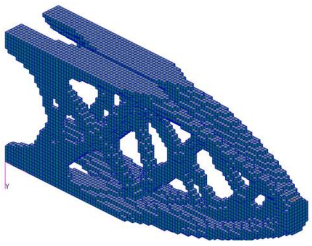
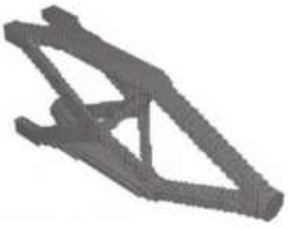
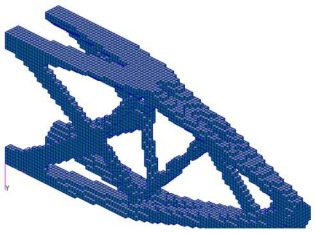
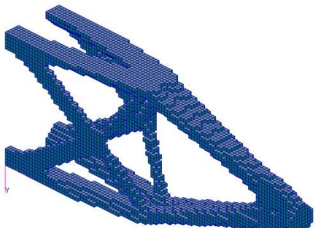
Iter. No.	Huang and Xie [21]	Algorithm used in this thesis
15		
30		
45		
60		
80		
100		

Table 8-3 demonstrates the same outcome with the 2D cantilever beam study. Those final topologies are almost the same but evolving histories are different due to soft-kill and hard-kill BESO differences. Since the final topologies are close enough, this case study proves that the constructed algorithm in this thesis can find well optimized topologies by BESO even for 3D structures. It took 100 iterations and 3.2 hours to optimize this 3D structure by this algorithm.

B. 3D Cantilever Beam Mesh-independency Study

BESO method is characterized by its mesh-independence which denotes the capability of the method to perform the optimization process without the need for a specific discretization of the design. This feature allows more flexibility in the design process, enables the efficient handling of highly complex geometries and makes BESO a versatile tool for structural optimization. Huang and Xie shared a mesh independence study to prove BESO is mesh-independent [23]. The related study is shared in Figure 8-4. In this thesis, mesh-independency of BESO is investigated by using the 3D Cantilever Beam Structure in Appendix A.3. Three different meshing are used and results are shared in Table 8-4. Exact meshing is from Appendix A.3 and there are additional coarse and fine mesh cases.

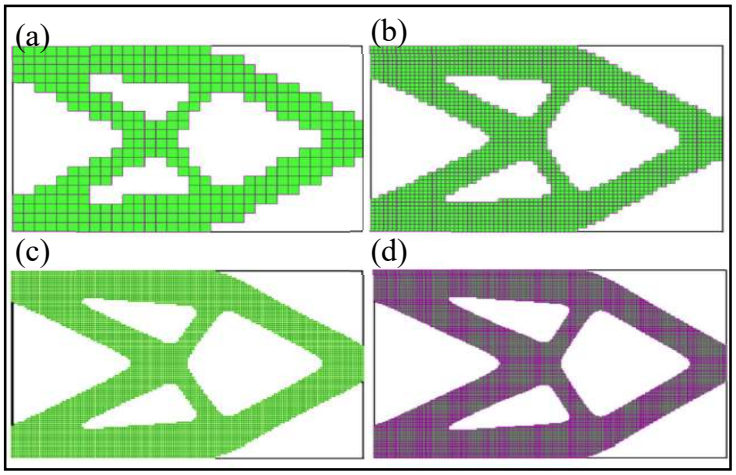
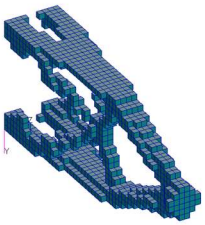
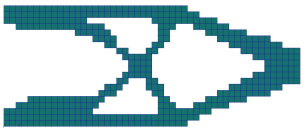
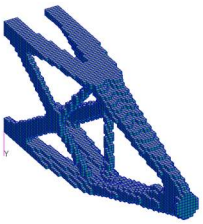
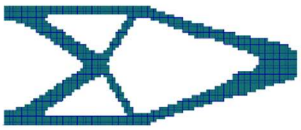
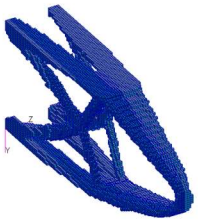
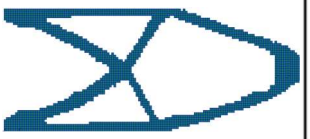


Figure 8-4 Mesh-independent Solutions of (a) 32x20, (b) 80x50, (c) 160x100, (d) 240x150 [23]

Table 8-4 Mesh-independency Results

Mesh	Isometric View	Left View	Mean Compliance (Nmm)
Coarse (50 x 2 x 5)			1680
Exact (100 x 40 x 10)			1664
Fine (133 x 53 x13)			1660

Results clearly state that BESO is not "fully" mesh-independent. The final topologies of coarse and fine mesh are not the same. Even though differences between final topologies are minor, selecting a finer mesh provides better and smoother results which provide more details about the design. However, it is always important to consider the computational time since topology optimization requires static or dynamic finite element analysis for every iteration. Selecting overly fine mesh may lead to excessive computational time, which is an undesired situation for most engineering problems.

C. Minimum Filter Radius Selection

Investigation for minimum filter radius (r_{min}) is done and results of 4 mm, 6 mm, 8 mm are shared in Figure 8-5, Figure 8-6 and Figure 8-7. Figure 8-8 and Figure 8-9 shows the evolution histories of mean compliance and maximum displacement values of these three cases. ER =1%, $AR_{max} = 5\%$, $p = 3$, and $x_{min} = 10^{-6}$ are the other common parameters.

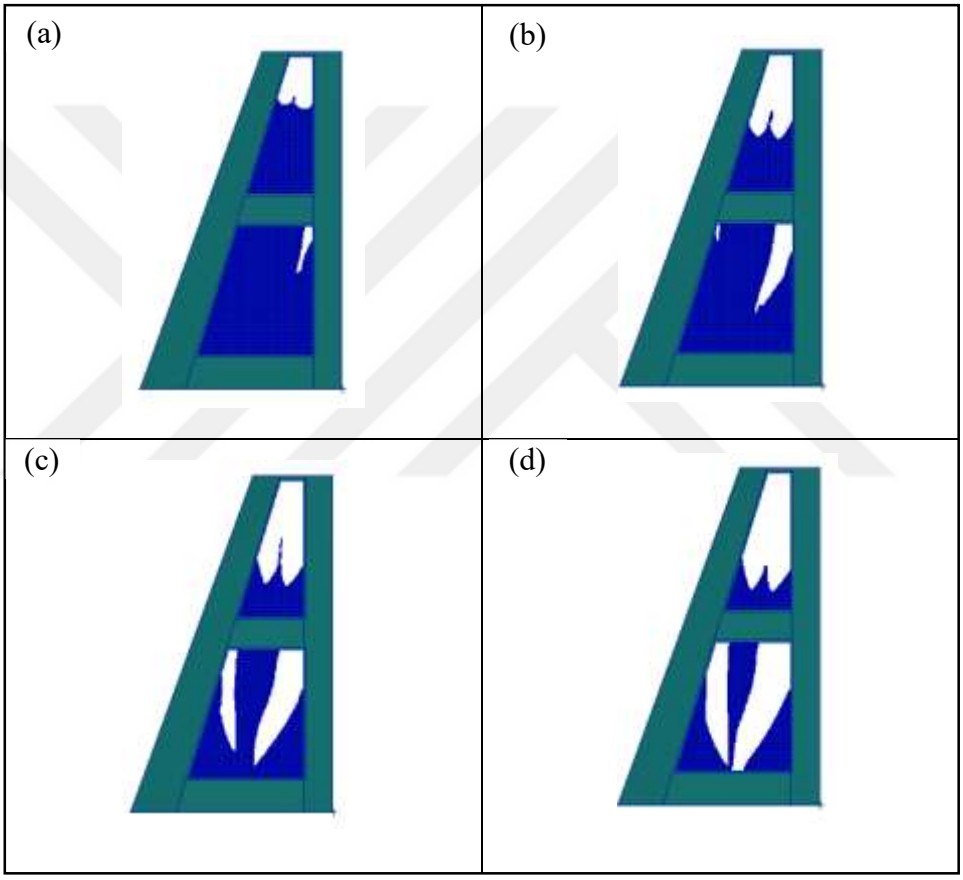


Figure 8-5 Iteration Steps for $r_{min} = 8\ mm$ (a) Iter. 30 (b) Iter. 60 (c) Iter. 90 (d) Iter. 120

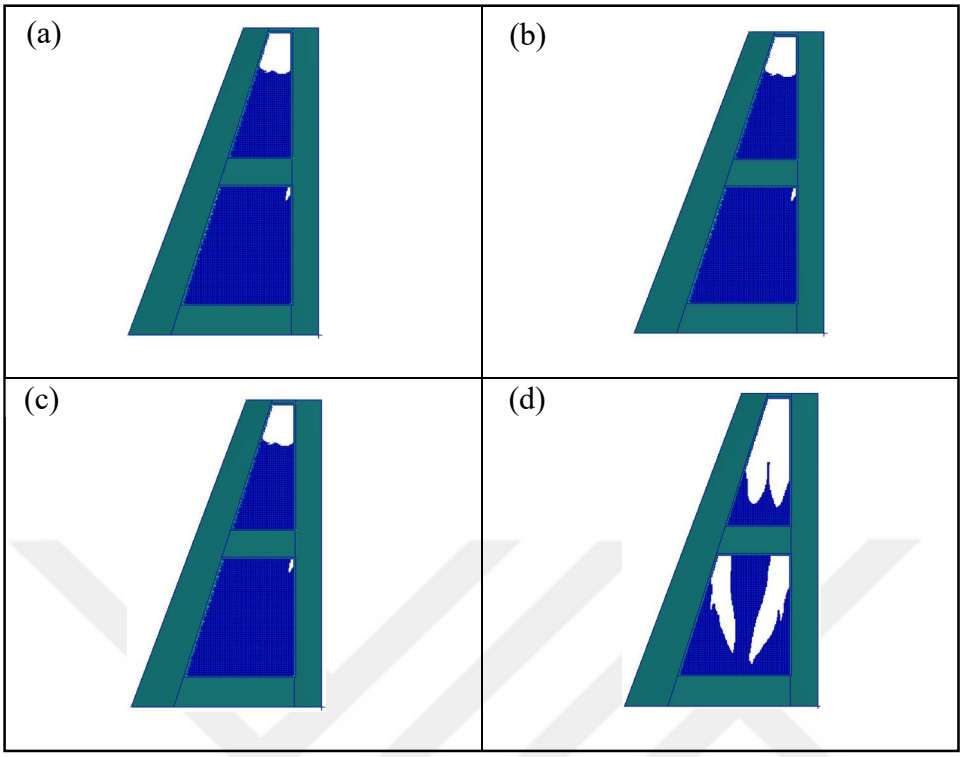


Figure 8-6 Iteration Steps for $r_{min} = 6\ mm$ (a) Iter. 30 (b) Iter. 60 (c) Iter. 90 (d) Iter. 120

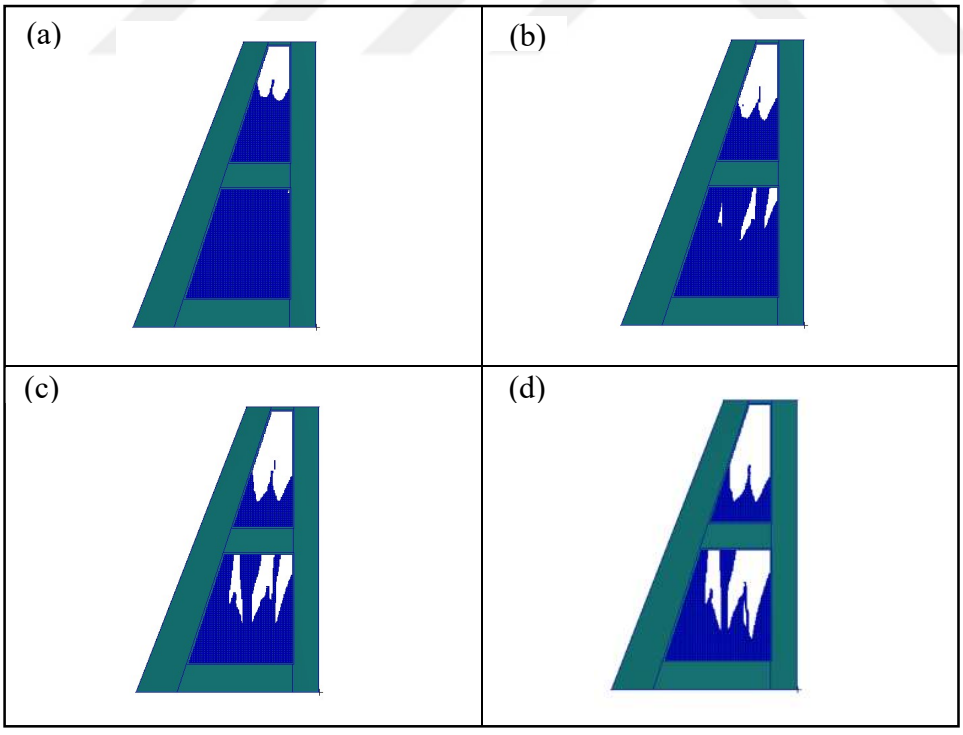


Figure 8-7 Iteration Steps for $r_{min} = 4\ mm$ (a) Iter. 30 (b) Iter. 60 (c) Iter. 90 (d) Iter. 120

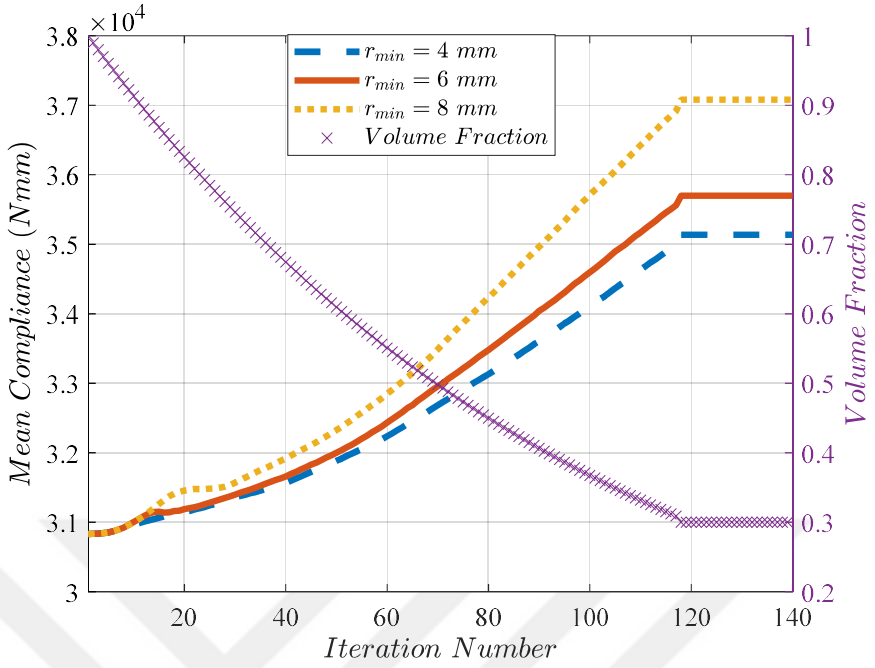


Figure 8-8 Evolution Histories of Mean Compliance and Corresponding Volume Fraction

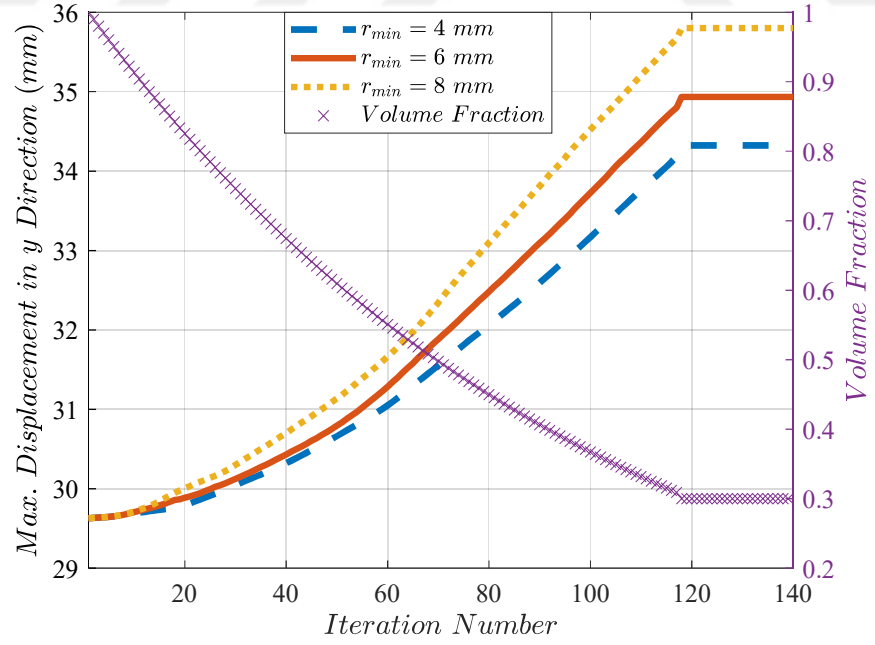


Figure 8-9 Evolution Histories of Maximum Tip Displacement and Corresponding Volume Fraction

Figure 8-8 and Figure 8-9 clearly demonstrate that mean compliance is minimum for $r_{min} = 4\ mm$ Case, which means that the final topology of this case has the maximum stiffness. However, this topology has some areas (Figure 8-10) which are complex and not suitable for conventional chip removal manufacturing methods.

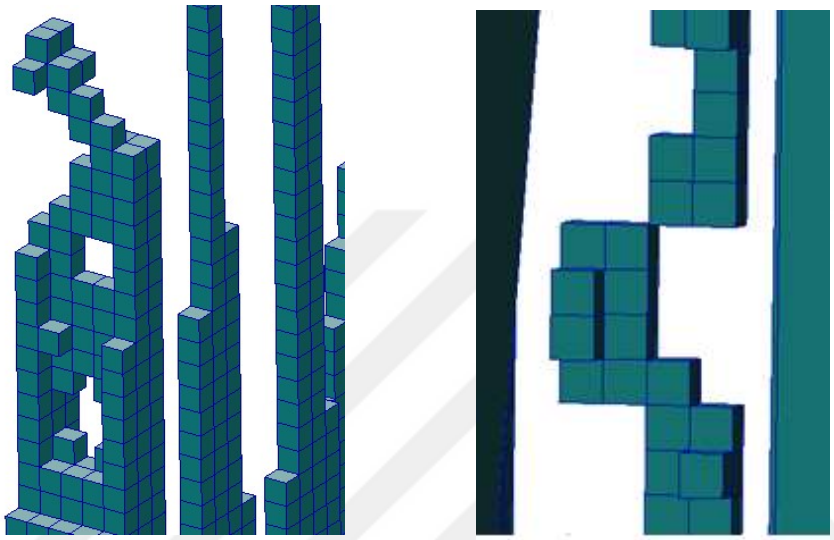


Figure 8-10 Complex Areas of $r_{min} = 4\ mm$ Case

Although $r_{min} = 8\ mm$ Case provides smooth and easy-to-manufacture topology, it has the worst stiffness value among all cases. Therefore, $r_{min} = 6\ mm$ is selected for all studies in this thesis since the final topology with this value has medium compliance and does not have any non-manufacturable zones. A similar study is done by Ürün, Şahin and Gürses in 2022 and it is presented in UHUK [39].

D. Stiffness Optimization for Load 2 and Load 3

Final topologies of stiffness optimization with Load 2 (only bending load) and Load 3 (only hinge moment) are shared in Figure 8-11 and Figure 8-12.

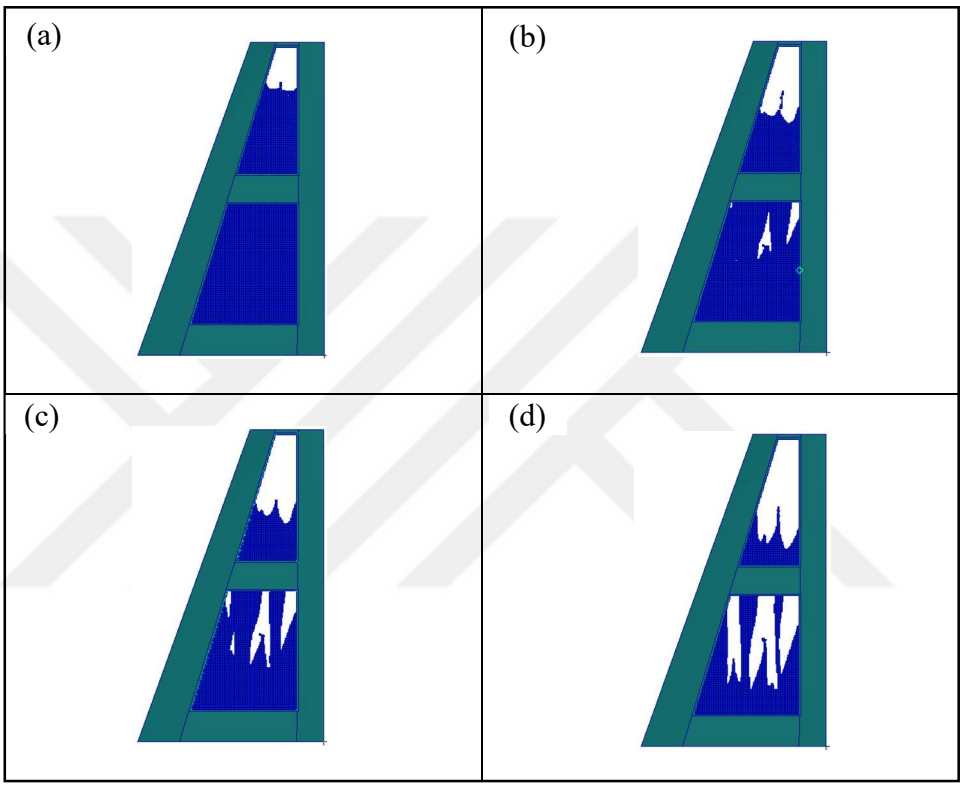


Figure 8-11 Iteration Steps for Load 2 (a) Iter. 30 (b) Iter. 60 (c) Iter. 90 (d) Iter. 120

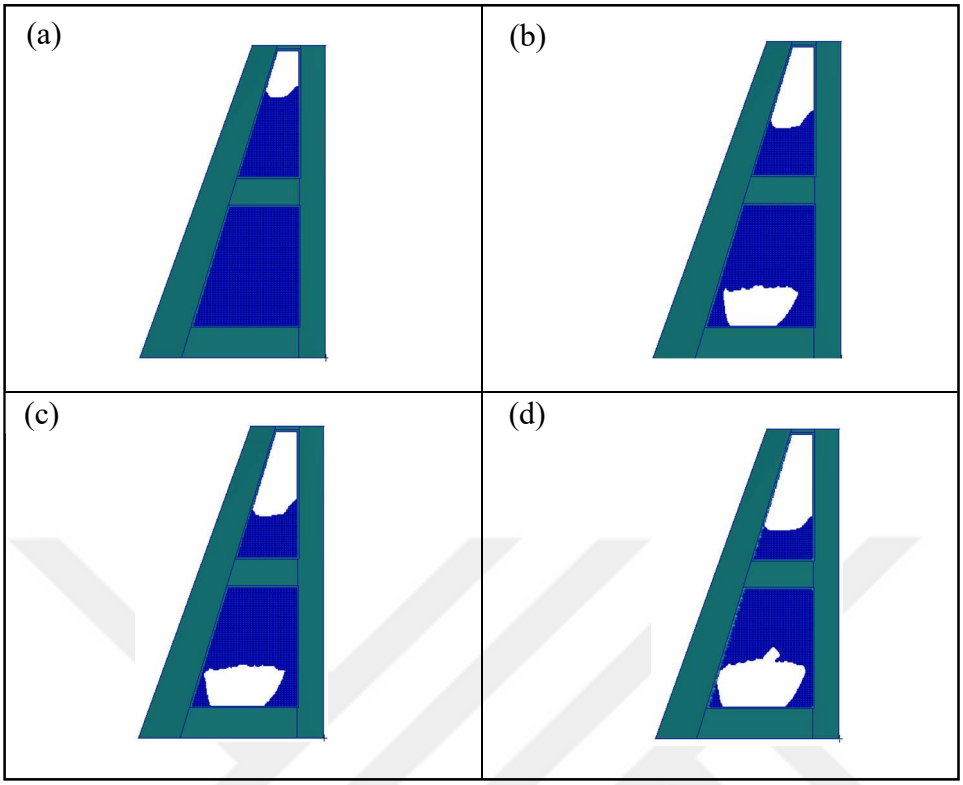


Figure 8-12 Iteration Steps for Load 3 a) Iter. 30 (b) Iter. 60 (c) Iter. 90 (d) Iter. 120

E. Effect of Initial Guess on Optimization of 2D Cantilever Beam

BESO has the capability to do topology optimization by using different initial guess designs that are feasible in addition to the full design. This approach may decrease the total number of iterations and the total computational time. In this sub-study, two different initial guess designs of the 2D Cantilever Beam presented in Appendix A.2 are optimized. Initial guess designs have a volume fraction of 0.5, which is the targeted final volume fraction at the same time. Figure 8-13 and Figure 8-14 show the first initial guess design and iteration steps while Figure 8-15 shows the evolution of the mean compliance and the corresponding volume fraction.



Figure 8-13 The First Initial Guess Design of 2D Cantilever Beam

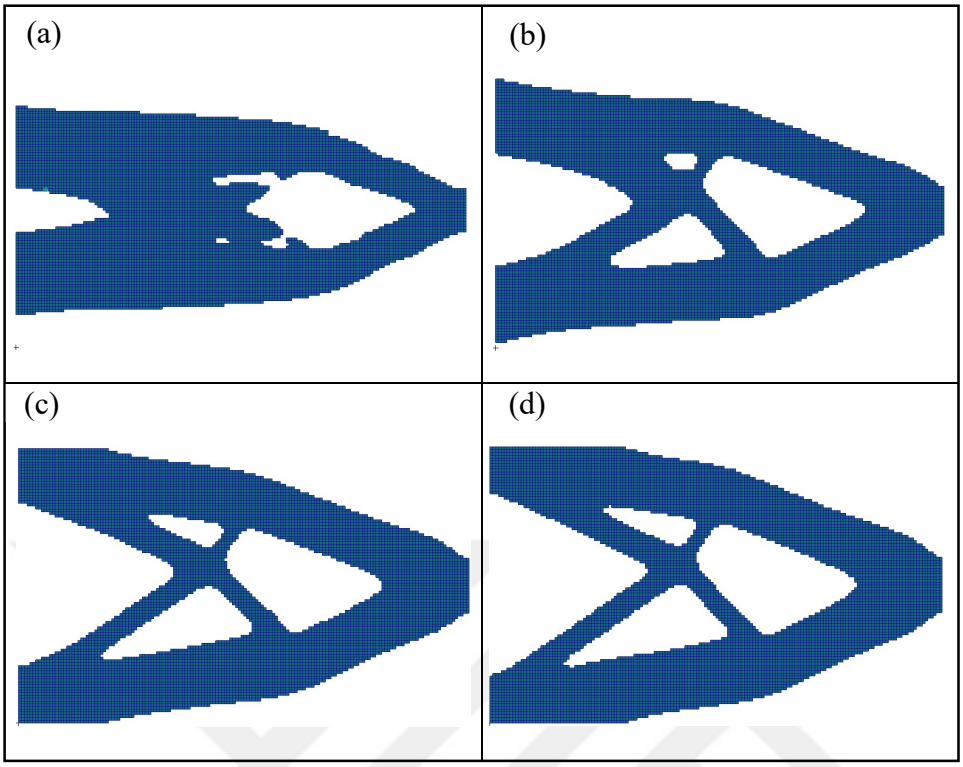


Figure 8-14 Iteration Steps for the First Initial Guess Design (a) Iter. 5 (b) Iter. 10 (c) Iter. 15 (d) Iter. 20

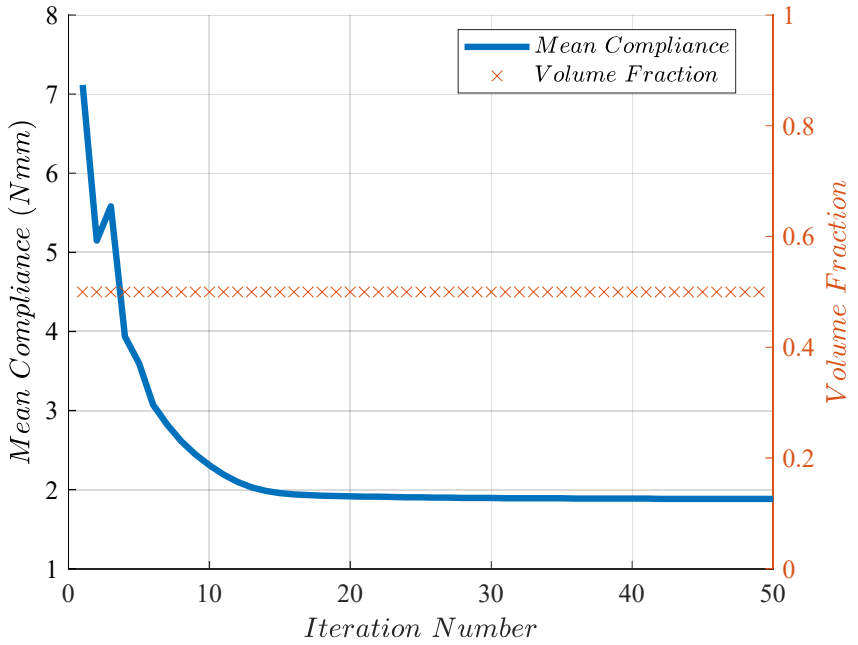


Figure 8-15 Evolution Histories of Mean Compliance and Corresponding Volume Fraction

The whole analysis took 50 iterations and 35 minutes. The final topology is demonstrated in Figure 8-16 and the mean compliance is 1.88 Nmm.

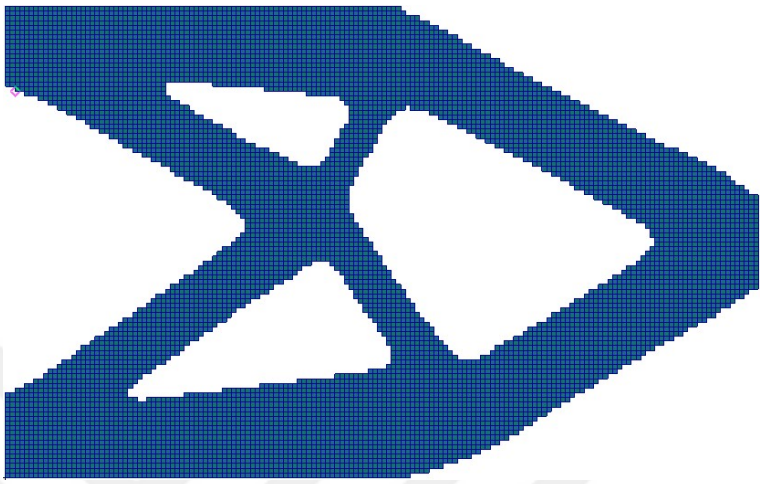


Figure 8-16 The Final Topology of 2D Cantilever Beam at Iteration 50

Figure 8-17 and Figure 8-18 show the second initial guess design and iteration steps while Figure 8-19 shows the evolution of the mean compliance and the corresponding volume fraction.

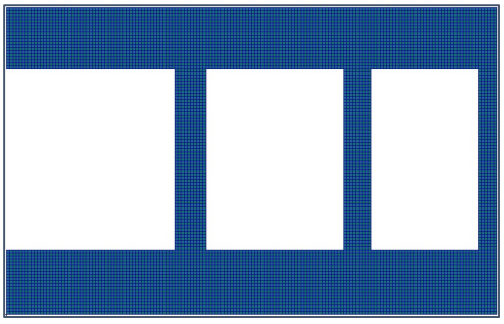


Figure 8-17 The Second Initial Guess Design of 2D Cantilever Beam

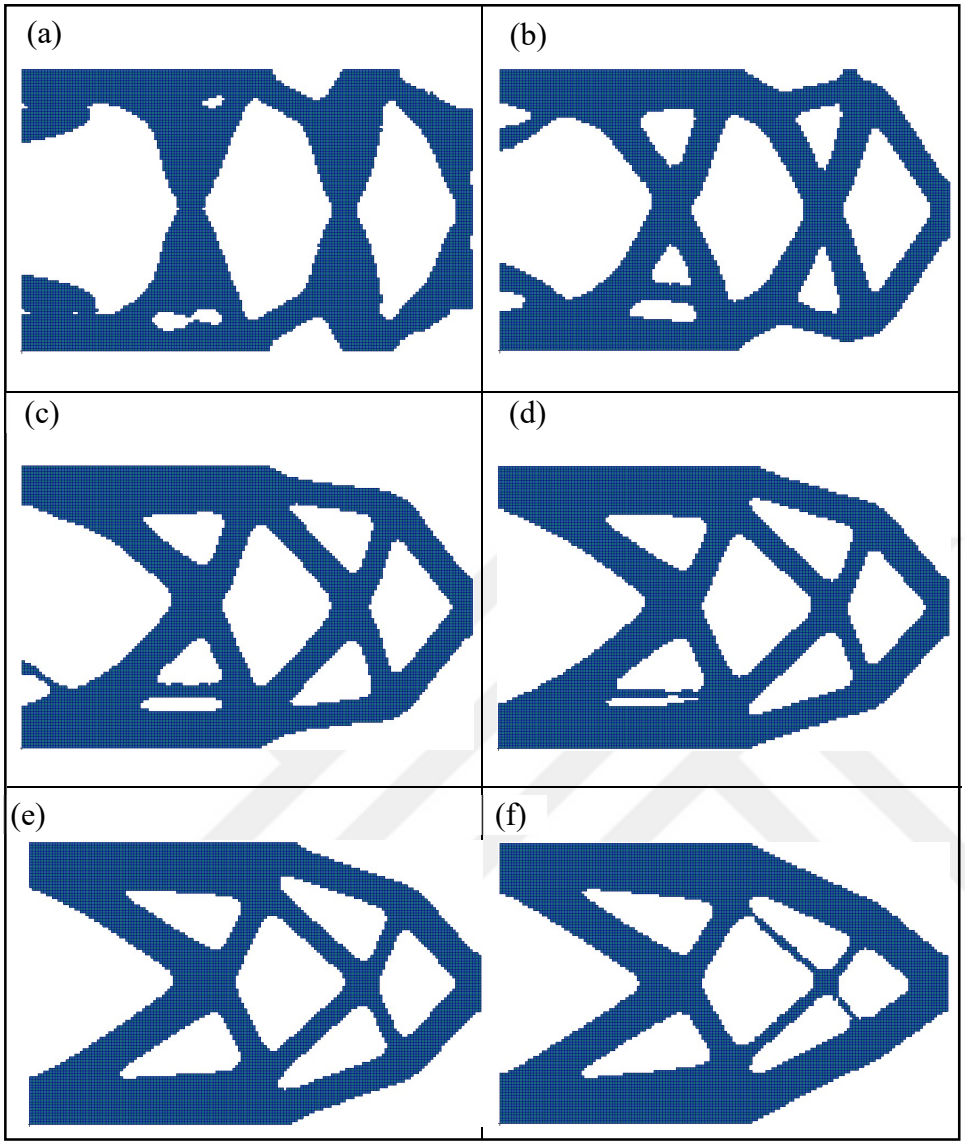


Figure 8-18 Iteration Steps for the Second Initial Guess Design (a) Iter. 5 (b) Iter. 10 (c) Iter. 15 (d) Iter. 20 (e) Iter. 25 (f) Iter. 80

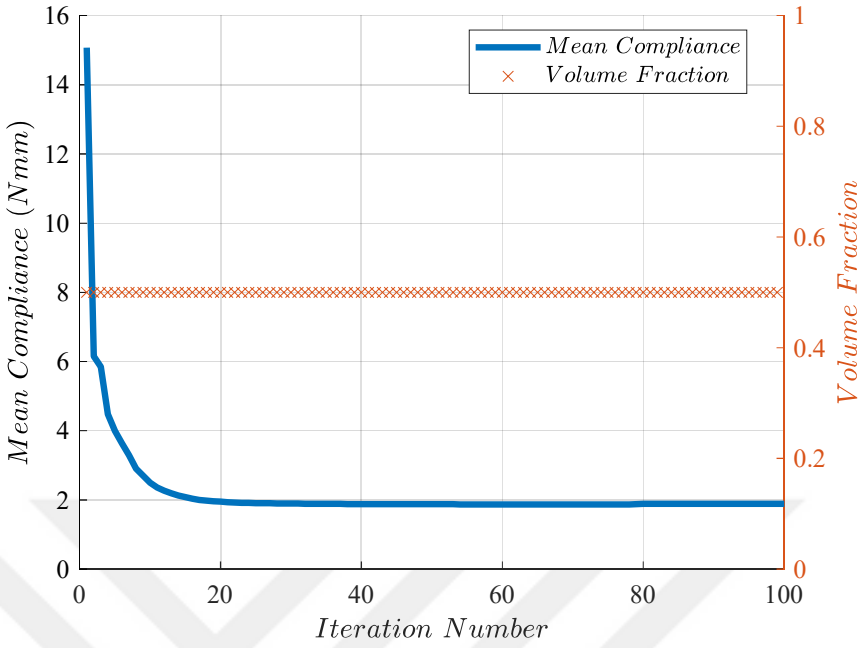


Figure 8-19 Evolution Histories of Mean Compliance and Corresponding Volume Fraction

The whole analysis took 95 iterations and 1.2 hours. The final topology is demonstrated in Figure 8-20. The mean compliance of the final topology is 1.87 Nmm, which is the same value of full design space optimization at the same time.

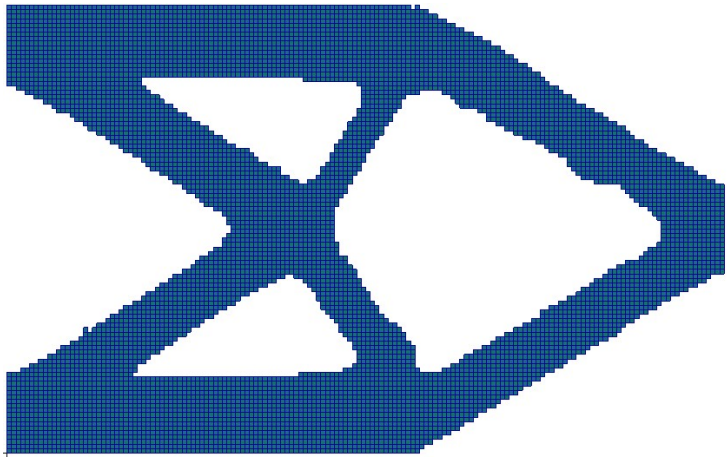


Figure 8-20 The Final Topology of 2D Cantilever Beam at Iteration 95

These two sub-studies with different initial topologies demonstrate that BESO is able to find similar final optimized designs for the problem considered and this outcome is shown in Figure 8-21. Furthermore, it is important to note that both final designs have very similar mean compliance values. The most important advantage of having an initial feasible guess design is the computational time. The first initial guess design converges in 50 iterations, and it finds a slightly worse topology compared to the second initial guess. The second initial guess design converges in 95 iterations, and it gives a slightly better design. Even though the optimum design is achieved with the almost same number of iterations of the full design case, it is possible to have slightly worse structures with less number of iterations by using larger convergence tolerance. For example, the topology at iteration 25 has a mean compliance of 1.9 Nmm, which is just 1.6% higher than the mean compliance of the final topology. In this way, the computational time of the optimization could be shortened in exchange for the efficiency of the final topology.

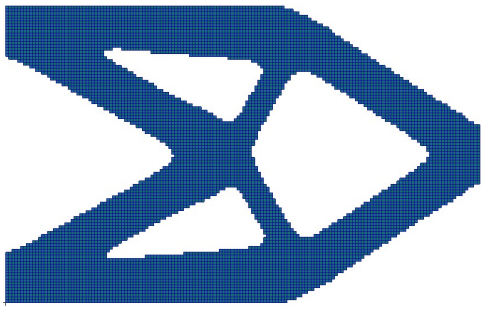
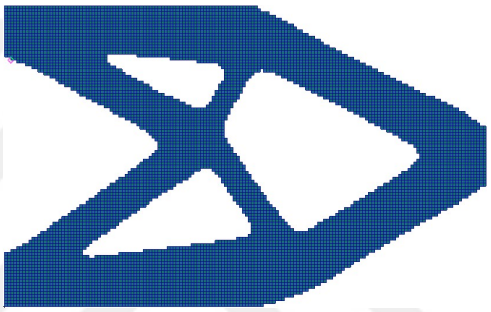
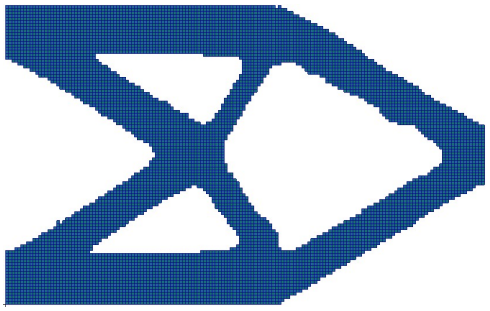
Full Design Space (Mean Compliance=1.87 Nmm)	
The First Initial Guess Design (Mean Compliance=1.88 Nmm)	
The Second Initial Guess Design (Mean Compliance=1.87 Nmm)	

Figure 8-21 Final Topologies of 2D Cantilever Beam According to Initial Guesses

F. Initial Guess Design for the Folding Wing

In this sub-study, the folding wing structure is optimized by using the initial guess design with the volume fraction of 0.3 under Load 1 with the stiffness criteria. The initial guess in Figure 8-22 is generated randomly and analysis goes until the convergence criterion is satisfied. Iteration steps are demonstrated in Figure 8-23 while Figure 8-24 shows the evolution of the mean compliance and the corresponding volume fraction.

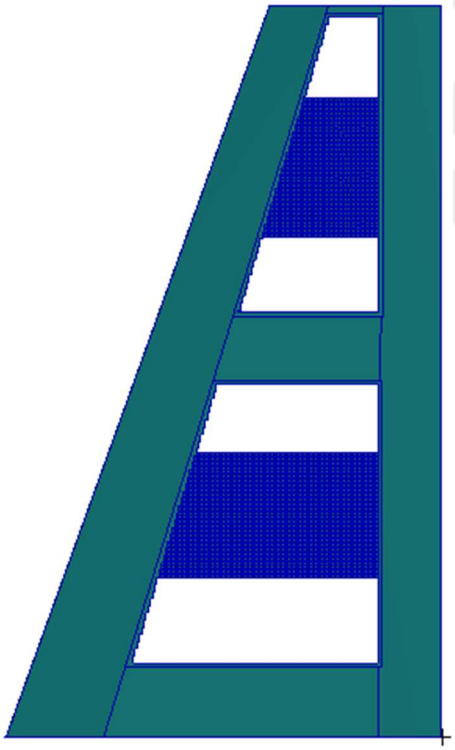


Figure 8-22 The Initial Guess Design of the Folding Wing with the Volume Fraction of 0.3

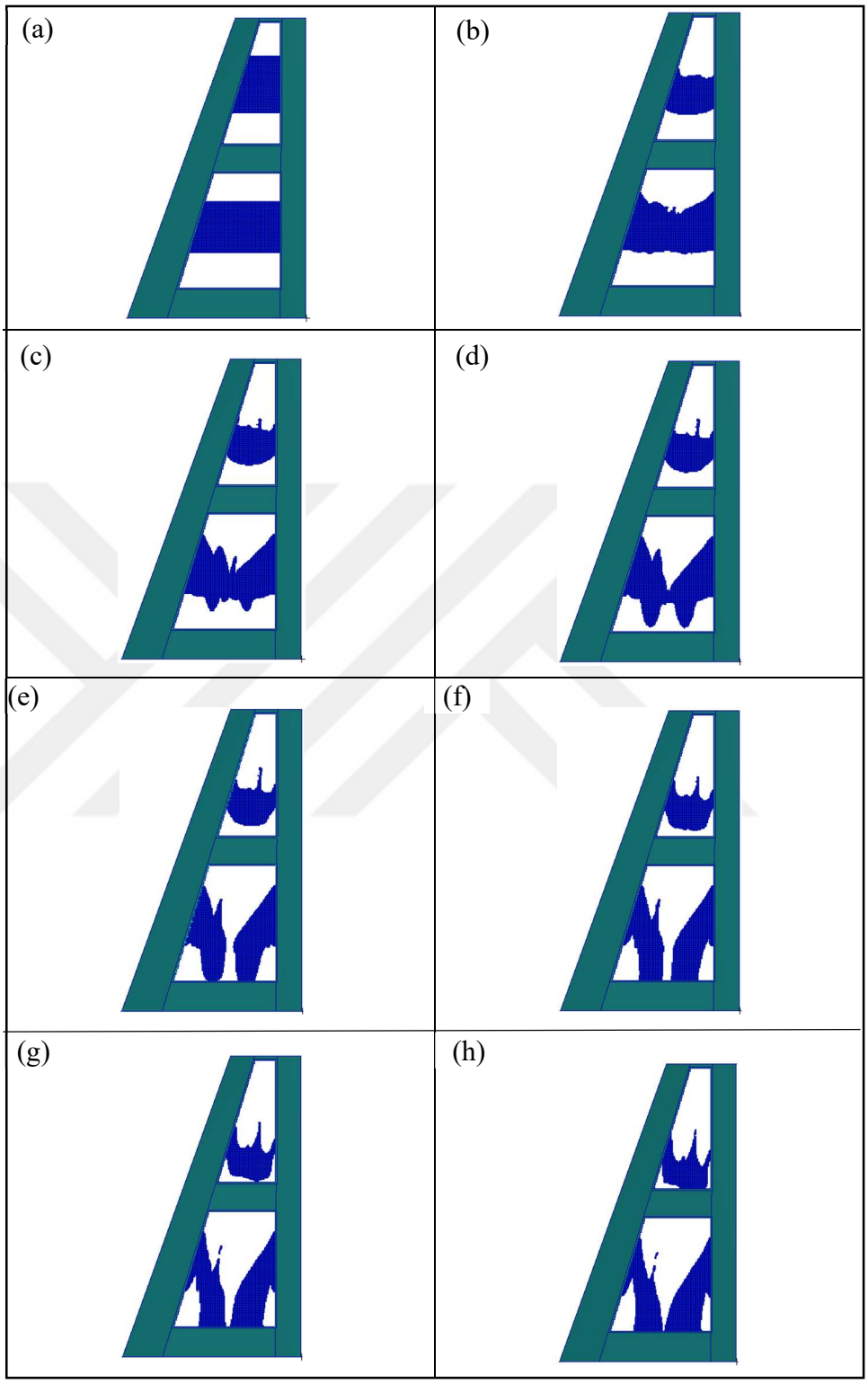


Figure 8-23 Iteration Steps for the Folding Wing Initial Guess Design (a) Iter. 1 (b) Iter. 15 (c) Iter. 30 (d) Iter. 45 (e) Iter. 60 (f) Iter. 75 (g) Iter. 90 (h) Iter. 105

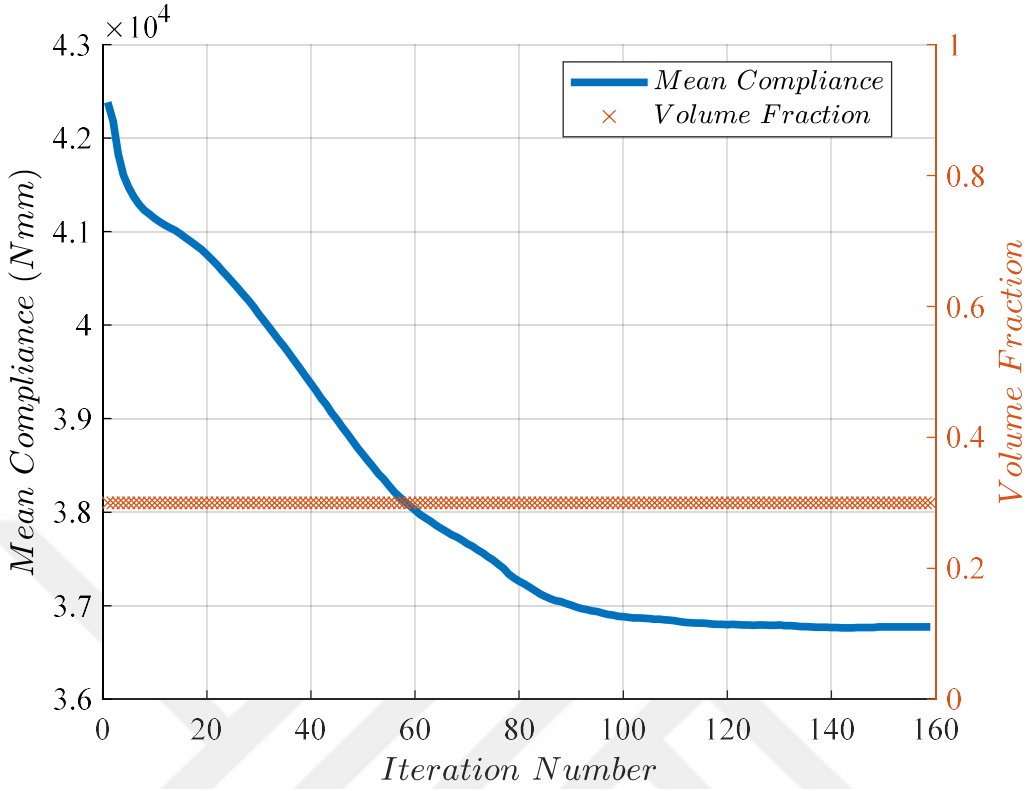


Figure 8-24 Evolution Histories of Mean Compliance and Corresponding Volume Fraction

Optimization took a total of 160 iterations and 5.2 hours. Figure 8-24 shows that the mean compliance value decreases with iterations and stiffness increases. The final topology (Figure 8-25 (a)) at iteration 160 has the mean compliance value of 3.68×10^4 Nmm, which is 3% greater than the mean compliance of the full design space study. This indicates that the optimized topology in this sub-study is not successful as the final topology of the full design space study, which is detailed in Section 5.3. In addition to objective values, this sub-study took almost two times more than the full design space study. To conclude, BESO has the capability to start from different initial points, but the optimized design could be worse than the case where the full domain is used as the start point.

(a) Mean Compliance
3.68×10^4 Nmm

(b) Mean Compliance
3.57×10^4 Nmm



Figure 8-25 Final Topologies for (a) Initial Guess Design (b) Full Design